

**FABRICATION, CHARACTERIZATION, AND PROPERTIES OF  
BIONANOHYBRIDS BASED ON BIOCOMPATIBLE POLYLACTIDE  
AND CARBON NANOTUBES**

by

**James Ramontja (M.Sc.)**

**Submitted in accordance with the requirements for the degree**

**PHILOSOPHIAE DOCTOR (Ph.D.)**

**Department of Chemistry**

**Faculty of Natural and Agricultural Sciences**

at the

**UNIVERSITY OF THE FREE STATE (QWAQWA CAMPUS)**

**University supervisor: Prof A.S. Luyt**

**CSIR supervisor: Prof S. Sinha Ray**

**November 2010**

## DECLARATION

We the undersigned, hereby declare that the research in this thesis is Mr Ramontja's own original work, which has not partly or fully been submitted to any other University in order to obtain a degree.

---

Mr J Ramontja

---

Prof AS Luyt

---

Prof S Sinha Ray

## **DEDICATION**

I would like to dedicate this work to my mother, Mpatjake Lisbeth Mashifane and my late uncle, Sekgekge Klaas Ramontja.

## ACKNOWLEDGEMENTS

I would like to thank God for always supplying me with the protection, strength, tolerance, patience, and wisdom that were needed to succeed in this work.

I would also like to express my sincere gratitude to my supervisors, Professor Adriaan Stephanus Luyt and Professor Suprakas Sinha Ray, for their compassionate, excellent supervision and personal respect they gave me. Their broad knowledge, dedication, and enthusiasm are what brought success in this work. I like the freedom I had to explore my potential on my own regarding this study. I don't have words to express my true inner feeling about how you opened new frontiers for my career, I thank you Professors.

I would also like to thank Dr Sreejarani Pillai for her contribution to this work, especially the discussions we always had on functionalization of carbon nanotubes.

I thank Jayita Bandyopadhyay for assisting me with small-angle X-ray scattering and polar optical microscopy measurements.

I would like to thank Thomas Malwela for assisting in the measurement and interpretation of the atomic force microscopy results.

I would like to thank my friend, Thabo Gcwabaza, for the positive comments he always made to this study.

My heartfelt gratitude goes to all the colleagues at National Centre for Nano-Structured Materials (NCNSM), CSIR.

I would like to thank my friends, Bethuel Nkgadime, Matome Ramusi, and Mabule Thobejane for encouraging me to continue studying up to this level.

I thank my mother Mrs Mpatjake Lisbeth Mashifane, my younger brother Raditsela Holiday Ramontja, and my little sister Virginia Kanyane Mashifane for having the faith and trust that I am capable of doing anything. Their encouragement, respect, and patience are highly appreciated.

I would like to thank the special one and only lady in my life, my fiancée Charity Elize Maepa, for always raising my hopes high even when the times seemed bad.

Lastly, I am very grateful for the financial support I received from Department of Science and Technology and Council for Scientific and Industrial Research (CSIR), South Africa.

## ABSTRACT

This work reports on the preparation and characterization of biodegradable polylactide (PLA) nanocomposites based on functionalized carbon nanotubes (f-MWCNTs). The nanocomposites were prepared by melt extrusion and solvent casting methods. A new method used for the functionalization of multiwalled carbon nanotubes (MWCNTs) with hexadecylamine (HDA) is also reported. Attenuated total reflectance Fourier-transform infrared (ATR-FTIR), Raman, and X-ray photoelectron spectroscopy confirmed the functionalization of the carbon nanotubes. The morphology and structure of the nanocomposites were investigated through scanning electron microscopy (SEM), transmission electron microscopy (TEM), polarized optical microscopy (POM), small angle X-ray scattering (SAXS), and atomic force microscopy (AFM). The influence of functionalized carbon nanotubes on the thermal, thermomechanical and tensile properties of the PLA matrix was also investigated.

Firstly, a PLA composite containing 1.5 wt.% of f-MWCNTs (with 10 % amine content, determined gravimetrically) was prepared through a melt extrusion technique. FTIR and Raman spectroscopy revealed the strong interaction between the f-MWCNT's surfaces and the PLA matrix. The POM (in the molten state) revealed a fairly homogeneous dispersion of f-MWCNTs with some micron-scale agglomeration. POM also revealed that the f-MWCNTs acted as nucleating agents for the crystallization of the PLA matrix. An increase in crystallinity was also observed from differential scanning calorimetry (DSC). Dynamic mechanical analyses (DMA) showed an enhancement of the elastic modulus, particularly above room temperature. An improvement in the tensile strength and elongation at break, without significant loss of modulus, was also reported.

Secondly, a composite containing 0.5 wt. % of f-MWCNTs (with 20 % amine content) was prepared by a melt extrusion technique. Improvement of the thermal stability in air was observed. The spherulitic morphology and structure was studied through POM and SAXS. An improvement in the thermomechanical properties was observed below and above the glass transition temperature. The presence of f-MWCNTs played a nucleation role for the crystallization of the polymer matrix. The dispersion was fairly homogeneous in the PLA matrix with some micro-scale agglomeration as observed in SEM.

Lastly, a PLA composite with f-MWCNTs (with 10 % amine content) was prepared by a solvent casting method using chloroform as a solvent. The effect of the incorporation of f-MWCNTs on the crystallization behaviour of biodegradable/biocompatible polylactide (PLA) was studied. The crystallization behaviour of the PLA in the absence and presence of f-MWCNTs was studied by using POM, DSC and AFM. The results showed that the f-MWCNTs did not actively nucleate the crystallization of PLA, and that the PLA crystals were perfectly grown in the case of the composite. Such an observation is quite uncommon to the general understanding of the role of CNTs in semicrystalline polymer crystallization.

## LIST OF ABBREVIATIONS

$\chi_c$	Crystallinity
AFM	Atomic force microscopy
ASTM	American society for testing and materials
ATR-FTIR	Attenuated total reflectance Fourier-transform infrared
CB	Carbon black
CCD-AFM	Charge coupled device atomic force microscopy
CNB	Carbon nanoballoons
CNH	Carbon nanohorns
CNTs	Carbon nanotubes
CVD	Chemical vapour deposition
dc	Direct current
DMA	Dynamic mechanical analysis
DSC	Differential scanning calorimetry
dTGA	Derivative TGA
FDA	Food and drug administration
FIB-SEM	Focused ion beam scanning electron microscopy
f-MWCNTs	Functionalized multiwalled carbon nanotubes
G'	Storage modulus
G''	Loss modulus
HDA	Hexadecylamine
MPa	Megapascal
MWCNT	Multiwalled carbon nanotubes
PAN	Polyacrylonitrile
PBS	Poly(butylene succinate)
PCL	Poly( $\epsilon$ -caprolactone)
PES	Poly(ethylene succinate)
PET	Poly(ethylene terephthalate)
PEVA	Poly(ethylene-co-vinylacetate)
PHB	Poly( $\beta$ -hydroxybuterate)
PHBV	Poly(3-hydroxybuterate-co-3-hydroxyvalerate)
PLA	Poly(L-lactide)

PMMA	Poly(methyl methacrylate)
POM	Polarized optical microscopy
PPDO	Poly(p-dioxane)
PVA	Polyvinyl alcohol
SAXS	Small-angle X-ray scattering
SEM	Scanning electron microscopy
SWCNT	Single-walled carbon nanotubes
tan $\delta$	Damping factor
TEM	Transmission electron microscopy
T <sub>g</sub>	Glass transition temperature
TGA	Thermogravimetric analysis
T <sub>m</sub>	Melting temperature
TMDSC	Temperature modulated DSC
TPa	Terapascal
WAXS	Wide angle X-ray scattering
XPS	X-ray photoelectron spectroscopy
$\Delta H_c$	Enthalpy of cold crystallization

# TABLE OF CONTENTS

<b>DECLARATION</b> .....	<b>ii</b>
<b>DEDICATION</b> .....	<b>iii</b>
<b>ACKNOWLEDGEMENTS</b> .....	<b>iv</b>
<b>ABSTRACT</b> .....	<b>vi</b>
<b>LIST OF ABBREVIATIONS</b> .....	<b>viii</b>
<b>TABLE OF CONTENTS</b> .....	<b>x</b>
<b>LIST OF FIGURES AND SCHEMATIC DIAGRAMS</b> .....	<b>xiv</b>
<b>LIST OF TABLES</b> .....	<b>xvi</b>
<b>Chapter 1</b> .....	<b>1</b>
<b>Introduction</b> .....	<b>1</b>
1.1 Overview .....	1
1.2 Objectives.....	3
1.4 References .....	5
<b>Chapter 2</b> .....	<b>8</b>
<b>Literature review</b> .....	<b>8</b>
2.1 Introduction .....	8
2.2 Chemistry and synthesis of lactic acid and PLA.....	9
2.2.1 Azeotropic dehydrative condensation .....	10
2.2.2 Direct polycondensation polymerisation.....	11
2.2.3 Ring opening polymerization .....	12
2.2.4. Solid state polymerization .....	12
2.3 Properties of poly(lactide).....	12
2.4 Applications of poly(lactide).....	13
2.4.1 Commodity applications .....	15
2.4.2 Medical applications .....	16
2.5 Carbon nanotubes .....	18
2.5.1 Types of carbon nanotubes.....	18
2.5.2 Synthesis of carbon nanotubes .....	21
2.5.2.1 Arc discharge.....	21
2.5.2.2 Laser ablation .....	23
2.5.2.3 Chemical vapour deposition.....	23
2.6 Properties of carbon nanotubes .....	24
2.7 Applications of carbon nanotubes .....	25

2.7.1	Composite materials .....	25
2.7.2	Hydrogen storage .....	25
2.7.3	Electrochemical devices .....	26
2.7.4	Sensors and nanoprobe s .....	26
2.7.5	Field emitting devices .....	26
2.7.6	Drug delivery systems .....	27
2.8	Functionalization of carbon nanotubes .....	27
2.9	Carbon nanotubes-containing PLA nanocomposites .....	28
2.10	Preparation methods of carbon nanotubes-containing PLA nanocomposites .....	30
2.10.1	Melt blending .....	30
2.10.2	Solution blending .....	30
2.10.3	In-situ polymerization .....	30
2.10.4	Bulk mixing.....	31
2.10.5	Latex technology .....	31
2.10.6	Other methods .....	31
2.11	Properties of nanocomposites.....	32
2.11.1	Thermal properties .....	32
2.11.2	Mechanical properties .....	33
2.11.3	Electrical properties.....	34
2.11.4	Rheological properties.....	34
2.11.5	Damping .....	36
2.12	References .....	36
<b>Chapter 3</b>	.....	<b>50</b>
<b>Sample preparation and experimental techniques</b>	.....	<b>50</b>
3.1	Introduction .....	50
3.2	Materials.....	50
3.2.1	Poly(lactide) .....	50
3.2.2	Multiwalled carbon nanotubes .....	50
3.2.3	Others .....	50
3.3	Methods.....	51
3.3.1	Preparation of samples .....	51
3.3.1.1	Functionalization of carbon nanotubes .....	51
3.3.1.2	Preparation of nanocomposites with melt mixing technique .....	51
3.3.1.3	Preparation of nanocomposites with solution mixing technique .....	52
3.3.2	Attenuated total reflectance Fourier-transform infrared spectroscopy .....	52
3.3.3	X-ray photoelectron spectroscopy.....	53
3.3.4	Raman spectroscopy.....	54
3.3.5	Thermogravimetric analysis.....	56
3.3.6	Differential scanning calorimetry.....	57
3.3.7	Scanning electron microscopy .....	57
3.3.8	Polarized optical microscopy .....	58
3.3.9	Dynamic mechanical analysis .....	59
3.3.10	Small- and wide angle X-ray scattering .....	60
3.3.11	Tensile testing .....	61

3.3.12	Electrical conductivity.....	62
3.3.13	Transmission electron microscopy.....	63
3.3.14	Atomic force microscopy.....	64
3.4	References.....	65
<b>Chapter 4.....</b>	<b>68</b>	
<b>High-performance carbon nanotube-reinforced bioplastic.....</b>	<b>68</b>	
4.1	Introduction.....	68
4.2	Results and discussion.....	68
4.2.1	Fourier-transform infrared spectroscopy: Functionalization of MWCNTs.....	68
4.2.2	X-ray photoelectron spectroscopy: Functionalization of MWCNTs.....	69
4.2.3	Raman spectroscopy: Functionalization of MWCNTs.....	70
4.2.4	Fourier-transform infrared spectroscopy: After composite formation.....	71
4.2.5	Raman spectroscopy: After composite formation.....	73
4.2.6	Differential scanning calorimetry.....	74
4.2.7	Polarized optical microscopy.....	75
4.2.8	Dynamic mechanical analysis.....	77
4.2.9	Tensile properties.....	79
4.2.10	Direct current measurements.....	80
4.3	Conclusions.....	80
4.4	References.....	81
<b>Chapter 5.....</b>	<b>82</b>	
<b>The effect of surface functionalized carbon nanotubes on the morphology, as well as thermal, thermomechanical, and crystallization properties of polylactide.....</b>	<b>82</b>	
5.1	Introduction.....	82
5.2	Results and discussion.....	82
5.2.1	Attenuated total reflectance Fourier-transform infrared (ATR-FTIR) spectroscopy.....	82
5.2.2	Raman spectroscopy.....	83
5.2.3	Scanning electron microscopy.....	84
5.2.4	Polarized optical microscopy.....	85
5.2.5	The effect of cooling rate on the non-isothermal crystallization behaviour of PLA.....	86
5.2.6	Effect of cooling rates on melting behaviour of PLA.....	89
5.2.7	Temperature modulated DSC.....	92
5.2.8	Wide angle X-ray scattering.....	94
5.2.9	Thermogravimetric analysis.....	96
5.2.10	Dynamic mechanical analysis.....	97
5.3	Conclusions.....	99
5.4	References.....	99
<b>Chapter 6.....</b>	<b>102</b>	

<b>Unusual crystallization behaviour of carbon nanotubes-containing biodegradable polylactide composite .....</b>	<b>102</b>
6.1 Introduction .....	102
6.2 Results and discussion.....	102
6.3 Conclusions .....	108
6.4 References .....	108
<b>Chapter 7.....</b>	<b>111</b>
<b>Conclusions, publications and conference presentations.....</b>	<b>111</b>
7.1 Conclusions .....	111
7.2 Publications from the project .....	112
7.3 Future work .....	113
7.4 Conference presentations .....	113

## LIST OF FIGURES AND SCHEMATIC DIAGRAMS

- Figure 2.1 Enantiomers of lactic acid
- Figure 2.2 Different routes for the synthesis of PLA
- Figure 2.3 Synthesis of PLA based on chirality
- Figure 2.4 TEM images of multi-walled carbon nanotubes
- Figure 2.5 Schematic diagram showing how a hexagonal sheet of graphite is 'rolled' to form a carbon nanotube
- Figure 2.6 Diagrams of the three types of nanotube: (a) armchair, (b) zigzag and (c) chiral
- Figure 2.8 Visualization of a possible carbon nanotube growth mechanism
- Figure 3.1 Schematic representation of infrared beam path in the ATR setup
- Figure 3.2 Operating principle of XPS
- Figure 3.3 Raman scattering of excited molecules and atoms
- Figure 3.4 Schematic representation of a TGA setup
- Figure 3.5 A schematic representation of scanning electron microscope
- Figure 3.6 A photo of a thermostatted chamber showing the clamped sample in a DMA
- Figure 3.7 An example of a typical stress-strain curve
- Figure 3.8 Schematic representation of four-point collinear probe set-up (all dimensions in mm)
- Figure 3.9 Schematic representation of a transmission electron microscope
- Figure 3.10 Schematic diagram showing the operating principles of the AFM in the contact mode
- Figure 4.1 Fourier-transform infrared spectra of (a) p-MWCNTs, (b) f-MWCNTs, and (c) pure HDA
- Figure 4.2 XPS spectra of (a) p-MWCNTs and (b) f-MWCNTs. The right side is the enlarged peak position of 'C 1S'
- Figure 4.3 Raman spectra of (a) p-MWCNTs and (b) f-MWCNTs. Excitation wavelength was 514.5 nm
- Figure 4.4 FTIR of (a) pure PLA, (b) PLA/f-MWCNTs composite, and (c) f-MWCNTs
- Figure 4.5 Raman spectra of (a) f-MWCNTs and (b) the PLA/f-MWCNTs composite. The inset is the Raman spectrum of the pure PLA matrix. The excitation wavelength was 514.5 nm

- Figure 4.6 DSC curves of (a) pure PLA and (b) the PLA/f-MWCNT composite. Both samples were annealed at 110 °C for 3h under vacuum prior to analysis
- Figure 4.7 Polarized optical micrographs of (a) pure PLA and (b) the PLA/f-MWCNT composite. Both samples were crystallized from their melts at 130 °C for 30 min
- Figure 4.8 POM image of the PLA/f-MWCNT composite taken at 190 °C in the transmittance mode. This is the most representative image after taking 5 pictures at different positions in the sample
- Figure 4.9 Temperature dependence of the dynamic mechanical properties of pure PLA and the composite: (a) storage modulus and (b)  $\tan \delta$
- Figure 4.10 Most representative (out of five tests for each sample) room temperature uniaxial tensile tests of neat PLA and composite samples at a constant cross head speed of 5 mm/min. Annealed (110 °C for 3h) injection moulded samples were used
- Figure 6.1 Polarized optical micrographs of (a) neat PLA and (b) the PLA/f-MWCNT composite. Both samples were crystallized at 130 °C from their melts
- Figure 6.2 DSC curves of neat PLA and the PLA/f-CNT composite: (a) during cooling from the melt and (b) during heating as soon as the cooling was finished
- Figure 6.3 The temperature dependence of elastic storage modulus and  $\tan \delta$  curves of neat PLA and the PLA/f-CNTs composite. Compression moulded, annealed (at 110°C for 3h under vacuum) samples were used
- Figure 6.4 (a) Field-emission scanning electron microscopic image of the freeze-fractured surface of the composite and (b) bright-field transmission electron microscopic image of the composite
- Figure 6.5 Tapping mode atomic force microscopy height images of (a, a') neat PLA and (b, b') PLA/f-CNTs composite thin films at two different magnifications

## LIST OF TABLES

Table 2.1	Physical properties of PLA
Table 4.1	Various properties of neat PLA and its composite with f-MWCNTs
Table 5.1	Cooling rate dependence of the total heat of fusion of two melting peaks of PLA estimated by the area under the endothermic region of the DSC curves
Table 5.2	TMDSC data for PLA and its nanocomposite

# Chapter 1

## Introduction

### 1.1 Overview

When introducing the subject of nanoscience and nanotechnology, it is almost customary to extract from RP Feynman's visionary 1959 lecture [1,2] "There is plenty of room at the bottom". The field of nanoscience and nanotechnology (concerned with the manipulation of matter on the nanoscale, which is now generally taken as the 1-100 nm range) is of the greatest interest to chemists, physicists and engineers (nanoparticles, nanostructured materials, nanoporous materials, nanopigments, nanotubes, nanoimprinting, quantum dots, etc.) and has already led to many innovative applications, particularly in materials science [2-5]. The main focus of this chapter shall be mainly on nanotechnology as it is a frequently used word, both in the scientific literature and in common language [6].

Perhaps the question to be asked should be: Why has nanoscience/nanotechnology attracted such a huge global interest? It has already been established that nanoscience/nanotechnology is concerned with properties, interactions and processing of units containing a notable number of atoms. These units, regardless of whether they are fullerenes, quantum dots, carbon nanotubes or biomolecules have novel electronic, optical and chemical properties by virtue of their nanometre dimensions. Varying the size and controlling the interactions of these units change fundamental properties of the nanostructured materials synthesized from these building blocks. These created an impression that nanoscience and nanotechnology has a huge potential to contribute in finding solutions for the four difficulties facing a greater part of the globe's population: health, food, energy, and pollution. It has thus sparked huge investments from governments and private sectors across the globe [7,8].

Nanotechnology employs two main approaches: (a) the "bottom-up" approach where materials and devices are built from molecular components which assemble themselves chemically by principles of molecular recognition, and (ii) "top-down" approach where

nanoscale-objects are constructed from larger ones without atomic-level manipulation [9]. However, it has become increasingly obvious that the top-down approach is subject to drastic limitations for dimensions smaller than 100 nm [10]. Thus, the bottom-up approach opens virtually unlimited possibilities regarding the design and construction of artificial molecular devices and machines capable of performing specific functions upon stimulation with external energy inputs [11,12]. Although nanoscience and nanotechnology are still in their infancy, new exciting results [13] and, sometimes, disappointments [14] alternate the scene as always happens in fields that have not yet reached maturity. The Project on Emerging Nanotechnologies estimates that over 1015 manufacturer-identified nanotech products are available to the public as of August 2009 [15]. For the past decade, various methods have been applied in the synthesis of nanomaterials categorized as fullerenes, carbon nanotubes, nanospheres, and inorganic nanoparticles/nanocrystals (made from metals, semiconductors or oxides). These are of great scientific interest as they effectively bridge the gap between bulk materials and atomic or molecular structures by virtue of their very high surface area to volume ratio.

In this study, our main focus is on the CNTs as fillers for polymeric composite systems. CNTs are graphite sheets rolled up into seamless cylinders that have revolutionized experimental low-dimensional physics and are utilized in a wide variety of state-of-the-art nanoscientific research. Since their discovery in 1991 at NEC Laboratories in Japan by Sumio Iijima, CNTs have been found to exhibit outstanding physical properties for a wide range of potential applications [16]. CNTs exhibit intrinsic properties such as high mechanical strength [17], structurally dependent electrical conductivity [18,19], and thermal conductivity [20]. It is also believed that the incorporation of CNTs into polymer matrices could lead to composites with unique properties [21] such as dramatically enhanced thermal stability, as well as mechanical and barrier properties [22-27]. There are two main approaches to achieve polymer nanomaterials. The most popular is to incorporate nanoscale particles into a polymer matrix to produce polymer/nanoparticle composites. The other is to manufacture polymeric materials themselves in the nanoscale dimension. Both approaches have been applied to many non-degradable and biodegradable polymer materials, giving rise to materials with good performance. The advantages of nanoscale particle incorporation can lead to a countless application possibilities where the analogous larger scale particle incorporation would not provide the adequate property profile for exploitation. These areas include polymer blend

compatibilization, membrane separation, electrical conductivity, barrier properties, impact modifications, UV screens and biomedical applications.

## 1.2 Objectives

The main objective of this project is to fabricate high performance new and novel bionanomaterials. Nanocomposites of anisotropic particles such as carbon nanotubes (CNTs) with biocompatible polylactide were prepared and characterized. The surfaces of the CNTs were fine-tuned by proper chemistry to enhance the compatibility of the CNT surface with the polylactide matrix. The correlation between the CNT geometries and nanocomposite morphologies on the one hand, and the mechanical, thermal, rheological, and electrical properties of the nanocomposites on the other hand were studied. The influence of surface modification and filler content on the nanocomposite morphology and properties was investigated. This was done to contribute to the knowledge needed to design new bionanohybrid materials with desired properties. However, because of the strong inter-tube Van der Waals interactions, the homogeneous dispersion-distribution of CNTs within a polymeric matrix remains a great scientific and engineering challenge. If CNTs are not dispersed as single tubes, the active surface area will not increase sufficiently for polymer-CNT surface interaction and as a result a very small amount of stress will be transferred between the filler and the matrix. While many techniques are recently available such as *in-situ* polymerization of monomers in the presence of CNTs, ultrasonic dispersion of CNTs in the polymer solution, melt processing, electrospinning and electrode chemistry, all the techniques failed to individually disperse the CNTs in the polymer matrix. For this reason, polymer nanocomposites based on CNTs have so far not shown a dramatic improvement in mechanical properties (maximum 30-40%) of the final composite materials.

Both improvements in and worsening of mechanical performance of CNT/polymer nanocomposites have been reported. The possible causes of such inconsistencies include variable specimen preparation methods, variations in CNTs quality and purity, dispersion, type, aspect ratio, degree of alignment, and, finally, differences in tube-polymer interfacial chemistry, both within a sample and among samples from different batches or laboratories.

In this project we used two innovative methods to disperse CNTs in the polymer matrix: The first method is the solution casting, which is achieved by dissolving a polymer and filler separately in a solution and then mixing the two to prepare the composites. The second method involves simple melt extrusion in which a polymer and filler are melt-mixed in a chamber at a pre-set temperature. The later method was also used by the Sinha Ray group [28-31] to disperse layered silicates in polyolefin matrices.

In the first part of this study, we focused on functionalizing the surface of multiwalled CNTs to improve the dispersion and interaction with the polylactide chains. We used the following techniques to characterise them:

- Attenuated total reflectance Fourier-transform infrared (ATR-FTIR) spectroscopy to confirm the functionalization.
- The presence of functional groups was also confirmed with x-ray photoelectron spectroscopy (XPS).
- Raman spectroscopy was used to confirm the nature of bonding between MWCNTs and the surfactant of interest.

The second part focused on nanocomposite preparation by melt extrusion, and the characterization and property determination by the following techniques:

- Scanning electron microscopy (SEM) to study the morphology.
- Polarized optical microscopy (POM) to study the influence of (f-MWCNTs) on the crystal growth behaviour of PLA nanocomposites.
- Differential scanning calorimetry (DSC) to study the melting and crystallization behaviour of the PLA nanocomposites.
- Thermogravimetric analysis (TGA) to study the influence of the presence of f-MWCNTs on the thermal stability of the PLA samples.
- Tensile testing to study the influence of f-MWCNTs on the mechanical properties of the PLA nanocomposites.
- Wide angle x-ray scattering (WAXS) to study the miscibility, crystallinity, and structure of the PLA nanocomposites.
- Dynamic mechanical analysis (DMA) to study the effect of the f-MWCNTs on thermomechanical properties of PLA.

### 1.3 Layout of the thesis

This thesis contains 7 chapters. Chapter 1 describes the general background and objectives of this study. Chapter 2 presents a literature review relevant to the project. Chapter 3 summarizes the characterization techniques (including brief discussions on how the techniques work) and materials used in this study. Chapters 4, 5, and 6 presents the discussion of results obtained. Finally, chapter 7 summarizes the main observations described in the thesis, and presents some concluding remarks.

### 1.4 References

- [1] R.P. Feynman. 1959. <http://www.zyvex.com/nanotech/Feynman.html> (originally published in the February 1960 edition of the Altech Engineering and Science Journal).
- [2] R.P Feynman. "There's plenty of room at the bottom". Engineering and Science 1960; 23:22-36.
- [3] S.J. Ainsworth. As nanometer-scale materials start making money, intellectual property issues are heating up. Chemical and Engineering News 2004; 82:17-22.
- [4] S.R. Morrissey. Harnessing nanotechnology. Chemical and Engineering News 2004; 82:30-33.
- [5] Nanotechnology. Innovation for tomorrow's world. European Commission, EUR 21151, p. 1-56, 2004.  
See at: [ftp://ftp.cordis.europa.eu/pub/nanotechnology/docs/nano\\_brochure\\_en.pdf](ftp://ftp.cordis.europa.eu/pub/nanotechnology/docs/nano_brochure_en.pdf)
- [6] M. Reisch. "A rose by any other name?". Chemical and Engineering News 2004; 82 (16):8.
- [7] P. Moriarty. "Nanostructured materials". Reports on Progress in Physics 2001; 64:297-381.
- [8] S.J. Fonash. Education and training of the nanotechnology workforce. Journal of Nanoparticle Research 2001; 3:79-82.
- [9] P. Rodgers, "Nanoelectronics: Single file". Nature Nanotechnology 2006. This is a one page article available on:  
<http://www.nature.com/nnano/reshigh/2006/0606/full/nnano.2006.5.html>

- [10] R.F. Service. Optical lithography goes to extremes – and beyond. *Science* 2001; 293:785-786.
- [11] G.M. Whitesides, J.P. Mathias, C.T. Seto. Molecular self-assembly and nanochemistry: a chemical strategy for the synthesis of nanostructures. *Science* 1991; 254:1312-1319.
- [12] D.B. Amabilino, J.F. Stoddard. Interlocked and Intertwined Structures and Superstructures. *Chemical Reviews* 1995; 95:2725-2828.
- [13] R.F. Service. Assembling Nanocircuits from the Bottom Up. *Science* 2001; 293:782-785.
- [14] R.F. Service. Next-Generation Technology Hits an Early Midlife Crisis. *Science* 2003; 302:556-559.
- [15] Project on Emerging Nanotechnologies (2010). Analysis: This is the first publicly available on-line inventory of nanotechnology-based consumer products.
- [16] S. Iijima. Helical microtubules of graphitic carbon. *Nature* 1991; 354:56-58.
- [17] M.M.J. Treacy, T.W. Ebbesen, J.M. Gibson. Exceptionally high Young's modulus observed for individual carbon nanotubes. *Nature* 1996; 381:678-680.
- [18] T.W. Ebbesen. Carbon nanotubes. *Annual Review of Material Science* 1994; 24:235-264.
- [19] J.W. Mintmire, B.D. Dunlap, C.T. White. Are Fullerene tubules metallic? *Physical Review Letters* 1992; 68:631-634.
- [20] J. Che, T. Cagin, W.A. Goddard III. Thermal conductivity of carbon nanotubes. *Nanotechnology* 2000; 11:65-69.
- [21] R. Dagani. Putting the "nano" into composites. *Chemical and Engineering News* 1999; 77(23):25-37.
- [22] M. Okamoto. Biodegradable Polymer/Layered Silicate Nanocomposites: A Review. *Journal of Industrial and Engineering Chemistry* 2004; 10:1156-1181.
- [23] T.B. Liu, C. Burger, B. Chu. Nanofabrication in polymer matrices. *Progress in Polymer Science* 2003; 28:5-26.
- [24] J.W. Kim, S.G. Kim, H.J. Choi, M.S. Jhon. A Commentary on "Synthesis and electrorheological properties of polyaniline-Na<sup>+</sup>-montmorillonite suspensions". *Macromolecular Rapid Communications* 1999; 20:450-452.
- [25] S.J. Park, K. Li, S.K. Hong. Preparation and characterization of layered silicate-modified ultrahigh-molecular-weight polyethylene nanocomposites. *Journal of Industrial and Engineering Chemistry* 2005; 11:561-566.

- [26] K. Ishizu, K. Tsubaki, A. Mori, S. Uchida. Architecture of nanostructured polymers. *Progress in Polymer Science* 2003; 28:27-54.
- [27] M. Pluta, M. A. Paul, M. Alexandre, P. Dubois. Plasticized polylactide/clay nanocomposites. I. The role of filler content and its surface organo-modification on the physico-chemical properties. *Journal of Polymer Science: Part B Polymer Physics* 2006; 44:299-311.
- [28] S.S. Ray, P. Maiti, M. Okamoto, K. Yamada, K. Ueda. New polylactide/ layered silicate nanocomposites. 1. Preparation, characterization, and properties. *Macromolecules* 2002; 35(8):3104–10.
- [29] S.S. Ray, K. Yamada, M. Okamoto, A. Ogami, K. Ueda. New polylactide/ layered silicate nanocomposites. 3. High-performance biodegradable materials. *Chemistry of Materials* 2003; 15(7):1456–65.
- [30] S.S. Ray, K Yamada, M. Okamoto, Y. Fujimoto, A. Ogami, K. Ueda. New polylactide/layered silicate nanocomposites. 5. Designing of materials with desired properties. *Polymer* 2003; 44(21):6633–46.
- [31] S.S. Ray, M. Bousmina. Biodegradable polymers and their layered silicate nanocomposites: In greening the 21st century materials world. *Progress in Materials Science* 2005; 50(8):962–1079.

## Chapter 2

### Literature review

#### 2.1 Introduction

Over the past century synthetic polymers have become an integral part of our lives. They are, however, not readily biodegradable and their persistent environmental pollution has become a global problem [1].

There are two ways that can be used to alleviate plastic wastes from the environment: (1) storage of plastic wastes at landfill sites, but these sites are limited due to the rapid development of society. (2) Recycling and incineration. Recycling appears to solve the problem, but it requires substantial costs of labour and energy for the removal of plastic wastes, separation according to the types of plastics, washing, drying, grinding, and then reprocessing to final products. Hence, this leads to more expensive packaging and the quality of the recycled plastic wastes is often lower than that produced directly by the primary manufacturer. Incineration of plastic wastes always produces a large amount of carbon dioxide which results in global warming. It also sometimes produces toxic gases such as nitrogen oxide, carbon monoxide, and nitrogen dioxide which again contribute to environmental pollution [2].

With this background, the development of biodegradable polymers has been a growing concern since the last decade of the 20<sup>th</sup> century. Biodegradable polymers are regarded as those that undergo microbially induced chain scission into smaller fragments, and ultimately into simple stable end-products [3]. Mineralization may be due to aerobic or anaerobic microorganisms, or biologically active processes (such as enzymatic reactions) or passive hydrolytic cleavage [4-6]. A range of biodegradable polymer materials have been prepared and industrialized [7-11].

Biodegradable polymers are classified into three major categories according to their different origins: (i) synthetic polymers, particularly aliphatic polyester poly(L-lactide) (PLA) [12-17],

poly( $\epsilon$ -caprolactone) (PCL) [18,19], poly(p-dioxane) (PPDO) [19-21], poly(butylene succinate) (PBS) [22-26], and poly(ethylene succinate) (PES) [27,28]; (ii) polyesters produced by microorganisms, which basically indicates different types of poly(hydroxyalkanoate)s, including poly( $\beta$ -hydroxybuterate) (PHB) and poly(3-hydroxybuterate-co-3-hydroxyvalerate) (PHBV) [29-31], (iii) polymers that originate from natural resources including starch, lignin, chitosan, cellulose, chitin, and proteins [32-39]. Even though biodegradable polymers have created massive opportunities, they are still far from taking over from conventional undegradable polymers, in that they generally have poor mechanical properties, are highly hydrophobic, and have poor processability which prohibits their utilization. One can now easily understand why there is a need for modification of these polymers into biodegradable materials with balanced properties. The use of inorganic or natural fillers for the preparation of blends or conventional composites is among the other routes to improve some of the properties of biodegradable polymers. Reinforcements of biodegradable polymers with nanometric materials promises to produce eco-friendly green materials with controlled properties such as thermal stability, strength, low melt viscosity, gas barrier properties, and slow biodegradation rate. These materials are called nanocomposites. The high aspect ratio and high surface area associated with nanometric fillers can improve the reinforcement efficiency of nanocomposites with only  $\pm 5$  wt.% loading to match that of conventional composites with 40 to 50 wt.% of loading of classical fillers.

This chapter aims to provide a detailed introduction of PLA and CNTs as a polymer and filler of interest. Both their properties, synthesis, and PLA nanocomposites containing CNTs shall be described. The characterization techniques shall be discussed in Chapter 3.

## **2.2 Chemistry and synthesis of lactic acid and PLA**

Poly lactide is synthesized from the monomer, lactic acid, which can be produced by carbohydrate fermentation and chemical methods of synthesis. However, lactic acid production by fermentation route is commonly favoured. This method is based on the fermentation of starch and other polysaccharides, which can be easily found from potatoes, corn, sugar cane, sugar beet, and other biomasses. Most of the commercially available lactic acid is produced by a bacterial fermentation route.

Lactic acid (2-hydroxy propanoic acid) is a chiral molecule which exists in two optically active configurations, D- and L- enantiomers (Figure 2.1). The D enantiomer differs from the L enantiomer in that it rotates the plane of polarized light counterclockwise, whereas the L enantiomer rotates the plane of polarized light clockwise.

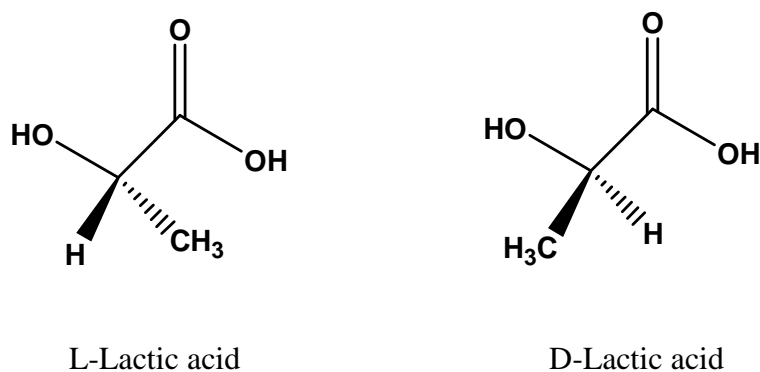


**Figure 2.1** Enantiomers of lactic acid

Chemical processes produce a racemic mixture of D and L enantiomers, optically inactive D, L or meso forms of lactic acid. L-lactic acid is currently produced through a popular bacterial fermentation route using various modified strains of *Lactobacillus* [40].

Although polymerization of lactic acid to high molecular weight PLA can be achieved in two ways, four methods are generally used for the synthesis of PLA (Figure 2.2).

### 2.2.1 Azeotropic dehydrative condensation

This method involves the use of an organic solvent. Lactic acid is condensed directly into a high molecular polymer. The removal of water is achieved azeotropically by balancing the equilibrium between a polymer and a monomer, whereas the solvent is dried and recycled back into the reaction. This technique produces a highly pure, high molecular weight PLA by allowing the reaction temperature to be below the melting point of the polymer, hence effectively preventing depolymerization and racemization during polymerization [41-45].

## 2.2.2 Direct polycondensation polymerisation

This method has the disadvantage that it is used only to obtain a low molecular weight polymer. The stereochemistry is also very difficult to control as lactic acid is polymerized in the presence of a catalyst at reduced pressure, hence it is very difficult to completely remove water from the highly viscous reaction mixture. A high molecular weight polymer can be obtained by coupling a low molecular weight polymer with isocyanates, epoxides or peroxides [45,46]. These chain coupling reagents react with either hydroxyl or carboxyl groups of low molecular weight PLA chains. Both carboxyl- and hydroxyl- terminated PLA chains serve as polymerization points to produce high molecular weight PLA.

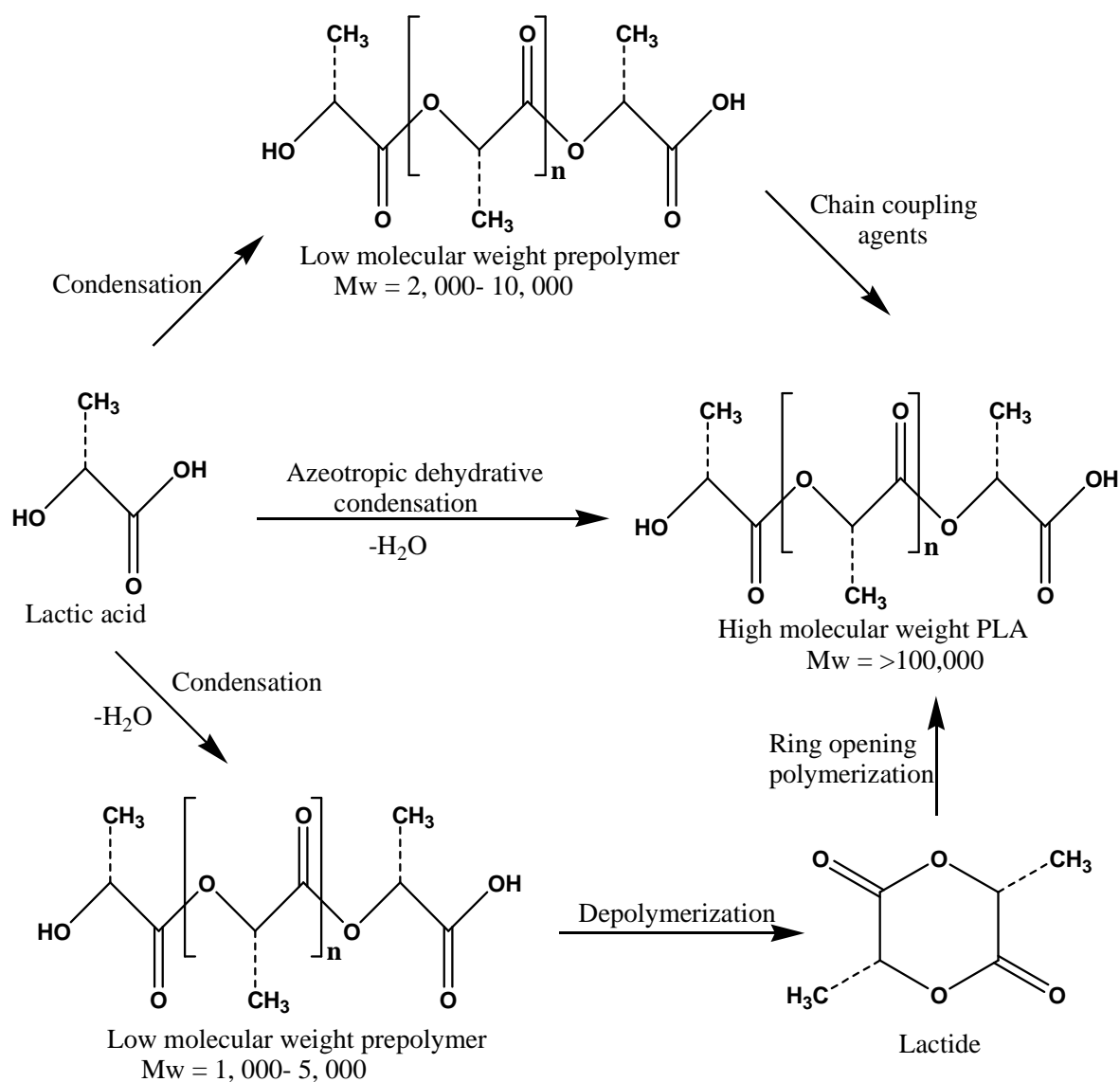


Figure 2.2 Different routes for the synthesis of PLA [45].

### **2.2.3 Ring opening polymerization**

This method is usually preferred for the synthesis of high molecular weight PLA as it provides better prospects of controlling stereochemistry. Lactide is obtained from the depolymerization of a low molecular weight pre-polymer, purified, and then polymerized to high molecular weight PLA [46].

### **2.2.4. Solid state polymerization**

This method offers advantages such as (a) no solvent is required, thus avoiding environmental pollution; (b) operating at low temperatures, thus able to control side reactions, thermal, hydrolytic, oxidative degradation with reduced discoloration and degradation of the final product; (c) polymers prepared from this method often have improved properties due to the ability to avoid side reactions and monomer cyclization.

## **2.3 Properties of poly(lactide)**

The physical properties of PLA polymers depend on molecular characteristics such as crystallinity, degree of chain orientation, spherulite size, and crystalline thickness. The purity of lactic acid stereocopolymer enantiomers also influences the physical properties of polylactide, for example, the polymerization of a 50 w/w mixture of L- and D-lactic acid produces DL-poly(lactic acid) which is amorphous (Figure 2.3).

Similarly, polymerization of D- and L- lactic acids respectively produces D- and L- poly(lactic acid), that have the same properties, but different stereochemistry. PLA can also be produced with varying fractions of L- and D-lactide. PLA resins having more than 93% of L-lactic acid are semicrystalline, while PLA with 50–93% L-lactic acid is amorphous [46]. Some of the physical properties of PLA are summarized in Table 2.1 [47].

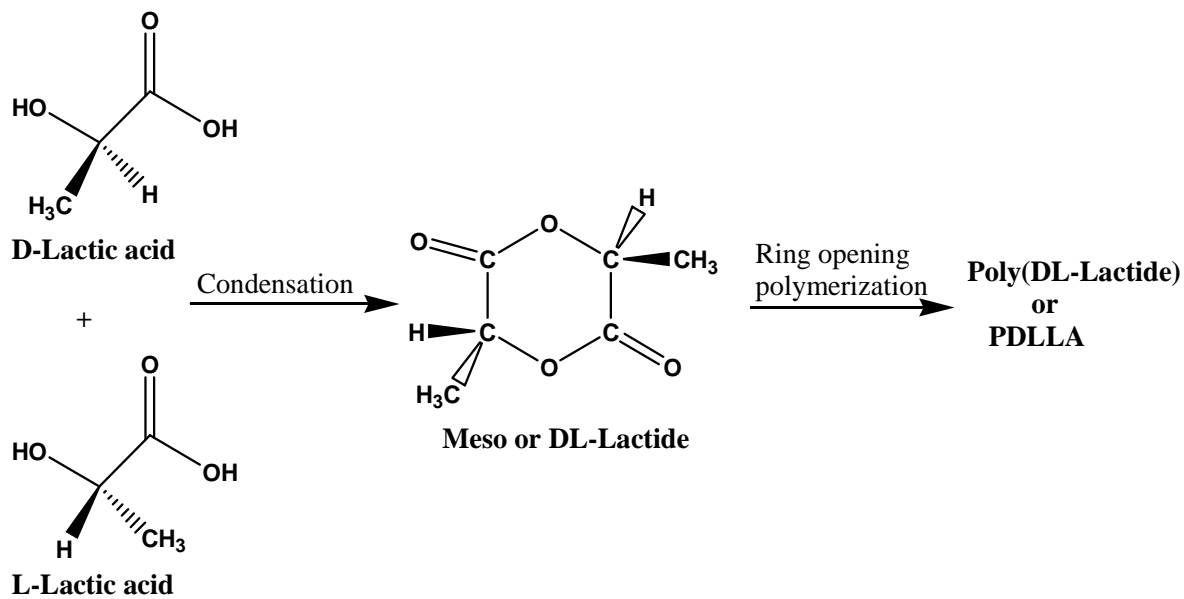


**Figure 2.3** Synthesis of PLA based on chirality.

The glass transition temperature ( $T_g$ ) and melting temperature ( $T_m$ ) are the most important parameters, because they both influence the type of applications the polymer will be used for [47,48]. Changes in polymer chain mobility occur at or above  $T_g$ .

PLA synthesized from 100% L-lactide has a melting temperature of 175 °C. Addition of D-lactide to the polymer structure reduces the melting temperature to between 130 °C to 160 °C [48,50].

## 2.4 Applications of poly(lactide)

Due to its good mechanical properties, biodegradability, and the eco-friendliness of its degradation products, PLA is used for a number of applications ranging from conventional thermoplastics (as in packaging, agricultural products and disposable products) to biomedicine, surgery and pharmaceuticals.

**Table 2.1 Physical properties of PLA [47]**

Property	Typical value
Molecular weight ( $\text{kg mol}^{-1}$ )	100–300
Glass transition temperature, $T_g$ ( $^{\circ}\text{C}$ )	55–70
Melting temperature, $T_m$ ( $^{\circ}\text{C}$ )	130–215
Heat of melting, $\Delta H_m$ ( $\text{J g}^{-1}$ )	8.1–93.1
Degree of crystallinity, $X$ (%)	10–40
Surface energy (dyn)	38
Solubility parameter, $\delta$ ( $\text{J}^{1/2} \text{ mL}^{-1/2}$ )	19–20.5
Density, $\rho$ ( $\text{kg m}^{-3}$ )	1.25
Melt flow rate, MRF (g/10 min)	2–20
Permeability of $\text{O}_2/\text{CO}_2$ ( $\text{mol m}^{-1} \text{ s}^{-1} \text{ Pa}^{-1}$ )	4.25/23.2
Tensile modulus, $E$ (GPa)	1.9–4.1
Yield strength (MPa)	70/53
Strength at break (MPa)	66/44
Flexural strength (MPa)	119/88
Elongation at break (%)	100–180
Notched Izod impact strength ( $\text{J m}^{-1}$ )	66/18
Decomposition temperature (K)	500–600
IR peaks ( $\text{cm}^{-1}$ )	
-OH (alcohol/carboxylic)	3700–3450
C=O	1750–1735
-COO	1600–1580
C-O	1200–1000
C-H	950–700

### 2.4.1 Commodity applications

Current developments in the production processes of PLA, along with improvements in material properties, has led to a variety of applications such as fibres, injection moulded articles, textile, and packaging. PLA is suitable for all these applications due to its [51]:

- (i) Low moisture absorption and high wicking properties superior to even that of poly(ethylene terephthalate) (PET), offering benefits for sports and performance apparel and products. The garments made from PLA or with wool or cotton are more comfortable with a silky touch.
- (ii) Low flammability and smoke generation [52-54]. The fibre shows improved self extinguishing characteristics. Fibres can be made by solvent or by melt spinning processes. The fibres produced by solvent spinning usually have better mechanical properties than the fibre produced by melt spinning, because of thermal degradation during melt spinning [55]
- (iii) High resistance to ultraviolet light, a benefit for performance apparel as well as for outdoor furniture and furnishing applications [56-61].
- (iv) Low index of refraction, which provides excellent colour characteristics. PLA possesses high transparency and it is an inherently polar material due to its basic repeating unit of lactic acid. This high polarity leads to a number of unique attributes such as high critical surface energy that yields excellent printability. Another benefit of PLA's polarity is the resistance to aliphatic molecules such as oils and terpenes.
- (v) Low density, making PLA fibres lighter in weight than others.
- (vi) Fibres coming from an annually renewable resource base that are readily melt-spun, offering manufacturing advantages resulting in greater consumer choice [62].

The textile sector is showing a great potential for PLA applications. For example, Fibreweb in France has shown webs and laminates made exclusively from PLA. The French have also extruded a range of melt-blown and spunlaid PLA fabrics under the name Deposa<sup>TM</sup> [63]. The garments showcased during the Nagano Olympics under the umbrella "*Fashion for the Earth*" were the products of Japan's Kanebo Ltd, which has produced PLA fibre under the brand name LACTROM<sup>TM</sup> [46].

### 2.4.2 Medical applications

The medical applications of PLA also rely on its biodegradability and the compatibility of lactic acid, as the degradation product, with the human body. The degradation behaviour of PLA was studied both *in vitro* and *in vivo*, and it was found to be influenced by environmental factors such as pH, air, temperature, and water [64].

In general, metal devices are used to fix fractured bones by aligning bone fragments into close proximity so that easy healing can take place. But the complete healing process relies on the bone's ability to carry normal weights, which is often compromised as the device also carries its own weight. Furthermore, the sudden removal of the device might temporarily leave the bone susceptible to re-fracture. However, with PLA devices, during the process of degradation, the fibrous connective tissues substitute the degrading implant. More importantly is the fact that no further surgery is required to remove the products since they slowly degrade in the body without any side effects [64]. The food and drug administration (FDA) of the United States of America has approved the use of PLA for certain human clinical applications such as sutures [65, 66].

Sutures are wound closure filaments designed in various shapes to keep tissues together in place until their natural healing is completed. However, the use of neat PLA for suture applications has been restricted by its inherent properties such as rigidity, slow degradation, and high crystallinity. In order to remedy this problem, companies such as Ethicon copolymerized (and commercialized) lactic acid with biodegradable monomers such as glycosidic acid to produce a copolymer with the required properties [67]. This introduces significant changes in physical properties and also increases the degradation rate of the PLA filament.

There is an urgent need for the development of systems to deliver therapeutic agents directly to the circulatory system, especially for drugs that undergo considerable inactivation by the liver. PLA and its copolymers have been playing a crucial role in drug delivery applications [67-70]. In the 1970s, protein based drugs and growth hormones were not attractive to use clinically, as methods to produce them, such as tissue extraction, were tedious. However, the advancement in molecular biology made it easier to synthesize and introduce proteins like insulin into bodies. PLA and its copolymers has been used to encapsulate and deliver these

proteins [71,72]. These drug systems have been developed based on reservoir devices. In the reservoir, the drug release takes place across a polymer membrane, while the drug activity remains unchanged. The drug is released steadily by hydrolytic degradation or morphological changes in the polymer [68,73]. PLA and PLA blend fibres with desired properties such as clearly designed porosity and biodegradability have been synthesized through dry-wet phase-inversion and electro spinning for drug release systems. Both methods have produced remarkable results. For example, Kenawy *et al.* [74] investigated the release of a drug from electrospun PLA, polyethylene-co-vinylacetate (PEVA) and their 50:50 blends. The drug, tetracycline hydrochloride, was solubilized in methanol, added to a PLA solution in chloroform, and the solution was electrospun to produce a nonwoven fabric sheet of very low thickness. The results showed immediate drug release with neat PLA compared to PEVA and its blend which showed a release of up to 120 days. This is an attractive characteristic of PLA blends, where short term continuous drug release is needed.

Another interesting application of PLA is in tissue engineering. This field is concerned about developing biological materials to help maintain, restore, and improve tissue function. The most fascinating aspects about tissue engineering are that there won't be a problem of transplant rejection since no donor is required. Patients with organ defects or malfunctions are treated by using their own cells grown on a polymer support so that a tissue part is regenerated from the natural cells. This is because the support disappears from the transplantation site with time, leaving behind a perfect patch of the natural tissue. PLA scaffolds may be designed into different shapes e.g. knitted, filament, film, braided, and nonwoven to achieve the requirements of organ manufacturing. These scaffolds serve as extracellular matrix to stick and grow cells leading to the development of new functional tissues. For example, Kellomäki *et al.* [75] reported on the design and manufacturing of different bioabsorbable scaffolds for guided bone regeneration and generation. They used self-reinforced PLA rods as scaffolds for bone formation in muscle by free tibial periosteal grafts. They found that, six weeks after implantation, new, histologically mature, bone had been generated in a pre-designed cylindrical form. Several other potential applications of PLA and its blends are summarized in a review by Lunt *et al.* [64].

## **2.5 Carbon nanotubes**

Graphitic sheets that are coiled up into seamless cylinders called CNTs, have dramatically changed the low-dimensional physics and are used in research by both scientists and engineers in the field of nanotechnology. It is the discovery of fullerenes (geometric cage-like structures of carbon atoms that are composed of hexagonal and pentagonal faces) by Smalley and co-workers [76] in the 1980s at Rice University that led to the discovery of CNTs. While looking for new carbon structures by an arc discharge method, Iijima [77] discovered long, slender fullerenes, often capped at the end. The walls of these fullerenes consisted of hexagonal carbonic structures, which were then labelled nanotubes due to their nanometre dimensions. Since then, the scientific community has been studying these materials intensely because of their potential applications invoked by their exceptional material properties, owing to their symmetric structure.

### **2.5.1 Types of carbon nanotubes**

Carbon nanotubes are classified mainly in two categories:

- (i) Single-walled CNTs. These consist of a single graphene sheet rolled seamlessly to form a cylinder with a diameter of the order of 1 nm and length of up to centimetres.
- (ii) Multiwalled CNTs. These consist of an array of cylinders formed concentrically and separated by a distance of 0.35 nm. They have diameters of 2-100 nm and lengths of tens of microns (see Figure 2.4, the coaxial arrangement of the tubes is clearly visible).

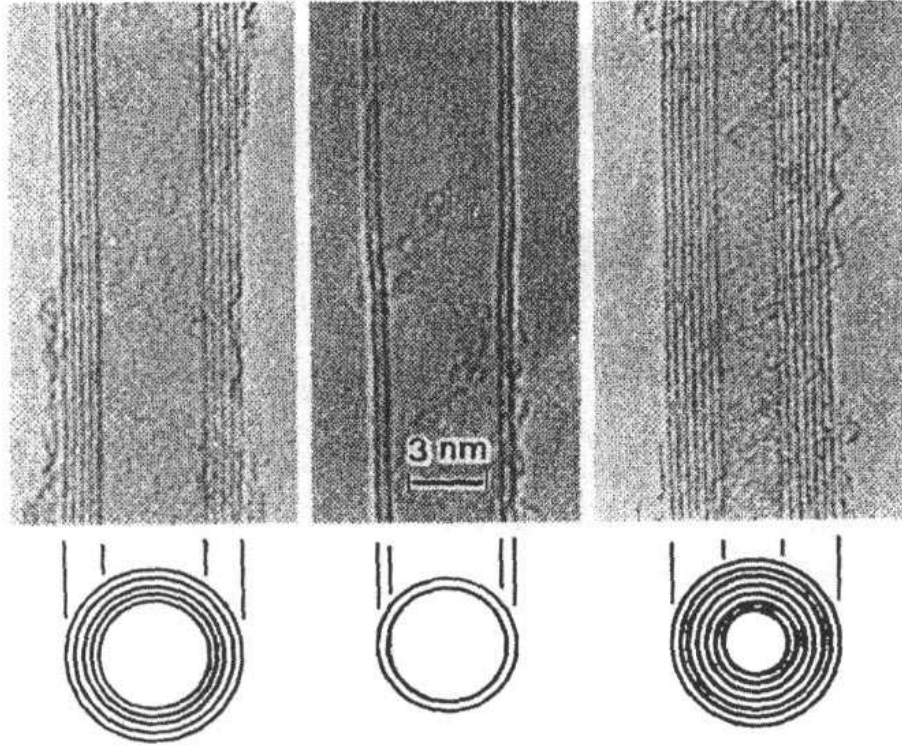


**Figure 2.4** TEM images of multi-walled carbon nanotubes [77].

A grapheme sheet may be rolled up in various ways to form single-walled CNTs with different structures, defined by the chiral vector,  $\vec{C}_h$ , and chiral angle,  $\theta$ , such that:

$$\vec{C}_h = n\vec{a}_1 + m\vec{a}_2 \quad (1)$$

where  $\vec{a}_1$  and  $\vec{a}_2$  are the basis vectors of the graphite lattice and  $m, n$  are integers representing the number of steps along the lattice (see Figure 2.5). The chiral vector covers the circumference of the tube.

The relationship between the graphite lattice basis vectors  $\vec{a}_1, \vec{a}_2$  and the chiral vector,  $\vec{C}_h$ , are used to characterize carbon nanotubes. Two limiting cases are shown:  $(n, 0)$  indices are associated with zigzag tubes whereas  $(n, n)$  indices are associated with armchair tubes. All other tubes are chiral. Figure 2.6 illustrates the different types of nanotube.

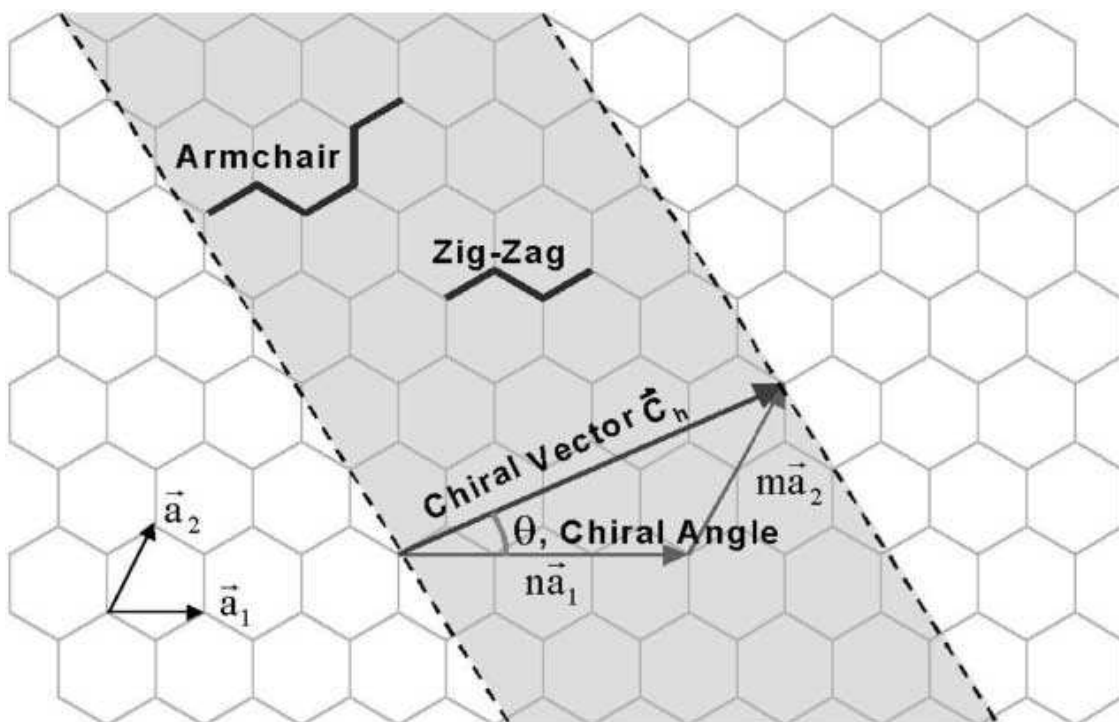


Figure 2.5 Schematic diagram showing how a hexagonal sheet of graphite is ‘rolled’ to form a carbon nanotube [78].

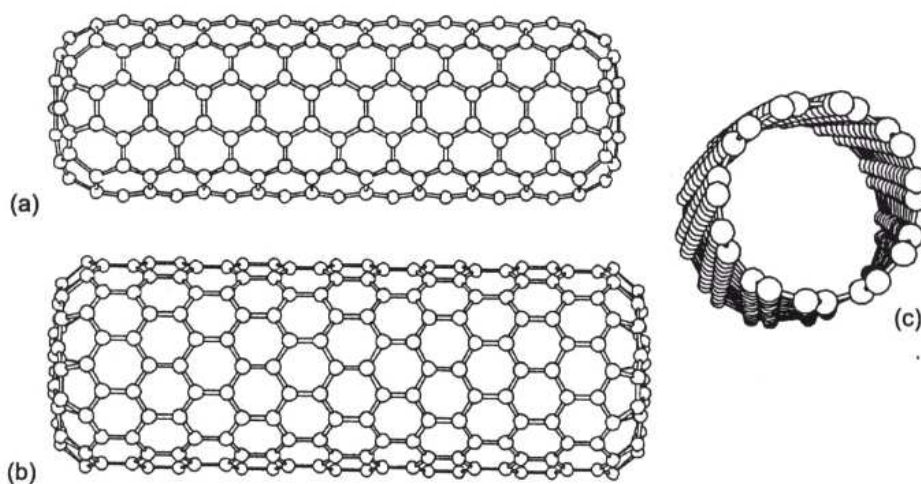


Figure 2.6 Diagrams of the three types of nanotube: (a) armchair, (b) zigzag and (c) chiral [79].

Chirality is an important characteristic of CNTs as it determines the type of properties they will have, such as electronic properties. For example, graphite has semi-metal properties, whereas CNTs are either metallic or semiconducting, depending on the nanotubes chirality.

## **2.5.2 Synthesis of carbon nanotubes**

Although scientists across the globe are still looking for more ways to produce carbon nanotubes, there are generally three main techniques so far. These are arc discharge, laser ablation, and chemical vapour deposition.

### **2.5.2.1 Arc discharge**

This method was initially used for the synthesis of C<sub>60</sub> fullerenes. Iijima [77] first observed nanotubes from the electric-arc discharge technique. This is the easiest technique to produce carbon nanotubes. However, it has a disadvantage of producing a mixture of components, so that the produced nanotubes still have to be purified before they can be useful. In this method, two carbon rods separated by about 1 mm are placed end to end in an inert environment of either argon or helium at low pressure, and they are arc-vaporized to produce CNTs.

The discharge vaporises one of the carbon rods and forms a small rod shaped deposit on the other rod. Both SWCNT and MWCNT can be selectively synthesized by this method depending on the exact set-up. To produce single-walled CNTs, the anode has to be doped with metal catalysts e.g. Mo, Co, Y, Fe, Ni, or mixtures of these [81]. Parameters such as system geometry, type of gas, metal concentration, current strength, and inert gas pressure influence the quality and quantity of the nanotubes obtained. The exact growth mechanism for nanotubes is not yet fully understood. However, there are some theories on the growth mechanisms (Figure 2.7).

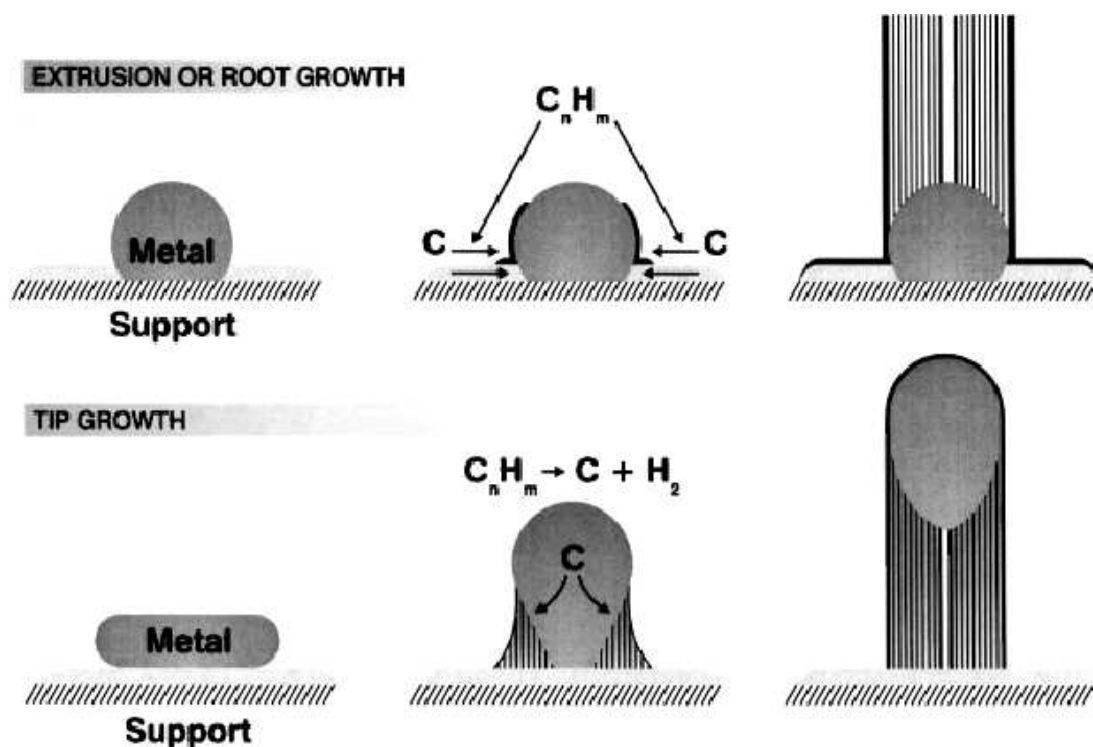


**Figure 2.7 Visualization of a possible CNTs growth mechanism [82].**

Figure 2.8 explains the two generally accepted theories: tip growth, and extrusion or root growth. Both mechanisms postulate that metal catalyst particles are floating or are supported on graphite or another substrate. The catalyst particles are spherical or pear-shaped. Extrusion or root growth takes place when the nanotube grows upwards from the metal particles that remain attached to the substrate. Tip growth takes place when the metal catalyst particles detach from the substrate and move to the head of the growing nanotube.

Although the diameter of the nanotubes can be fairly well controlled, the problem with this method is that there are a lot of metal catalyst impurities, and purification is difficult to perform. If MWCNTs are preferred, both electrodes are graphite. However, other products such as graphite sheets, amorphous carbon, and fullerenes are also formed. Purification is therefore needed, which causes defects on the walls and a loss of structure. The absence of metallic catalysts, however, means that the nanotubes can be produced with only a few defects, since there won't be a need for heavy acid treatment.

### 2.5.2.2 Laser ablation

At first, laser ablation was used for the initial synthesis of fullerenes, and the technique was modified to allow for the synthesis of SWCNTs. In 1995, a pulsed or continuous laser was used by Smalley and co-workers [83] to vaporise a carbon target in an oven at 1200 °C.

The oven is filled with argon or helium gas to maintain a certain pressure. The condensed material is then collected on a water cooled target. To synthesize SWCNTs, the graphite target is doped with metal catalysts, whereas pure graphite produces MWCNTs. In general, laser ablation produces high yields of SWCNTs with better purity (up to 90%), better properties and a narrower size distribution than in arc discharge. However, the two methods are similar in that they both need an inert atmosphere and a catalyst mix.

### 2.5.2.3 Chemical vapour deposition

Often called thermal or catalytic CVD to distinguish it from other CVDs used for various purposes, CVD is a simple and cost-effective technique for producing carbon nanotubes at a moderately low temperature and at ambient pressure. It is quite flexible in that it allows for the use of various hydrocarbons in any form like gas, solid or liquid. It also allows the use of different substrates and enables nanotube growth in various forms such as powder, thin or thick films, straight or coiled, aligned or entangled. It is generally reported that low temperatures (600 to 900 °C) favour the growth of MWCNTs, while high temperatures (900 to 1200 °C) favour the growth of SWCNTs. The catalyst particle size has been found to dictate the nanotube diameter, growth rate, wall thickness, morphology and microstructure. Solid organometalocene catalysts such as nickelocene, ferrocene, and cobaltocene, producing nanometal particles *in situ*, are preferred for the synthesis of nanotubes. Various forms of CVD techniques such as thermal CVD, laser assisted CVD, vapour phase growth CVD, plasma enhanced CVD, aero gel-supported CVD, and alcohol catalytic CVD, have been developed for the synthesis of CNTs [84].

Chemical vapour deposition can be regarded as an extremely versatile technique for the production of carbon nanotubes in that it: (i) is relatively easy to scale up; (ii) successfully uses a variety of hydrocarbons, catalysts, and catalyst supports; (iii) can fabricate various

alignments and patterns of nanotubes; and (iv) the CNTs can be produced continuously, which provides a good way for the production of large quantities of nanotubes under relatively controlled conditions.

Before CNTs can reach their full potential, they need to be purified as they are produced with a lot of impurities. Currently, the following techniques are employed by various research groups for the purification of CNTs: Oxidation (to remove metal catalysts and other carbon based impurities, usually with peroxides and sulphuric acid), annealing, micro filtration, ultrasonication, cutting, chromatography, functionalization, acid treatment, and magnetic purification [84].

## 2.6 Properties of carbon nanotubes

CNTs are regarded as one-dimensional systems. This is due to their small diameter (in nanometers) and long length (up to microns), leading to large aspect ratios. The large aspect ratios are important for electronic, molecular and structural properties. Carbon nanotubes generally possess three special properties:

*Electrical conductivity:* Depending on the chirality of their atomic structure, CNTs can be either metallic or semiconducting. The difference in conducting properties results from their molecular structure (armchair, zigzag, or chiral) with different band structures, and therefore different band gaps [85]. The electronic properties of perfect MWCNTs are similar to those of perfect SWCNTs, because the coupling between the concentric cylinders in MWCNTs is weak.

*Chemical reactivity:* A distinction must be made between the sidewall and the end caps of nanotubes, because the CNTs reactivity is directly related to the  $\pi$ -orbital mismatch caused by an increased curvature. In comparison with a grapheme sheet, nanotubes' reactivity is enhanced by the curvature of the surfaces of the nanotubes. Covalent chemical modifications of either sidewalls or end caps have proved to be possible. However, further experiments on the influence of chemical modifications on the nanotubes' behaviour are difficult, as it is not easy to produce or to find highly pure nanotubes [85].

*Mechanical strength:* The small-diameter CNTs are quite stiff and exceptionally strong, meaning that they have a high Young's modulus ( $\sim 1$  TPa) and high tensile strength ( $\sim 60$  TPa), as well as unique deformation behaviour [86]. CNTs are also very flexible due to their

great length, which makes them potentially suitable for future applications in composite materials with anisotropic properties.

*Optical properties:* It is expected that the optical properties of CNTs will be affected by their physical properties such as chirality, since theoretical studies have shown that optical activity of chiral nanotubes disappears if the nanotubes become larger [87]. Optical activity of CNTs might lead to optical devices.

## **2.7 Applications of carbon nanotubes**

As extensive research is ongoing on the applications of CNTs, we summarize here some of the most promising applications from the literature.

### **2.7.1 Composite materials**

Due to the interesting properties that they possess, CNTs can potentially be used in the development of super-strong and super-stiff polymer composite materials with CNT reinforcement [88–93]. The first achieved major commercial application of MWCNTs is their use as electrically conducting components in polymer composites [95]. The nanofibre morphology of the MWCNTs allows electronic conductivity to be achieved at low loading levels. Other performance aspects, such as mechanical properties and low melt flow viscosity, are either minimized or avoided. These are needed for thin-wall moulding applications.

### **2.7.2 Hydrogen storage**

Because they are cylindrical and hollow, CNTs have the potential to be used for hydrogen storage, e.g. for fuel cells that power electric vehicles or laptop computers. However, it is still impossible to assess these application potentials, because the reports of high storage capacities have shown to be inconsistent [96-98].

### **2.7.3 Electrochemical devices**

CNTs are attractive as electrodes for devices that use electrochemical double-layer charge injection, because they have high electrochemically accessible surface areas, good electronic conductivity, and good mechanical properties. Supercapacitors are good examples, as they have huge capacitances compared to ordinary dielectric-based capacitors and electromechanical actuators. Supercapacitors with CNT electrodes can be used for applications that require much higher power capabilities than batteries, and much higher storage capacities than ordinary capacitors like hybrid electric vehicles that can provide rapid acceleration and store braking energy electrically [99,100].

### **2.7.4 Sensors and nanoprobes**

CNTs are also used as scanning probe tips for equipment such as atomic force and scanning tunnelling microscopes, because they allow imaging in narrow, deep crevices and improve resolution compared to metal tips or silicon tips. These tips also have enhanced probe life and do not damage the sample during repeated hard crashes into substrates [101,102]. Nanoscopic tweezers may be used as nanoprobes for assembly because they are driven by the electrostatic interaction between two nanotubes on a probe tip.

### **2.7.5 Field emitting devices**

Both SWCNTs and MWCNTs can be used as field emitting electron sources for lamps, flat panel displays, x-ray and microwave generators, and gas discharge tubes providing surge protection. The emission behaviour depends on the nanotubes tip structure. Enhanced emission results from the opening of the tip of either an SWCNT or an MWCNT. Nanotube field emitting surfaces are fairly easy to produce by screen printing nanotube pastes and do not deteriorate in moderate vacuum, which is an advantage over tungsten and molybdenum tip arrays that are difficult to manufacture [103,104].

### 2.7.6 Drug delivery systems

Currently, CNTs have generated an enormous interest in biological systems, where a well designed CNTs can serve as vaccine delivery systems or protein transporters [105-107]. Carbon nanotubes can be functionalised with bioactive peptides, proteins, nucleic acids and drugs, and can be used to deliver their cargos to cells and organs because they display low toxicity and are not immunogenic.

### 2.8 Functionalization of carbon nanotubes

Because of their atomically smooth surface and the limited solubility in most organic solvents, it is very difficult to disperse CNTs homogeneously into the polymer matrix. Over the last few years there has been a great research interest in preparing homogeneous dispersions/solutions of CNTs, suitable for processing into thin films and composites, and exploiting the unrivalled properties of the CNTs. The main routes consist of end and/or sidewall functionalization, use of surfactants with sonication or high-shear mixing [108-111], polymer wrapping of nanotubes' outer surfaces [112-115], and protonation by super-acids [116]. Among all the reported methods, grafting of CNTs' outer surfaces with amines has been widely investigated in preparing soluble CNTs in various solvents. For example, Wong *et al.* [117] reported the modification of MWCNTs *via* amide bond formation between carboxyl functional groups, bonded to the open ends of the tubes, and the amines. Chen *et al.* [118] have demonstrated that SWCNTs can be solubilized in common organic solvents by non-covalent (ionic) functionalization of the carboxylic acid groups by using octadecyl amine. They found that the same dissolution process, applied to arc-produced MWCNTs (average length <1mm), only gave rise to very unstable suspensions in organic solvents. And that they were visually scattered. Qin *et al.* [119] showed that, by modifying Haddon's method [120] using two Soxhlet extractors, large quantities of solubilized MWCNTs could be obtained. The conventional approach of amine functionalization is tedious with a typical reaction time of 4-8 days which involves steps such as carboxylation, acylchlorination, and amidation. Although these methods are quite successful, however, they often indicate cutting of the tubes into smaller pieces. This may be due to the oxidative induced cutting during the refluxing with a strong acid for a long time, thus partly losing the high aspect ratio (length/diameter) of CNTs. For the structural applications such as the fabrication of CNT-based composites, full-length

CNTs are always preferred because of their high aspect ratio. However, the dissolution of pristine CNTs without losing the structural integrity still remains a significant research challenge.

## **2.9 Carbon nanotubes-containing PLA nanocomposites**

Polymer composites prepared with conventional fillers usually contain 10-70 wt.% filler, which leads to composites with high densities and high material cost. The modulus and strength of these composites is often traded for high fracture toughness [121]. Unlike ordinary polymer composites prepared with micron scale fillers, preparation of polymer composites containing CNTs results in very short distances between the fillers, thereby hugely modifying their properties at very low filler content.

Polymer/CNT nanocomposites can be classified as structural or functional composites [122]. For the structural composites, the unique mechanical properties of CNTs, such as the high modulus, tensile strength and strain to fracture, are explored to obtain structural materials with much improved mechanical properties. As for CNT/polymer functional composites, many other unique properties of CNTs such as electrical, thermal, optical and damping properties, along with their excellent mechanical properties, are utilized to develop multi-functional composites for applications in the fields of heat resistance, chemical sensing, electrical and thermal management, photoemission, electromagnetic absorbance, and energy storage [123]. In 1994, Ajayan *et al.* [124] first reported the preparation of a polymer/CNT nanocomposite. Following this, many research attempts have been made to understand their structure-property relationship and find useful applications in different fields. These efforts have become more pronounced in the beginning of the 21st century after the realization of CNT fabrication on an industrial scale at lower cost.

Recently, a number of papers have appeared on the preparation, characterization, and properties of CNT-reinforced PLA composite materials. Moon *et al.* [125] reported mechanical, thermal, and electrical properties of MWCNTs containing PLA composites, which were fabricated by a solution blending technique using chloroform as a solvent. Besides a slight increase in Young's modulus, an improvement in electromagnetic wave shielding effectiveness was reported by adding 10 wt.% MWCNTs. Tshuji *et al.* [126] studied

the effects of incorporation of nano-structured carbon fillers such as fullerene ( $C_{60}$ ), SWCNTs, carbon nanohorns (CNH), carbon nanoballoons (CNB), and carbon black (CB) on the conductivity, thermal properties, crystallization, and enzymatic degradation of poly(L-lactic acid) (PLLA). Results showed that the addition of CNH, CNB, and CB increased the thermal stability of PLLA, whereas the thermal stability of PLLA decreased after incorporation of SWCNTs. However, the addition of SWCNTs enhanced the enzymatic degradation of PLLA. Wu and Liao [127] prepared PLA/MWCNT composites by melt-blending of acrylic-acid-grafted PLA (PLA-g-AA) and multihydroxyl-functionalized MWCNTs (MWCNT-OHs). In this study, the authors tried to correlate the interaction between the MWCNT-OH with the PLA-g-AA matrix with the tensile properties. A significant enhancement in the thermal and mechanical properties of PLA was observed. For example, there was a 77 °C increase in initial decomposition temperature with the addition of only 1 wt% MWCNTs-OH. The thermal and mechanical analyses showed that the optimal amount of MWCNT-OH was 1 wt%, because excess MWCNT-OH caused separation of the organic and inorganic phases and lowered their compatibility. McCullen *et al.* [128] reported the preparation of MWCNTs containing PLA fibres by electro-spinning from a PLA solution to develop a scaffold for tissue engineering. With the addition of MWCNTs, the fibre diameter was drastically reduced by 70% to form fibres with a mean diameter of 700 nm. This was believed to be due to an increased surface charge density for the MWCNT/polymer solution. Transmission electron microscopy validated the alignment of the MWCNTs within the fibres. The presence of MWNTs showed an increase in the conductance of the scaffold and in the tensile modulus at an optimal loading level of 0.25 wt %.

Villmow *et al.* [129] studied the influence of twin-screw extrusion conditions on the degree of dispersion of MWCNTs in a PLA matrix. The main aim was to establish a guideline for the processing of PLA/MWCNT composites using the master-batch dilution technique. A high rotation speed (500 rpm), that still ensures a certain residence time of the melt, combined with a screw profile containing mainly mixing elements, were found to be highly convenient to disperse and distribute the MWNTs in the PLA matrix during the master-batch production and during the dilution step. Under these processing conditions a percolation threshold for electrical conductivity was achieved on compression moulded samples at MWCNT contents below 0.5 wt%.

The above are some of several reports on the preparation and characterization of CNTs-containing PLA composites by using pure and surface oxidized CNTs as reinforcing filler. Most of the reported works focused on enhancing the modulus and thermal and electrical properties of the final composite materials. However, other mechanical properties such as strength and elongation at break have not been considered by most of the published studies on CNTs containing polymer composites, particularly in the case of PLA/CNT composites [125-129]. This is because these mechanical properties are directly related to the degree of interfacial interactions between the filler surface and the polymer matrix, that is the CNT dispersion in the PLA matrix.

## **2.10 Preparation methods of carbon nanotubes-containing PLA nanocomposites**

### **2.10.1 Melt blending**

This is the most preferred method in the industry, and it only uses high temperature and a high shear force to disperse CNTs in a polymer matrix. Another interesting feature is that no solvent is required for the dispersion of the CNTs. However, it may be less effective compared to other methods such as solution blending, because it is only limited to low filler concentration due to the high viscosities of the nanocomposites at high CNTs contents [130].

### **2.10.2 Solution blending**

This is the most common used method for the preparation of CNT/polymer composites. It involves the mixing of the two components in a preferred solvent and evaporating the solvent to form a composite film. Usually the CNT powder is dispersed in a solvent by either vigorous stirring or sonication [124], mixed with a polymer solution and evaporating the solvent with or without vacuum.

### **2.10.3 In-situ polymerization**

In this method, monomers are polymerized to produce polymer-grafted tubes mixed with free polymer chains. There is a high homogeneity of the resulting composites compared to mixing the polymer and CNTs in solution due to the small size of the monomeric molecules. This

method produces composites with high CNT weight fraction. Jia and co-workers [131] initially used this method for the preparation of PMMA composites.

#### **2.10.4 Bulk mixing**

This method has been used mainly to shorten the length of carbon nanostructures [132]. For example, Xia *et al.* [133] used a solid state mechanochemical pulverization process to prepare CNT/polypropylene composite powder, which was subsequently melt-mixed with a twin-roll masticator to obtain a homogenous composite. The length of the CNTs was found to be reduced from a few micrometers to ~500 nm. A reasonable level of dispersion of CNTs into the polymer matrix was observed leading to the improvement of the physical properties of the samples.

#### **2.10.5 Latex technology**

This method differs from *in situ* polymerization in that, the polymer is synthesized first and then follows the addition of CNTs. It makes it possible to disperse CNTs in many polymers produced by emulsion polymerization, or those that can be brought in the form of an emulsion. The process is also safe and eco-friendly because water is used as a solvent.

#### **2.10.6 Other methods**

Recently, new methods have been developed to produce CNT/polymer nanocomposites with high CNT content or for some specific applications. These methods include pulverization, densification, layer-by-layer deposition, and spinning of coagulant [123]. The nanocomposite materials field has not yet reached maturity, and therefore most of these methods are still under investigation. It is hoped that nanocomposites with unique structures and properties for specialised applications will be produced.

## 2.11 Properties of nanocomposites

### 2.11.1 Thermal properties

Due to the excellent thermal properties of CNTs, like high thermal conductivity and good thermal stability, it was thought that CNTs will greatly improve the thermal properties of polymers. However, this phenomenon did not quite materialise, except for a very few cases. By means of thermogravimetric analysis, a number of research groups reported improved thermal conductivity in CNT/polymer composites relative to the neat polymers. Choi and co-workers [134] prepared an epoxy composite with 3 wt.% SWCNT and reported a 300% increase in thermal conductivity at room temperature with an additional 10% when aligned magnetically. Biercuk and co-workers [134] reported a thermal conductivity increase of about 125% from an epoxy composite containing 1 wt.% of SWCNTs. Cai and Song [136] used latex technology to prepare polyurethane/CNT composites. The thermal conductivity of the composites increased by about 200% with 3 wt.% CNTs.

So far, the most promising result on the improvement of thermal conductivity by nanotubes in polymer composites was reported by Huang and co-workers [137]. They embedded the aligned MWCNT array (synthesised from CVD) with silicone elastomers using injection moulding. The composite film they prepared had MWCNTs tips protruding on both sides, which made better contact with the heat source. This composite, containing 0.3 wt.% of aligned MWCNTs, was found to have a thermal conductivity of ~115-280% higher than either the pristine polymer or a composite with 0.3 wt.% of randomly dispersed MWCNTs.

Incorporation of CNTs also enhances thermal stability and flame retardant properties. To be specific, the onset temperature and the temperature of maximum weight loss rate are generally higher in the nanocomposites. For example, 5 wt.% MWCNT/ polyacrylonitrile (PAN) composite fibres showed a 24 °C increase in onset temperature compared to that of neat PAN [138]. Velasco-Santos *et al.* [139] prepared a 1.0 wt.% SWCNT/polymethylmethacrylate (PMMA) composite which gave rise to a 40 °C increase in the  $T_g$  of the PMMA. CNT/PMMA composites have also been reported to have flame retardant properties, and the mechanisms of these had been studied [140,141]. Overall, the thermal properties of CNT/polymer composites depend on the dispersion of the carbon nanotubes, their interfacial interactions with the polymer matrices, aspect ratio, filler content, and filler alignment.

### 2.11.2 Mechanical properties

Dispersion is the most important aspect in manufacturing CNT/polymer composites. Good dispersion ensures more surface area availability for bonding with the polymer matrix, and also prevents aggregated filler from acting as stress concentrators [141]. The aspect ratio must also be large enough to maximize the load transfer between the CNTs and the matrix material to achieve enhanced mechanical properties. In general, the tensile modulus and strength of polymer-rich nanotube composites were found to increase with nanotube loading, dispersion, and alignment in the matrix. Dalton and co-workers [143] used a coagulation method and spun several hundred meters of SWCNT/polyvinyl alcohol (PVA) composite fibres. These composite fibres contained 60% w/w SWCNTs. This super tough composite had a tensile stress at break of 1.8 GPa, which is comparable to that of the silk fibre produced by a spider. Qian and co-workers [144] prepared a 1.0 wt.% CNT/polystyrene nanocomposite and observed 25 and 35% improvements in the tensile strength and elastic modulus, respectively. A number of papers on CNT/polymer composites available in the literature were recently summarized in a review by Ma *et al.* [123]. It has been well established that the performance of a fibre-reinforced composite depends critically on the interfacial characteristics between the reinforcement and the matrix material. Liao *et al.* [145] used molecular mechanics simulations and elasticity calculations to study the interfacial characteristics of a CNT-reinforced polystyrene composite. They found that in the absence of atomic bonding between the reinforcement and the matrix material, there is no interfacial stress transfer ability, which is a critical parameter controlling material performance. It should be noted that functional moieties on nanotubes provide better interfacial load transfer through bonding and/or entanglement with the polymer matrix. Geng and co-workers [146] fabricated a poly(ethyleneoxide) composite containing 1.0 wt.% fluorinated SWCNTs, and reported 145 and 300% increase in tensile modulus and yield strength, respectively. It is important to understand the mechanism of interfacial adhesion at the molecular level to further optimize the interface in nanocomposite systems. Further investigations are necessary to understand and then optimize nanotube/polymer interfaces.

### 2.11.3 Electrical properties

CNT/polymer composites were found to be electrically conductive with small loadings of 0.1 wt.% CNTs or less [147]. Electrical conductivity in the bulk material is achieved when the filler content exceeds the percolation threshold (characterized by a sharp jump in the conductivity by many orders of magnitude which is attributed to the formation of a 3-dimensional conductive network of the fillers within the matrix). Above the percolation threshold, the electrical conductivity of the composite often shows saturation because multiple electron pathways exist in the matrix. Below the percolation threshold, the electrical properties are dominated by the matrix material as electron pathways do not exist. To accomplish conducting networks in the composite, the amount of conducting filler must be above the percolation threshold. Even though there is no obvious consensus on percolation thresholds, most polymers show a transition from insulator to a conductor when the CNT content is below 5 wt.% [148]. It is generally agreed that the electrical properties of CNT/polymer nanocomposites are affected by the type of CNTs (SWCNT or MWCNT), aspect ratio of CNTs, their dispersion (homogenous distribution of individual CNTs or CNT agglomerates on microscopic scale), and disentanglement of CNT agglomerates on the nano scale [149-152].

Functionalization of CNTs also plays a crucial role in improving the electrical properties of polymer nanocomposites. However, the use of strong acids with higher concentrations should be avoided as they have the potential of fragmenting CNTs into smaller pieces, resulting in low aspect ratios that are critical for the formation of conducting networks in composites. Introduction of many heterogeneous atoms on the surface of CNTs destabilises the  $\pi$  electrons, thereby altering the inherent electrical properties on the nanotubes. However, the high cost associated with CNTs, particularly the SWCNTs, continues to limit the widespread uses of conducting polymers based on nanotubes.

### 2.11.4 Rheological properties

Rheology is defined as the study of the flow behaviour of a material, primarily in the liquid state, but also as 'soft solids' or solids under conditions in which they respond with plastic flow rather than deforming elastically in response to an applied force. Rheological properties

are related to the materia's microstructure, the state of the nanotube dispersion, orientation of nanotubes, the aspect ratio, and the interactions between nanotubes and polymer chains. In general, the rheology of polymer melts depends strongly on the temperature at which the measurement is made. For thermorheologically simple materials, bilogarithmic plots of the isotherms of the storage modulus  $G'(\omega)$ , loss modulus  $G''(\omega)$ , and complex viscosity ( $|\eta^*|$ ) can be superimposed by horizontal shifts of  $\log(a_T)$ , along  $\log(\omega)$ , and vertical shifts given by  $\log(b_T)$ , such that:

$$b_T G'(a_T \omega, T) = G'(\omega, T_{\text{ref}}) \quad (2)$$

$$b_T G''(a_T \omega, T) = G''(\omega, T_{\text{ref}}) \quad (3)$$

$$(b_T / a_T) |\eta^*(a_T \omega, T_{\text{ref}})| = |\eta^*(\omega, T_{\text{ref}})| \quad (4)$$

where  $T_{\text{ref}}$  is the reference temperature. All isotherms measured for neat polymers and for various nanocomposites can be superimposed in this way.

For polymer samples, the temperatures and frequencies at which the rheological measurements are taken are expected to exhibit characteristic homopolymer-like terminal flow behavior, expressed by the power-laws  $G' \propto \omega^2$  and  $G'' \propto \omega$ . The rheology of a polymer/CNT composite also displays a transition from a rheological state to a solid-like behaviour at a point called the rheological percolation threshold [153-155]. Abbasi and co-workers [153] reported a decrease in the percolation threshold from 0.8 wt.% to about 0.3 wt.% upon increasing the temperature from 210 to 300 °C in MWCNT/polycarbonate nanocomposites. Improved dispersion of functionalized CNTs also decreases the rheological percolation threshold of CNT containing nanocomposites. Mitchell and co-workers [156] reported an improved SWCNT dispersion in polystyrene with a reduced rheological percolation threshold from 3.0 to 1.5 wt.%. Viscosity also lowers with the better dispersion of nanotubes.

Oscillatory frequency sweep measurements showed that addition of about 2.0 wt% F-MWNTs led to a solid-like response where a percolated network structure formed, and the composites exhibited remarkable improvement of rheological properties in the melt state as compared with that of neat PLA [157].

PLA nanocomposites with various functionalized MWCNTs were prepared by melt mixing for morphological, rheological and thermal measurements. The results show that PLA/carboxylic MWCNTs present a typical solid-like viscoelastic response at low frequencies under small amplitude oscillatory shear flow and, the percolation threshold is lower than 3 wt% [158].

Other independent reports also found that in general, improved dispersion of functionalized CNTs decreases percolation threshold [159-160]

### **2.11.5 Damping**

Damping properties are concerned with the tendency of materials to decrease the amplitude of oscillations in an oscillatory system. As with elastic mechanical properties, improved CNT dispersion can increase the damping properties of nanocomposites. Frictional sliding of the CNTs within the polymer matrix can cause considerable dissipation of energy, even when they are present in small amounts. This phenomenon leads to an enhancement of the damping properties of the CNT/polymer nanocomposites, which is largely due to the CNTs having large surface areas, low mass densities, and weak interfacial bonding with the polymer [161]. For polycarbonate nanocomposites prepared using SWCNTs and MWCNTs the damping properties were found to be higher compared to pristine polycarbonate [162]. The loss modulus of the SWCNT/polycarbonate nanocomposite was found to be considerably higher than that of the MWCNT/polycarbonate nanocomposite, suggesting that the inner layers of MWCNTs did not contribute to the interfacial frictional sliding with the polymer matrix for energy dissipation.

## **2.12 References**

- [1] V.A. Fomin, V.V. Guzeev. Biodegradable polymers, their present state and future prospects. *Progress in Rubber and Plastics Technology* 2001; 17:186-204.
- [2] M. Yiu-Wing, Y. Zhong-Zhen. *Polymer Nanocomposites*. Woodhead Publishing Limited, Cambridge, England, p.57-129 (2006).

- [3] D.J. Mooney, K. Sano, M.P. Kaufmann, K. Majahod, B. Schloo, J.P. Vacanti, *et al.* Long term engraftment of hepatocytes transplanted on biodegradable polymer sponges. *Journal of Biomedical Materials Research* 1997; 37:413-420.
- [4] G.L. Griffith. *Polymeric Biomaterials*. *Acta Materialia* 2000; 48:263-277.
- [5] D.W. Hutmacher. Scaffolds in tissue engineering bone and cartilage. *Biomaterials* 2000; 21:2529-2543.
- [6] D. Satyanarayana, P.R. Chatterji. Biodegradable polymers: Challenges and strategies. *Polymer Reviews* 1993; 33:349-368.
- [7] K.M. Stridsberg, M. Ryner, A.C. Albertsson. Controlled ring-opening polymerization: Polymers with designed macromolecular architecture. *Advances in Polymer Science* 2002; 157:41-65.
- [8] H.R. Kricheldorf. Biodegradable polymers with variable architectures via ring-expansion polymerization. *Journal of Polymer Science Part A: Polymer Chemistry* 2004; 42:4723-4742.
- [9] M.S. Lindblad, Y. Liu, A.C. Albertsson, E. Ranucci, S. Karlsson. Polymers from renewable resources. *Advances in Polymer Science* 2002; 157: 139-161.
- [10] A.C. Albertsson, I.K. Varma. Aliphatic polyesters: Synthesis, properties and applications. *Advances in Polymer Science* 2002; 157:1-40.
- [11] M. Okada. Chemical synthesis of biodegradable polymers. *Progress in Polymer Science* 2002; 27:87-133.
- [12] J.H. Lee, T.G. Park, H.S. Park, D.S. Lee, Y.K. Lee, S.C. Yoon, J.D. Nam. Thermal and mechanical characteristics of poly(L-lactic acid) nanocomposite scaffold. *Biomaterials* 2003; 24:2773-2778.
- [13] Y.J. Wee, J.N. Kim, H.W. Ryu. Biotechnological production of lactic acid and its recent applications. *Food Technology and Biotechnology* 2006; 44:163–172.
- [14] S. Jacobsen, P.H. Degee, H.G. Fritz, P. H. Dubois, R. Jerome. Polylactide (PLA) - A new way of production. *Polymer Engineering and Science* 1999; 39:1311-1319.
- [15] K.E. Perepelkin. Polylactide fibres: Fabrication, properties, use, prospects. A review. *Fibre Chemistry* 2002; 34:85-100.
- [16] Y. You, S.W. Lee, S.J. Lee, W.H. Park. Thermal interfibre bonding of electrospun poly(L-lactic acid) nanofibres. *Materials Letters* 2006; 60:1331-1341.
- [17] H.Y. Li, A. Debuigne, R. Jerome, P. Lecomte. Synthesis of macrocyclic poly( $\epsilon$ -caprolactone) by intramolecular cross-linking of unsaturated end groups of chains

- precyclic by the initiation. *Angewandte Chemie International Edition* 2006; 45:2264-2267.
- [18] E. Luong-Van, L. Grondahl, K. N. Chua, K.W. Leong, V. Nurcombe, S.M. Cool. Controlled release of heparin from poly(epsilon-caprolactone) electrospun fibres. *Biomaterials* 2006; 27:2042-2050.
- [19] M.A. Sabino, S. Gonzalez, L. Marquez, J.L. Feijoo. Study of the hydrolytic degradation of polydioxanone PPDx. *Polymer Degradation and Stability* 2000; 69:209-216.
- [20] M.A. Sabino, J.L. Feijoo, A.J. Muller. Crystallisation and morphology of poly(*p*-dioxanone). *Macromolecular Chemistry and Physics* 2000; 201:2687-2698.
- [21] A.P.T. Pezzin, G.O.R. van Ekenstein, E.A.R. Duek. Melt behaviour, crystallinity and morphology of poly(*p*-dioxanone). *Polymer* 2001; 42:8303-8306.
- [22] D.N. Bikiaris, D.S. Achilias. Synthesis of poly(alkylene succinate) biodegradable polyesters. I. Mathematical modelling of the esterification reaction. *Polymer* 2006; 47:4851-4860.
- [23] J. Kim, J.H. Kim, T.K. Shin, H.J. Choi, M.S. Jhon. Miscibility and rheological characteristics of biodegradable aliphatic polyester and linear low density polyethylene blends. *European Polymer Journal* 2001; 37:2131-2139.
- [24] J. Kim, T.K. Shin, H.J. Choi, M.S. Jhon. Miscibility of biodegradable synthetic aliphatic polyester and poly(epichlorohydrin) blends. *Polymer* 1999; 40(24):6873-6.
- [25] S. Carroccio, P. Rizzarelli, C. Puglisi, G. Montaudo, MALDI investigation of photooxidation in aliphatic polyesters: Poly(butylene succinate). *Macromolecules* 2004; 37:6576-6586.
- [26] T. Dong, K.M. Shin, B. Zhu, Y. Inoue. Nucleation and crystallization behaviour of poly(butylene succinate) induced by its  $\alpha$ -cyclodextrin inclusion complex: Effect of stoichiometry. *Macromolecules* 2006; 39:2427-2428.
- [27] S. Salhi, M. Tessier, J.C. Blais, R. El Gharbi, A. Fradet. Synthesis of aliphatic-aromatic copolyesters by a high temperature bulk reaction between poly(ethylene terephthalate) and cyclodi(ethylene succinate). *Macromolecular Chemistry and Physics* 2004; 205:2391-2397.
- [28] A. Oishi, M. Zhang, K. Nakayama, T. Masuda, Y. Taguchi. Synthesis of poly(butylene succinate) and poly(ethylene succinate) including diglycollate moiety. *Polymer Journal* 2006; 38:710-715.

- [29] C.S.K. Reddy, R. Ghai, Rashmi, V.C. Kalia. Polyhydroxyalkanoates: An overview. *Bioresource Technology* 2003; 87:137–146.
- [30] D.K.Y. Solaiman, R.D. Ashby, T.A. Foglia, W.N. Marmer. Conversion of agricultural feedstock and coproducts into poly(hydroxyalkanoates). *Applied Microbiology and Biotechnology* 2006; 71:783-789.
- [31] R.W. Lenz, R.H. Marchessault. Bacterial polyesters: Biosynthesis, biodegradable plastics and biotechnology. *Biomacromolecules* 2005; 6:1-8.
- [32] A. Rouilly, L. Rigal. Agro-materials: A bibliographic review. *Journal of Macromolecular Science Part C: Polymer Reviews* 2002; 42:441-479.
- [33] D.L. Woerdeman, W.S. Veraverbeke, R.S. Parnas, D. Johnson, J. Delcour, I. Verpoest, C.J.G. Plummer. Designing new materials from wheat protein. *Biomacromolecules* 2004; 5:1262-1269.
- [34] S.N. Swain, S.M. Biswal, P.K. Nanda, P.L. Nayak. Biodegradable soy-based plastics: opportunities and challenges. *Journal of Polymers and the Environment* 2004; 12:35-42.
- [35] D.S. Zimmitsky, T.L. Yurkshtovich, P.M. Bychkovsky. Synthesis and characterization of oxidized cellulose. *Journal of Polymer Science Part A: Polymer Chemistry* 2004; 42:4785-4791.
- [36] C. Peniche, W. Arguelles-Monal, H. Peniche, N. Acosta. Chitosan: An attractive biocompatible polymer for microencapsulation. *Macromolecular Bioscience* 2003; 3:511-520.
- [37] H.A. Lim, T. Raku, Y. Tokiwa. A new method for the evaluation of biodegradable plastic using coated cellulose paper. *Macromolecular Bioscience* 2004; 4:875-881.
- [38] D.G. Liu, L.N. Zhang. Structure and properties of soy protein plastics plasticized with acetamide. *Macromolecular Materials and Engineering* 2006; 291:820-828.
- [39] R.M.D. Soares, F.F. Scremin, V. Soldi. Thermal stability of biodegradable films based on soy protein and corn starch. *Macromol Symposia* 2005; 229:258-265.
- [40] J.R. Dorgan, H. Lehermerier, M. Mang. Thermal and rheological properties of commercial-grade poly(lactic acid). *Journal of Polymers and the Environment* 2000; 8:1-9.
- [41] S. Shyamroy, B. Garnaik, S. Sivaram. Structure of poly(L-lactic acid)s prepared by the dehydropolycondensation of L-lactic acid with organotin catalysts. *Journal of Polymer Science Part A: Polymer Chemistry* 2005; 43:2164–77.

- [42] M. Ajioka, K. Enomoto, K. Suzuki, A. Yamaguchi. The basic properties of poly(lactic acid) produced by the direct condensation polymerization of lactic acid. *Journal of Polymers and the Environment* 1995; 3:225–234.
- [43] A. Takasu, Y. Narukawa, T. Hirabayashi. Direct dehydration polycondensation of lactic acid catalyzed by water-stable Lewis acids. *Journal of Polymer Science Part A: Polymer Chemistry* 2006; 44:5247-5253.
- [44] S.H. Kim, Y.D. Kim. Direct condensation polymerization of lactic acid. *Macromolecular Symposia* 1999; 144:277-87.
- [45] J. Lunt. Large scale production, properties and commercial applications of polylactic acid polymers. *Polymer Degradation and Stability* 1998; 59:145-152.
- [46] J. Lunt, A.L. Shafer. Polylactic acid polymers from corn: applications in the textiles industry. *Journal Industrial Textiles* 2000; 29:191-205.
- [47] S. Sinha Ray, J. Ramontja. *Biodegradable polymer blends and composites*. John Wiley & Sons 2008: ISBN-13: 9780470146835, 389-409.
- [48] H. Tsuji, Y. Ikada. Crystallization from the melt of poly(lactide)s with different optical purities and their blends. *Macromolecular Chemistry and Physics* 1996; 197:3483-3499.
- [49] D.R. Witzke. Ph.D. thesis, Michigan State University, East Lansing, MI 1997; p.389.
- [50] R. Auras, Bruce Harte, Susan Selke. An overview of polylactides as packaging materials. *Macromolecular Biosciences* 2004; 4:835-864.
- [51] G. Gupta, N. Revagade, J. Hilborn. Poly(lactic acid): An overview. *Progress in Polymer Science* 2007; 32:455-482.
- [52] K. Kim, Y.K. Luu, C. Chang, D. Fang, B.S. Hsiao, B. Chu, et al. Incorporation and controlled release of a hydrophilic antibiotic using poly(lactide-co-glycolide)-based electrospun nanofibrous scaffolds. *Journal of Controlled Release* 2004; 98:47-56.
- [53] J.A. Cicero, J.R. Dorgan. Physical properties and fibre morphology of poly(lactic acid) obtained from continuous two-step melt spinning. *Journal of Polymers and the Environment* 2001; 9:1–10.
- [54] A.K. Agrawal, R. Bhalla. Advances in production of poly(lactic acid) fibres: A Review. *Journal of Macromolecular Science Part C: Polymer Reviews* 2003; 43:479–503.
- [55] J.P Penning, H. Dijkstra, A.J Pennings. Preparation and properties of adsorbable fibres from L-lactide copolymers. *Polymer* 1993; 34:942–951.

- [56] S.S. Ray, K. Yamada, M. Okamoto, Y. Fujimoto, A. Ogami, K. Ueda. New polylactide/layered silicate nanocomposites. 5. Designing of materials with desired properties. *Polymer* 2003; 44:6633–6646.
- [57] S.S. Ray, K. Yamada, M. Okamoto, K. Ueda. New polylactide-layered silicate nanocomposites. 2. Concurrent improvements of material properties, biodegradability and melt rheology. *Polymer* 2003; 44:857-866.
- [58] S.S. Ray, M. Okamoto. Polymer/layered silicate nanocomposites: A review from preparation to processing. *Progress in Polymer Science* 2003; 28:1539-1641.
- [59] M. Pluta. Morphology and properties of polylactide modified by thermal treatment, filling with layered silicates and plasticization. *Polymer* 2004; 45:8239–8251.
- [60] M.A. Paul, C. Delcourt, M. Alexandre, P. Dege´e, F. Monteverde, P. Dubois. Polylactide/montmorillonite nanocomposites: Study of the hydrolytic degradation. *Polymer Degradation and Stability* 2005; 87:535-542.
- [61] M. Okamoto. Biodegradable polymer/layered silicate nanocomposites: A review. In: S.K. Mallapragada, B. Narasimhan (Ed). *Handbook of Biodegradable Polymeric Materials and Their Applications*, Vol. 1. American Scientific Publishers (2005) p.1-45.
- [62] D. Plackett, T.L. Andersen, W.B. Pedersen, L. Nielsen. Biodegradable composites based on -polylactide and jute fibres. *Composites Science and Technology* 2003; 63:1287-1296.
- [63] Crop-based polymers for nonwovens. Insight Conference, Toronto. Calvin Woodings Coultling Ltd. (2000).
- [64] D.W. Farrington, J. Lunt, S. Davies, R.S. Blackburn. Poly(lactic acid) fibres. In: Blackburn RS (Ed.). *Biodegradable and Sustainable Fibres*. Cambridge: Woodhead Publishing Ltd (2005) 191-219.
- [65] S.S. Davis, L. Illum , S. Stolnik. Polymers in drug delivery. *Current Opinion in Colloid and Interface Science* 1996; 1:660-666.
- [66] B.C. Benicewicz, P.K. Hopper. Polymers for absorbable surgical sutures. *Journal of Bioactive and Compatible Polymers* 1990; 5:453-472.
- [67] B.X. Fu, B.S. Hsiao, G. Chen, J. Zhou, I. Koyfman, D.D. Jamiolkowski, et al. Structure and property studies of biodegradable poly(glycolide-co-lactide) fibre during processing and in-vitro degradation. *Polymer* 2002; 43:5527-5534.

- [68] O. Laitinen, P. Törmälä, R. Taurio, K. Skutnabb, K. Saarelainen, T. Iivonen, et al. Mechanical properties of biodegradable ligament augmentation device of poly(L-lactide) in vitro and in vivo. *Biomaterials* 1992; 13:1012-1016.
- [69] Y. Hu, X. Jiang, Y. Ding, L. Zhang, C. Yang, J. Zhang, et al. Preparation and drug release behaviors of nimodipineloaded poly(caprolactone)poly(ethylene oxide)polylactide amphiphilic copolymer nanoparticles. *Biomaterials* 2003; 24:2395-2404.
- [70] T. Ouchi, T. Saito, T. Kontani, Y. Ohya. Encapsulation and/or release behavior of bovine serum albumin within and from polylactide-grafted dextran microspheres. *Macromolecular Bioscience* 2004; 4:458-463.
- [71] T.G. Park, M.J. Alonso, R. Langer. Controlled release of proteins from poly(L-lactic acid) coated polyisobutylcyanoacrylate microcapsules. *Journal of Applied Polymer Science* 1994; 52:1797-807.
- [72] T. Chandy, G.S. Das, R.F. Wilson, G.H.R. Rao. Development of polylactide microspheres for protein encapsulation and delivery. *Journal of Applied Polymer Science* 2002; 86:1285-1295.
- [73] R. Langer, N. Peppas. Chemical and physical structure of polymers as carriers for controlled release of bioactive agents: A review. *Journal of Macromolecular Science – Reviews in Macromolecular Chemistry and Physics* 1983; 23:61-126.
- [74] E. Kenawy, G.L. Bowlin, K. Mansfield, J. Layman, D.G. Simpson, E.H. Sanders, et al. Release of tetracycline hydrochloride from electrospun poly(ethylene-co-vinylacetate), poly(lactic acid) and a blend. *Journal of Controlled Release* 2002; 81:57-64.
- [75] M. Kellomäki, H. Niiranen, K. Puumanen, N. Ashammakhi, T. Waris, P. Törmälä. Bioabsorbable scaffolds for guided bone regeneration and generation. *Biomaterials* 2000; 21:2405-2495.
- [76] H.W. Kroto, J.R. Heath, S.C. O'Brien, R.F. Curl, R.E. Smalley. C<sub>60</sub>: Buckminsterfullerene. *Nature* 1985; 318:162-163.
- [77] S. Iijima. Helical microtubules of graphitic carbon. *Nature* 1991; 354:56-58.
- [78] M.S. Dresselhaus, G. Dresselhaus, P.C. Eklund. *Science of Fullerenes and Carbon Nanotubes* 1996 (San Diego, CA: Academic). ISBN 0-12221-820-5.
- [79] S.J. Tans, M.H. Devoret, H. Dai, A. Thess, R.E. Smalley, L.J. Geerligs, C. Dekker. Individual single-wall carbon nanotubes as quantum wires. *Nature* 1997; 386:474-477

- [80] Yu-Chun Chen, *Diamond Chemical Vapour Deposition and Practical Applications*, dissertation, Auburn University, 2009.
- [81] C. Journet, P. Bernier. Production of carbon nanotubes. *Applied Physics A – Materials Science & Processing* 1998; 67:1-9.
- [82] S.B. Sinnott, R. Andrews, D. Qian, A.M. Rao, Z. Mao, E.C. Dickey, F. Derbyshire. Model of carbon nanotube growth through chemical vapour deposition. *Chemical Physics Letters* 1999; 315:25-30.
- [83] T. Guo, P. Nikolaev, A. Thess, D.T. Colbert, R.E. Smalley. Catalytic growth of single-walled nanotubes by laser vaporization. *Chemical Physics Letters* 1995; 243:49-54.
- [84] M. Daenen, R.D. de Fouw, B. Hamers, P.G.A. Janssen, K. Schouteden, M.A.J. Veld. *The Wondrous World of Carbon Nanotubes – A Review of Current Carbon Nanotube Technologies*, Eindhoven University of Technology, 2003.
- [85] S. Niyogi, M.A. Hamon, H. Hu, B. Zhao, P. Bhowmik, R. Sen, M.E. Itkis, R.C. Haddon. Chemistry of single-walled carbon nanotubes. *Accounts of Chemical Research* 2002; 35:1105-1113.
- [86] P.M. Ajayan, J.M. Tour. Nanotube composites. *Nature* 2007; 447:1066-1068.
- [87] M. Damnjanović, I. Milošević, T. Vuković, R. Sredanović. Full symmetry, optical activity, and potentials of single-wall and multiwall nanotubes. *Physical Review B* 1999; 60:2728-2739.
- [88] R.H. Baugman, A.A. Zakhidov, W.A. de Heer. Carbon nanotubes – The route toward applications. *Science* 2002; 279:787-792.
- [89] J.N. Coleman, M. Cadek, R. Blake, V. Nicolosi, K.P. Ryan, C. Belton, A. Fonseca, J. B. Nagy, Y. K. Gun'ko, W. J. Blau. High performance nanotube-reinforced plastics: understanding the mechanism of strength increase. *Advanced Functional Materials* 2004; 14:791-798.
- [90] Z.-D. Xiang, T. Chen, Z.-M. Li, X.-C. Bian. Negative temperature coefficient of resistivity in lightweight conductive carbon nanotube/polymer composites. *Macromolecular Materials and Engineering* 2009; 294:91-95.
- [91] R. Srivastava, S. Banerjee, D. Jehnichen, B. Voit, F. Bohme. In situ preparation of polyimide composites based on functionalized carbon nanotubes. *Macromolecular Materials and Engineering* 2009; 294:96-102.
- [92] M. Sangermano, E. Borella, A. Priola, M. Messori, R. Taurino, P. Postschke. Use of single-walled carbon nanotubes as reinforcing fillers in UV-curable epoxy systems. *Macromolecular Materials and Engineering* 2008; 293:708-713.

- [93] A. Almasri, Z. Ounaies, Y.S. Kim, J. Grunlan. Characterization of solution-processed double-walled carbon nanotube/poly(vinylidene fluoride) nanocomposites. *Macromolecular Materials and Engineering* 2008; 293:123-131.
- [94] L. Valentini, S.B. Bon, J.M. Kenny. Anisotropic electrical transport properties of aligned carbon nanotube/PMMA films obtained by electric-field-assisted thermal annealing. *Macromolecular Materials and Engineering* 2008; 293:867-871.
- [95] The Web site of Hyperion Catalysis International, Inc. is available at [www.fibrils.com](http://www.fibrils.com).
- [96] C. Zandonella. Is it all just a pipe dream? *Nature* 2001; 410:734-735.
- [97] G.G. Tibbets, G.P. Meisner, C.H. Olk. Hydrogen storage capacity of carbon nanotubes, filaments and vapour-grown fibres. *Carbon* 2001; 39:2291-2301.
- [98] A.C. Dillon, M.J. Heben. Hydrogen storage using carbon adsorbents: Past, present and future. *Applied Physics A* 2001; 72:133-142.
- [99] K.H. An, K.K. Jeon, W.S. Kim, Y.S. Park, S.C. Lim, D.J. Bae, Y.H. Lee. Electrochemical properties of high-power supercapacitors using single-walled carbon nanotube electrodes. *Advanced Functional Materials* 2001; 11:387-392.
- [100] R.H. Baughman, C. Cui, A.A. Zakhidov, Z. Iqbal, J.N. Barisci, G.M. Spinks, G.G. Wallace, A. Mazzoldi, D. De Rossi, A.G. Rinzler, O. Jaschinski, S. Roth, M. Kertesz. Carbon nanotube actuators. *Science* 1999; 284:1340-1344.
- [101] H. Dai, J.H. Hafner, A.G. Rinzler, D.T. Colbert, R.E. Smalley. Nanotubes as nanoprobe tips in scanning probe microscopy. *Nature* 1996; 384:147-150.
- [102] J.H. Hafner, C.L. Cheung, C.M. Leiber. Growth of nanotubes for probe microscopy tips. *Nature* 1999; 398:761-762.
- [103] W.A. de Heer, A. Châtelain, D. Ugarte. A carbon nanotube field-emission electron source. *Science* 1995; 270:1179-1180.
- [104] Y. Saito, S. Uemura. Field emission from carbon nanotubes and its applications to electron sources. *Carbon* 2000; 38:169-182.
- [105] C.R. Martin, P. Kohli. The emerging field of nanotube biotechnology. *Nature Reviews Drug Discovery* 2003; 2:29-37.
- [106] N.W. Shi Kam, H. Dai. Carbon nanotubes as intracellular protein transporters: Generality and biological functionality. *Journal of the American Chemical Society* 2005; 127:6021-6026.
- [107] A. Bianco, M. Prato. Can carbon nanotubes be considered useful tools for biological applications? *Advanced Materials* 2003; 15:1765-1768.

- [108] J.M. Bonard, T. Stora, J.P. Salvetat, F. Maier, T. Stöckli, C. Duschl, László Forró, W.A. de Heer, A. Châtelain. Purification and size-selection of carbon nanotubes. *Advanced Materials* 1997; 9:827-831.
- [109] B. Vigolo, A. Pénicaud, C. Coulon, C. Sauder, R. Pailler, C. Journet, P. Bernier, P. Poulin. Macroscopic fibres and ribbons of oriented carbon nanotubes. *Science* 2000; 290:1331-1334.
- [110] M.F. Islam, E. Rojas, D.M. Bergey, A.T. Johnson, A.G. Yodh. High weight fraction surfactant solubilization of single-wall carbon nanotubes in water. *Nano Letters* 2003; 3:269-273.
- [111] V.C. Moore, M.S. Strano, E.H. Haroz, R.H. Hauge, R.E. Smalley. Individually suspended single-walled carbon nanotubes in various surfactants. *Nano Letters* 2003; 3:1379-1382.
- [112] A.B. Dalton, C. Stephan, J.N. Coleman, B. McCarthy, P.M. Ajayan, S. Lefrant, P. Bernier, W.J. Blau, H.J. Byrne. Selective interaction of a semiconjugated organic polymer with single-wall nanotubes. *Journal of Physical Chemistry B* 2000; 104:10012-10016.
- [113] A. Star, J. Fraser Stoddart, D. Steuerman, M. Diehl, A. Boukai, E.W. Wong, X. Yang, S.W. Chung, H. Choi, J.R. Heath. Preparation and properties of polymer-wrapped single-walled carbon nanotubes. *Angewandte Chemie International Edition* 2001; 40:1721-1725.
- [114] M.J. O'Connell, P. Boul, L.M. Ericson, C. Huffman, Y. Wang, C. Haroz, C. Kuper, J. Tour, K.D. Ausman, R.E. Smalley. Reversible water-solubilization of single-walled carbon nanotubes by polymer wrapping. *Chemical Physics Letters* 2001; 342:265-271.
- [115] J. Chen, H. Liu, W.A. Weimer, M.D. Halls, D.H. Waldeck, G.C. Walker. Noncovalent engineering of carbon nanotube surfaces by rigid functional conjugated polymers. *Journal of the American Chemical Society* 2002; 124:9034-9035.
- [116] S. Ramesh, L.M. Ericson, V.A. Davis, R.K. Saini, C. Kittrell, M. Pasquali, W.E. Billups, W.W. Adams, R.H. Hauge, R.E. Smalley. Dissolution by direct protonation and nematization of pristine single-walled carbon nanotubes in superacids. *Journal of Physical Chemistry B* 2004; 108:8794-8798.
- [117] S.S. Wong, E. Joselevich, A.T. Woolley, C.L. Cheung, C.M. Lieber. Covalently functionalized nanotubes as nanometer probes for chemistry and biology. *Nature* 1998; 394:52-55.

- [118] J. Chen, A.M. Rao, S. Lyuksyutov, M.E. Itkis, M.A. Hamon, H. Hu, R.W. Cohn, P.C. Eklund, D.T. Colbert, R.E. Smalley, R.C. Haddon. Dissolution of full-length single-walled carbon nanotubes. *Journal of Physical Chemistry B* 2001; 105:2525-2528.
- [119] Y. Qin, L. Liu, J. Shi, W. Wu, J. Zhang, Z.X. Guo, Y. Li, D. Zhu. Large-scale preparation of solubilised carbon nanotubes. *Chemistry of Materials* 2003; 15:3256-3260.
- [120] S. Niyogi, M.A. Hamon, H. Hu, B. Zhao, P. Bhowmik, R. Sen, M.E. Itkis, R.C. Haddon. Chemistry of single-walled carbon nanotubes. *Accounts of Chemical Research* 2002; 35:1105-1113.
- [121] P.M. Ajayan, L.S. Schadler, P.V. Braun. *Nanocomposite Science and Technology*. Weinheim: Wiley-VCH (2003) p.77-80.
- [122] J.H. Du, J. Bai, H.M. Cheng. The present status and key problems of carbon nanotube based polymer composites. *Express Polymer Letters* 2007; 1:253-273.
- [123] P.-C. Ma, N.A. Siddiqui, G. Marom, J.-K. Kim. Dispersion and functionalization of carbon nanotubes for polymer-based nanocomposites: A review. *Composites Part A* 2010; 41:1345-1367.
- [124] P.M. Ajayan, O. Stephan, C. Colliex, D. Trauth. Aligned carbon nanotube arrays formed by cutting a polymer resin-nanotube composite. *Science* 1994; 265:1212-1214.
- [125] S. Moon, F. Jin, C.-J. Lee, S. Tsutsumi, S.-H. Hyon. Novel carbon nanotube/poly(L-lactic acid) nanocomposites; Their Modulus, Thermal Stability, and Electrical Conductivity. *Macromolecular Symposia* 2005; 224:287-296.
- [126] H. Tsuji, Y. Kawashima, H. Takikawa, S. Tanaka. Poly(L-lactide)/nano-structured carbon composites: Conductivity, thermal properties, crystallization, and biodegradation. *Polymer* 2007; 48:4213-4225.
- [127] C.-S. Wu, H.-T. Liao. Study on the preparation and characterization of biodegradable polylactide/multi-walled carbon nanotubes nanocomposites. *Polymer* 2007; 48:4449-4458.
- [128] S.D. McCullen, K.L. Stano, D.R. Stevens, W.A. Roberts, N.A. Monteiro-Riviere, L.I. Clarke, R.E. Gorge. Development, optimization, and characterization of electrospun poly(lactic acid) nanofibres containing multi-walled carbon nanotubes. *Journal of Applied Polymer Science* 2007; 105:1668-1678.
- [129] T. Villmow, P. Potschke, S. Pegel, L. Haussler, B. Kretzschmar. Influence of twin-screw extrusion conditions on the dispersion of multi-walled carbon nanotubes in a poly(lactic acid) matrix. *Polymer* 2008; 49:3500-3509.

- [130] M. Moniruzzaman, K.I. Winey. Polymer nanocomposites containing carbon nanotubes. *Macromolecules* 2006; 39:5194-205.
- [131] Z. Jia, Z. Wang, C. Xu, J. Liang, B. Wei, D. Wu, et al. Study on poly(methylmethacrylate): carbon nanotube composites. *Materials Science and Engineering A* 1999; 271:395-400.
- [132] N. Pierard, A. Fonseca, Z. Konya, I. Willems, G. van Tendeloo, J.B. Nagy. Production of short carbon nanotubes with open tips by ball milling. *Chemical Physics Letters* 2001; 335:1-8.
- [133] H. Xia, Q. Wang, K. Li, G.H. Hu. Preparation of CNT/polypropylene composite powder with a solid state mechanochemical pulverization process. *Journal of Applied Polymer Science* 2004; 93:378-386.
- [134] E.S. Choi, J.S. Brooks, D.L. Eaton, M.S. Al-Haik, M.Y. Hussaini, H. Garmestani, D. Li, K. Dahmen. Enhancement of thermal and electrical properties of carbon nanotube polymer composites by magnetic field processing. *Journal of Applied Physics* 2003; 94:6034-6039.
- [135] M.J. Biercuk, M.C. Llaguno, M. Radosavljevic, J.K. Hyun, A.T. Johnson, J.E. Fischer. Carbon nanotube composites for thermal management. *Applied Physics Letters* 2002; 80: 2767-2769.
- [136] D. Cai, M. Song. Latex technology as a simple route to improve the thermal conductivity of a carbon nanotube/polymer composite. *Carbon* 2008; 46:2107-2112.
- [137] H. Huang, C. Liu, Y. Wu, S. Fan. Aligned carbon nanotube composite films for thermal management. *Advanced Materials* 2005; 17:1652-1656.
- [138] J. Ge Jason, H. Hou, Q. Li, J. Graham Matthew, A. Greiner, H. Reneker Darrell, W. Harris Frank, Z.D. Cheng Stephen. Assembly of well-aligned multiwalled carbon nanotubes in confined polyacrylonitrile environments: electrospun composite nanofibre sheets. *Journal of the American Chemical Society* 2004; 126:15754-15761.
- [139] C. Velasco-Santos, A.L. Martínez-Hernández, F.T. Fisher, R. Ruoff, V.M. Castaño. Improvement of thermal and mechanical properties of carbon nanotube composites through chemical functionalization. *Chemistry of Materials* 2003; 15:4470-4475.
- [140] T. Kashiwagi, F. Du, J.F. Douglas, K.I. Winey, R.H. Harris, J.R. Shields. Nanoparticle networks reduce the flammability of polymer nanocomposites. *Nature Materials* 2005; 4:928-933.

- [141] B. Schartel, P. Pötschke, P.U. Knoll, M. Abdel-Goad. Fire behaviour of polyamide6/multiwall carbon nanotube nanocomposites. *European Polymer Journal* 2005; 41:1061-1070.
- [142] L.Q. Liu, H.D. Wagner. Rubbery and glassy epoxy resins reinforced with carbon nanotubes. *Composites Science and Technology* 2005; 65:1861-1868.
- [143] A.B. Dalton, S. Collins, E. Munoz, J.M. Razal, V.H. Ebron, J.P. Ferraris, J.N. Coleman, B.G. Kim, R.H. Baughman. Super-tough carbon-nanotube fibres. *Nature* 2003; 423:703-703.
- [144] D. Qian, E.C. Dickey. Load transfer and deformation mechanisms in carbon nanotube polystyrene composites. *Applied Physics Letters* 2000; 76:2868-2870.
- [145] K. Liao, S. Li. Interfacial characteristics of a carbon nanotube–polystyrene composite system. *Applied Physics Letters* 2001; 79:4225-4227.
- [146] H. Geng, R. Rosen, B. Zheng, H. Shimoda, L. Fleming, J. Liu, O. Zhou. Fabrication and properties of composites of poly(ethylene oxide) and functionalized carbon nanotubes. *Advanced Materials* 2002; 14:1387-1390.
- [147] M.B. Bryning, M.F. Islam, J.M. Kikkawa, A.G. Yodh. Very low conductivity threshold in bulk isotropic single-walled carbon nanotube-epoxy composites. *Advanced Materials* 2005; 17:1186-1191.
- [148] W. Bauhofer, J.Z. Kovacs. A review and analysis of electrical percolation in carbon nanotube polymer composites. *Composites Science and Technology* 2009; 69:1486-1498.
- [149] C.A. Martina, J.K.W. Sandler, A.H. Windle, et al. Electric field-induced aligned multi-wall carbon nanotube networks in epoxy composites. *Polymer* 2005; 46:877-886.
- [150] P.C. Ma, B.Z. Tang, J.K. Kim. Effect of CNT decoration with silver nanoparticles on electrical conductivity of CNT–polymer composites. *Carbon* 2008; 46:1497-1505.
- [151] J. Li, P.C. Ma, W.S. Chow, C.K. To, B.Z. Tang, J.K. Kim. Correlations between percolation threshold, dispersion state and aspect ratio of carbon nanotube. *Advanced Functional Materials* 2007; 17:3207-3215.
- [152] A. Moysala, Q. Li, I.A. Kinloch, A.H. Windle. Thermal and electrical conductivity of single- and multi-walled carbon nanotube-epoxy composites. *Composites Science and Technology* 2006; 66:1285-1288.

- [153] S. Abbasi, P.J. Carreau, A. Derdouri, M. Moan. Rheological properties and percolation in suspensions of multiwalled carbon nanotubes in polycarbonate. *Rheologica Acta* 2009; 48:943-959.
- [154] Z. Fan, S.G. Advani. Rheology of multiwall carbon nanotube suspensions. *Journal of Rheology* 2007; 51:585-604.
- [155] Y.Y. Huang, S.V. Ahir, E.M. Terentjev. Dispersion rheology of carbon nanotubes in a polymer matrix. *Physical Review B* 2006; 73:125422-125429.
- [156] C.A. Mitchell, J.L. Bahr, S. Arepalli, J.M. Tour, R. Krishnamoorti. Dispersion of functionalized carbon nanotubes in polystyrene. *Macromolecules* 2002; 35:8825-8830.
- [157] Z. Xu, Y. Niu, L. Yang, W. Xie, H. Li, Z. Gan, Z. Wang. Morphology, rheology and crystallization behaviour of polylactide composites prepared through addition of five-armed star polylactide grafted multiwalled carbon nanotubes. *Polymer* 2010; 51:730–737.
- [158] D. Wu, L. Wu, M. Zhang, Y. Zhao. Viscoelasticity and thermal stability of polylactide composites with various functionalized carbon nanotubes. *Polymer Degradation and Stability* 2008; 93:1577–1584.
- [159] Y.Y. Huang, S.V. Ahir, E.M. Terentjev. Dispersion rheology of carbon nanotubes in a polymer matrix. *Physical Reviews B* 2006; 73:1254221-1254229.
- [160] D. Wu, L. Wu, W. Zhou, Y. Sun, M. Zang. Relations between the aspect ratio of polylactide/carbon nanotube composites. *Journal of Polymer Science: Part B: Polymer Physics* 2010; 48:479-489.
- [161] N.A. Koratkar, B.Q. Wei, P.M. Ajayan. Carbon nanotube films for damping applications. *Advanced Materials* 2002; 14:997-1000.
- [162] J. Suhr, N. Koratkar. Energy dissipation in carbon nanotube composites: a review. *Journal of Materials Science* 2008; 43:4370-4382.

## **Chapter 3**

### **Sample preparation and experimental techniques**

#### **3.1 Introduction**

The experimental techniques used in this study include a bench-top counter-rotating twin-screw mini-extrusion, injection moulding, hot melt pressing, attenuated total reflectance Fourier-transform infrared spectroscopy, X-ray photoelectron spectroscopy, Raman spectroscopy, focused ion beam scanning electron microscopy, dynamic mechanical analysis thermogravimetric analysis, differential scanning microscopy, and polarized optical microscopy.

#### **3.2 Materials**

##### **3.2.1 Poly(lactide)**

Poly(lactide) (with an average molecular weight =  $188 \text{ kg}\cdot\text{mol}^{-1}$  and a D-lactide content of 1.1–1.7%) used in this study was obtained from Unitika Co. Ltd, Japan. Prior to use, the PLA was dried at  $80 \text{ }^\circ\text{C}$  for 2 days under vacuum.

##### **3.2.2 Multiwalled carbon nanotubes**

The MWCNTs used in this study were purchased from Sigma-Aldrich, with more than 95% purity (inner diameter  $\approx 10 \text{ nm}$ ; outer diameter  $\approx 20 \text{ nm}$ ; length  $\approx 500 \mu\text{m}$ ).

##### **3.2.3 Others**

HDA, chloroform, and ethanol were also purchased from Sigma-Aldrich.

### **3.3 Methods**

#### **3.3.1 Preparation of samples**

##### **3.3.1.1 Functionalization of carbon nanotubes**

In a typical functionalization process, a mixture of 1 g pure MWCNTs and 5 g HDA was transferred to a conical flask and heated at 180 °C for 6 h in an oil bath. After cooling to room temperature, the excess HDA was removed from the reaction mixture by washing with ethanol several times. The black solid was collected by Nylon membrane filtration (0.45µm pore size) and dried at 110 °C overnight to get a constant weight. The mass increase of the functionalised MWCNTs (f-MWCNTs) was ~10 %, determined gravimetrically.

##### **3.3.1.2 Preparation of nanocomposites with melt mixing technique**

For the preparation of the PLA/MWCNT composites, the f-MWCNTs (1.5 wt.% in powder form, with an amine content of ~10%, determined gravimetrically) and the PLA (pellet form) were first dry-mixed in a polyethylene bottle. The mixture was then extruded by using a counter-rotating twin-screw mini-extruder (bench-top Haake Minilab II, Thermo Scientific) operated at 180 °C (screw speed = 30 rpm, time = 5 min) to yield black coloured composite strands. These strands were chopped into pieces and compression moulded by pressing at 2 MPa pressure at 180 °C for 2 min. For tensile property measurements, injection moulded dumbbell-shaped specimens were used. The dried neat PLA and nanocomposite strands were injection-moulded using an injection-moulder (bench-top Haake Minijet II) operated at 180 °C at a mould temperature of 80 °C (ASTM D-638). Pure PLA and nanocomposite samples were annealed at 110 °C under vacuum, prior to all characterizations and property measurements.

Another PLA/f-MWCNT was prepared through this method. This composite contained 0.5 wt.% of f-MWCNTs with an amine content of ~20%, determined gravimetrically. This composite was treated in the same way as was described in the first paragraph.

A PLA composite with untreated MWCNTs was also prepared and analysed, but the results are not presented here, because of high variability due to extremely poor dispersion of the MWCNTs when prepared under the same conditions.

### **3.3.1.3 Preparation of nanocomposites with solution mixing technique**

A portion of the f-MWCNTs was accurately weighed and dissolved into 200 ml of chloroform. The undissolved f-MWCNTs were dried overnight at 90 °C under vacuum and weighed again to determine the exact amount dissolved in chloroform. From this solution, 1.5 wt.% f-MWCNTs was calculated and the composite was prepared by sonicating with PLA at  $\pm 40$  °C. The solvent was evaporated overnight at ambient temperature to collect thin films of about 1 mm thickness. The thin films were further left in a vacuum oven at 60 °C overnight to completely remove the chloroform. These were then melt-pressed for 5 minutes at 180 °C using a pressure of 2 metric tons in a Carver hot-melt press for various characterizations.

Although a PLA composite with untreated MWCNTs was prepared using this technique, the analysis results on this composites are also not presented in this work, because of the same reasons mentioned in the previous section.

### **3.3.2 Attenuated total reflectance Fourier-transform infrared spectroscopy**

Infrared spectroscopy is a chemical analytical technique, which measures infrared intensity versus wavelength of light by detecting the vibrations characteristic of chemical functional groups in a sample. Infrared light is classified as far infrared, mid infrared, and near infrared with wavelengths  $4 \sim 4000 \text{ cm}^{-1}$ ,  $400 \sim 4000 \text{ cm}^{-1}$ , and  $4000 \sim 14000 \text{ cm}^{-1}$  respectively.

Attenuated total reflectance (ATR) is a sampling technique used in conjunction with infrared spectroscopy which allows samples to be examined directly in the solid, liquid or gas state without further preparation [2]. ATR measurements are conducted by placing the sample in close contact with the surface of a prism made of a highly refractive material that transmits infrared light. Thus close contact between the sample and the prism is very important. The commonly used prisms include germanium (Ge), zinc selenide (ZnSe) and diamond. Even

though it is expensive, diamond is by far the best ATR crystal because of its robustness and durability. Figure 3.1 shows the infrared beam path in the ATR setup.

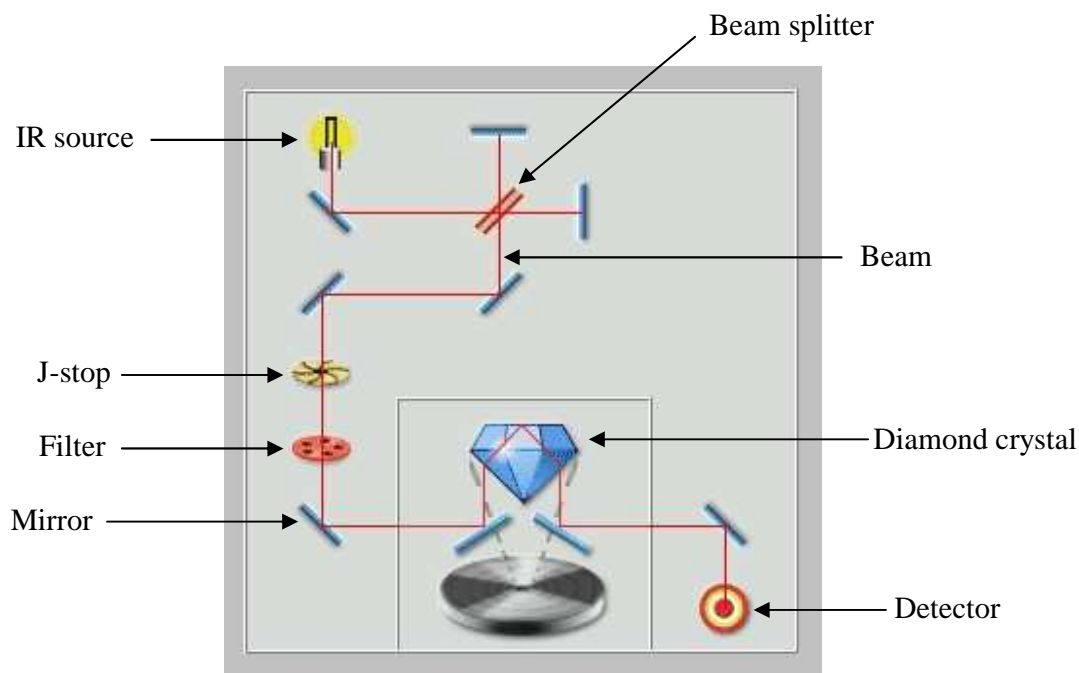


**Figure 3.1 Schematic representation of infrared beam path in the ATR setup [2].**

ATR-FTIR analyses of MWCNTs, HDA, f-MWCNTs, PLA, and the composites were carried out using a Perkin Elmer Spectrum 100 instrument with a resolution of  $4.0 \text{ cm}^{-1}$ .

### 3.3.3 X-ray photoelectron spectroscopy

XPS is an analytical technique used to estimate the elemental composition and chemical state of the elements on the surface of a material, by projecting soft X-rays (with a photon energy of 200-2000 eV) onto the surface and detecting the energy of photoelectrons emitted from areas a few nm (top 1–10 nm usually) from the surface [4]. Every element has a particular characteristic binding energy associated with each core atomic orbital, which means each element will give rise to a distinctive set of peaks in the photoelectron spectrum at kinetic energies determined by the photon energy and the respective binding energies [4,5]. The existence of peaks at particular energies therefore indicates the existence of a specific element in the sample under study. The intensity of the peaks is also related to the concentration of the

element within the sampled region [6]. The operating principle of XPS is schematically shown in Figure 3.2.

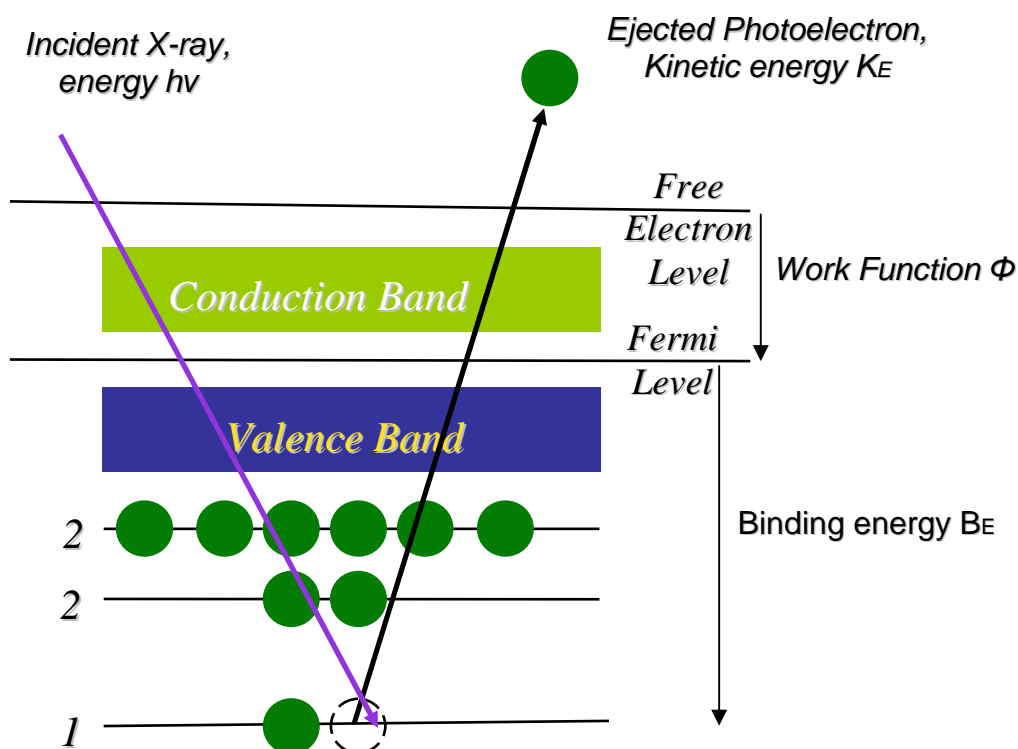


**Figure 3.2** Operating principle of XPS [7].

Elemental mapping of pure MWCNT and f-MWCNT samples was performed XPS on a Kratos Axis Ultra device, with a monochromatic Al X-ray source (1486.6 eV). Survey spectra were acquired at 160 eV and region spectra at 20 eV pass energies.

### 3.3.4 Raman spectroscopy

Raman spectroscopy is a spectroscopic technique in which the frequency of photons in monochromatic light changes upon interaction with a sample. Photons of the laser light are absorbed by the sample and then reemitted. The frequency of the reemitted photons is shifted up or down in comparison to an original monochromatic frequency, which is called the Raman effect. This shift provides information about vibrational, rotational and other low frequency transitions in molecules. Raman spectroscopy can be used to study solid, liquid and gaseous samples [8-10]. The Raman scattering and infrared spectra for a given species often

resemble one another quite closely. There are, however, enough differences between the kinds of groups that are infrared active and those that are Raman active to make the techniques complementary rather than competitive. An important advantage of Raman spectra over infrared lies in the fact that water does not cause interference. Glass or quartz cells can be used, thus avoiding the inconvenience of working with sodium chloride or other atmospherically unstable confinements. Thus aqueous solutions can be studied by Raman spectroscopy, but not by IR. Despite these advantages, Raman spectroscopy is subject to interference by fluorescence or impurities in the sample. Raman spectra are obtained by irradiating a sample with a powerful laser source of visible or infrared monochromatic radiation. This radiation usually has a wavelength that is well away from any absorption peaks of the sample. The scattered radiation is of three types, namely Stokes (found at wavenumbers that are 218, 314, and 495 $\text{cm}^{-1}$  smaller than the Rayleigh peak), anti-Stokes (occur at 218, 314, and 459 $\text{cm}^{-1}$  greater than the wavenumber of the source), and Rayleigh (wavelength is exactly that of the excitation source, and is significantly more intense than either of the two types) (Figure 3.3) [11].

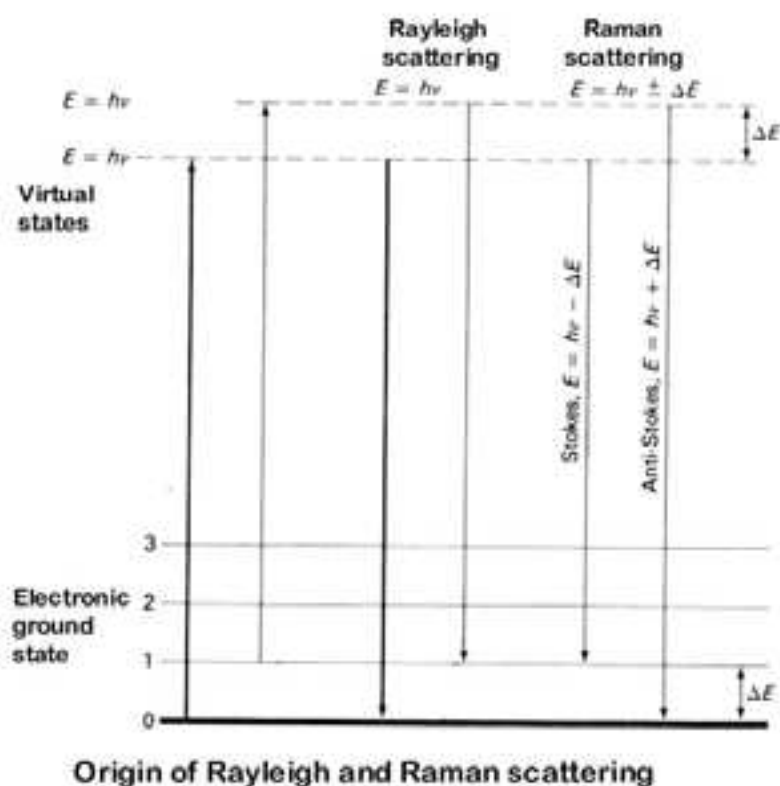


**Figure 3.3** Raman scattering of excited molecules and atoms [12].

Raman spectra of MWCNTs, f-MWCNTs, PLA, and PLA/MWCNTs nanocomposites were recorded using a Lab Raman system (Jobin-Yvon Horiba T64000 Spectroscopy) equipped with an Olympus BX-40 microscope. The excitation wavelength was 514.5 nm with an energy setting of 1.2 mW from a Coherent Innova Model 308 argon ion laser.

### 3.3.5 Thermogravimetric analysis

TGA is a technique that studies thermal stability of materials under inert conditions (dehydration, carbonization, spontaneous chain degradation), and in an oxygen environment (oxidation) [13]. This method monitors the weight loss of a sample in a chosen atmosphere as a function of time or temperature. It is composed of a recording balance, a furnace, a temperature programmer, a sample holder, an enclosure for establishing the required atmosphere, and a means of recording and displaying the data (Figure 3.4). Balance sensitivity is usually approximately one microgram, with a total capacity of a few hundred milligrams.

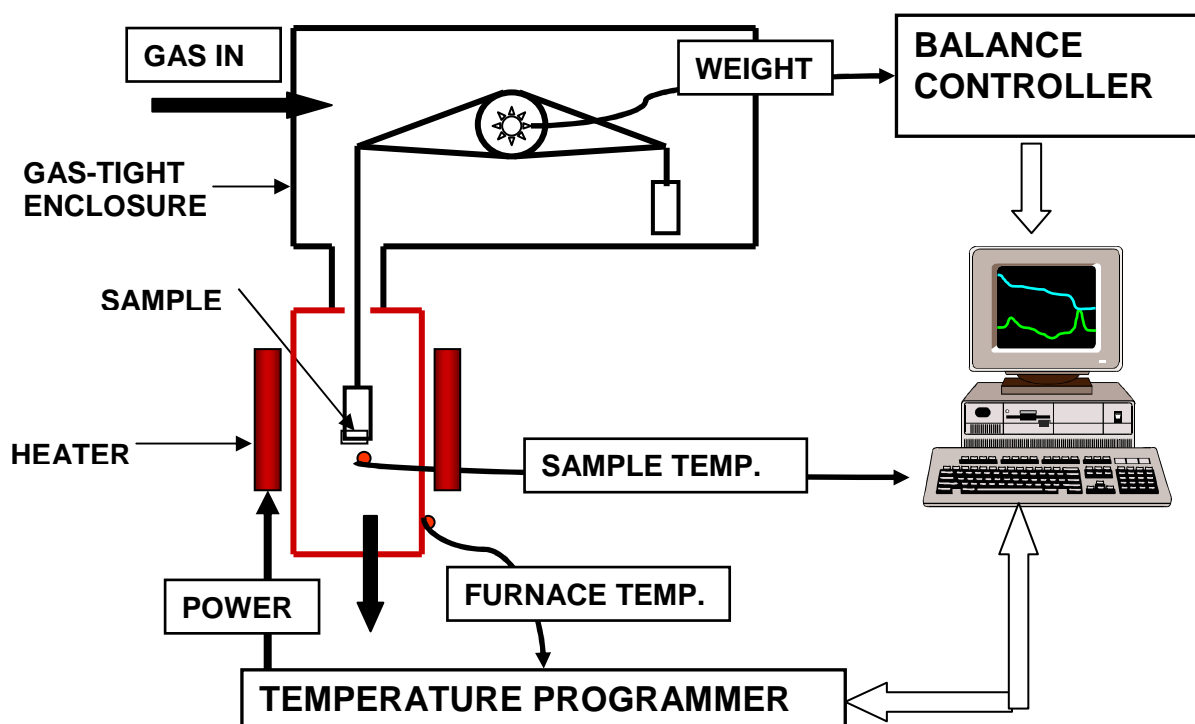


Figure 3.4 Schematic representation of a TGA setup.

Thermogravimetric analyses of all the samples were carried out on a TGA Q500 (TA Instruments) at the specified heating rates under thermo-oxidative conditions, from ambient temperature to 650 °C.

### **3.3.6 Differential scanning calorimetry**

DSC is a thermoanalytical technique which analyzes thermal transitions occurring in samples when they are heated or cooled. In polymers, melting and glass transition temperatures can be determined as well as the various transitions in liquid crystalline mesophases. In a typical DSC experiment, two pans are placed on a pair of identically positioned platforms connected to a furnace by a common heat flow path. One pan contains the sample, the other one is empty (often called the reference pan). Then the two pans are heated at a specific heating rate. A plot is created where the difference in heat flow between the sample and reference is plotted as a function of temperature. [15].

The melting and glass transition temperatures as well as crystallinity of the PLA matrix before and after nanocomposite formation were studied in a DSC instrument (TA Instruments model Q2000) under a constant nitrogen flow of 50 mL min<sup>-1</sup> and a heating rate of 20 °C min<sup>-1</sup>. The DSC samples were weighed such that all the samples had an identical PLA content. The DSC instrument was calibrated by determining the temperature and melting enthalpy of an indium standard, and the baseline was checked according to the TA Instruments protocols.

### **3.3.7 Scanning electron microscopy**

SEM is one of the most versatile instruments available for microstructure morphology examination and chemical composition characterization [16]. In the scanning electron microscope, an image is formed by a very fine electron beam which is scanned across the surface of a sample in a series of lines and frames called a raster; at any given moment, the specimen is bombarded with electrons over a very small area. These electrons may be elastically reflected with no loss of energy (backscattered electrons), they may be absorbed and give rise to secondary electrons of very low energy (together with X-rays), they may be absorbed and give rise to the emission of visible light, and they may give rise to electric currents within the specimen. All these effects can be used to produce images. The contrast in

the image is determined by the sample morphology. A high-resolution image can be obtained because of the small diameter of the primary electron beam (Figure 3.5) [15,16].

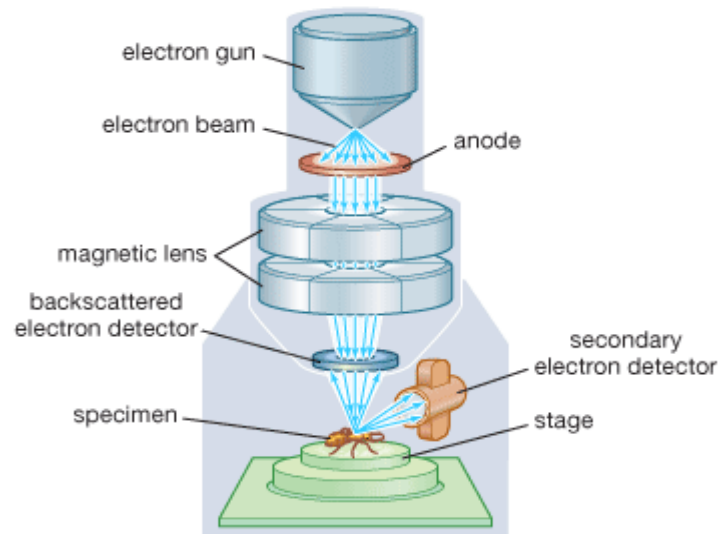


**Figure 3.5** A schematic representation of scanning electron microscope [17].

Both PLA and nanocomposite samples were freeze fractured in liquid nitrogen, sputter coated with carbon, and the morphology was studied with a Carl Zeiss SMT Neon 40, Cross Beam Series FIB-SEM in SEM mode, with an acceleration voltage of 2 kV and a filament current of 2.38 A (Figure 3.8).

### 3.3.8 Polarized optical microscopy

Polarized optical microscopy is a technique that exploits the interference of the split light rays, as they are re-united along the same optical path, to extract information about anisotropic materials. The polarized light microscope is designed to scrutinize and take pictures of specimens that are visible primarily due to their optically anisotropic character. To achieve this, the microscope must be equipped with both a polarizer, positioned in the light path somewhere before the specimen, and an analyzer (a second polarizer) placed in the optical pathway between the objective rear aperture and the observation tubes or camera port. Image contrast arises from the interaction of plane-polarized light with a birefringent (or doubly-refracting) specimen to produce two individual wave components that are each polarized in mutually perpendicular planes. The velocities of these components, that are

termed the ordinary and the extraordinary wavefronts, are different and vary with the propagation direction through the specimen. [16,18].

The spherulitic growth behaviour of the PLA matrix at various temperatures and the degree of dispersion of MWCNTs in the PLA matrix was studied with a Carl Zeiss Imager Z1M polarized optical microscope. A compression moulded thin films of PLA and the composite were placed between two covering glasses on a Linkam hot stage (Linkam Scientific Instruments Ltd, UK), mounted on the microscope. The samples were heated to 190 °C at specified heating rates while OM images were taken, held at that temperature for 5 min, and then OM images were taken again during cooling.

### **3.3.9 Dynamic mechanical analysis**

DMA is concerned with the measurement of the thermomechanical properties of a specimen as a function of temperature. DMA is a sensitive probe of molecular mobility within materials and is most commonly used to measure the glass transition temperature and other transitions in macromolecules, or to follow changes in the thermomechanical properties brought about by chemical reactions [19]. For this type of measurement the sample is subjected to an oscillating stress. In this test the sample, having the form of a strip, is clamped firmly at the upper end, while an oscillating disc is fastened to the lower end (Figure 3.6). The turning motion of this disc can be followed optically and continuously recorded. A thermostatted chamber that can be heated or cooled surrounds the test sample.



**Figure 3.6** A photo of a thermostatted chamber showing the clamped sample in a DMA

The storage modulus, being in-phase with the applied stress, represents the elastic component of the material's behaviour, whereas the loss modulus corresponds to the viscous nature of the material. The tangent of the ratio between the loss and storage moduli ( $G''/G'$ ) gives the useful quantity known as the mechanical damping factor ( $\tan \delta$ ) which is a measure of the amount of deformational energy that is dissipated as heat during each cycle.

The dynamic mechanical properties of neat PLA and PLA/MWCNTs composite samples were determined using an Anton Paar-Physica MCR501 Rheometer in the tension-torsion mode. The temperature dependence of the storage modulus ( $G'$ ) and  $\tan \delta$  of neat PLA and composite samples, were measured at a constant frequency of  $6.28 \text{ rad s}^{-1}$  with a strain amplitude of 0.02% (selected after a series of strain sweep tests at different temperatures to determine the linear region) and in the temperature range of  $-20$  to  $160 \text{ }^\circ\text{C}$  at a heating rate of  $2 \text{ }^\circ\text{C min}^{-1}$ .

### **3.3.10 Small- and wide angle X-ray scattering**

SAXS is a technique where the elastic scattering of X-rays by a sample, which has inhomogeneities in the nanometre range, is recorded at very low angles (typically  $0.1$  to  $10^\circ$ ). In the past decade, small angle X-ray scattering has been widely used to study the phase dispersion in matrices, polymerization, emulsification, colloidal stabilization, shear-induced structures, polymer crystallization, and the phase domain behaviour in polymers [20]. SAXS data provides information about the size and shape of particles that are present in a system and also gives information about the presence of different particle populations and types of interactions [21]. SAXS analysis is mainly applicable for randomly oriented and statistically distributed particle systems. Hence, their three-dimensional scattering pattern represents the orientational average of their structure [22-24].

SAXS experiments of the PLA and nanocomposite samples were carried out in an Anton Paar SAXSess instrument operated at  $40 \text{ kV}$  and  $50 \text{ mA}$  with a line collimation geometry. The radiation used was a Ni filtered  $\text{CuK}_\alpha$  radiation of wavelength  $0.154 \text{ nm}$  (PAN Analytical X-ray source). Intensity profiles were obtained with a slit collimated SAXSess and recorded with a two-dimensional imaging plate. The sample-to-detector distance was  $264.5 \text{ mm}$  and covered the length of the scattering vector ( $q$ ) from  $0.084$  to  $28 \text{ nm}^{-1}$ . The read-out angles

were calculated from the pixel size, and the obtained q-scale was cross-checked by measuring silver behenate whose equidistant peak positions are known. SAXS data were collected at room temperature. All the samples were exposed to the X-rays for 5 min.

### 3.3.11 Tensile testing

Uniaxial tensile testing is a well known and universal test to determine material parameters such as yield strength, Young's modulus, % elongation, % area of reduction and ultimate strength. Tensile testing is carried out by applying longitudinal or axial load at a specific extension rate to a standard tensile specimen with known dimensions (gauge length and cross sectional area perpendicular to the load direction) until failure.

The primary output from a tensile test is the load vs. elongation curve of the specimen, which is recorded in real-time using a load cell and an extensometer. This curve is then used to determine the stress-strain curve (Figure 3.7).

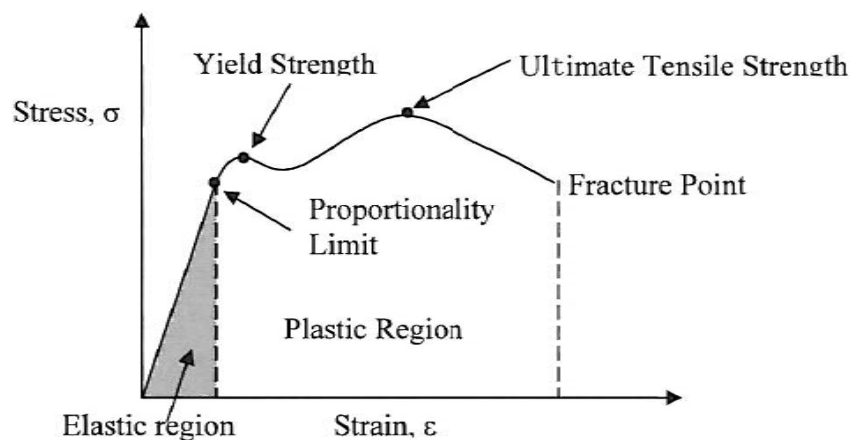


**Figure 3.7** An example of a typical stress-strain curve [26].

The tensile properties of the pure polymer and nanocomposite samples were measured using a Hounsfield H10KT tensile tester (Tinius Olsen Ltd) at room temperature. The microinjection moulded dumbbell-shaped specimens of thickness 3 mm, width 3 mm, and length 64 mm were used. For these tests, a gauge length of 25 mm and a cross-head speed of 5 mm min<sup>-1</sup> were employed. Five measurements were carried out for each specimen, and the results were averaged to obtain a mean value.

### 3.3.12 Electrical conductivity

The resistivity of a semiconductor is often determined using a four-point probe technique. This technique involves bringing four equally spaced probes in contact with a material of unknown resistance. The probe array is placed in the centre of the material, as shown in Figure 3.8.

The two outer probes are used for sourcing current and the two inner probes are used for measuring the resulting voltage drop across the surface of the sample. The four probes eliminate measurement errors due to the probe resistance, the spreading resistance under each probe, and the contact resistance between each metal probe and the semiconductor material [27].

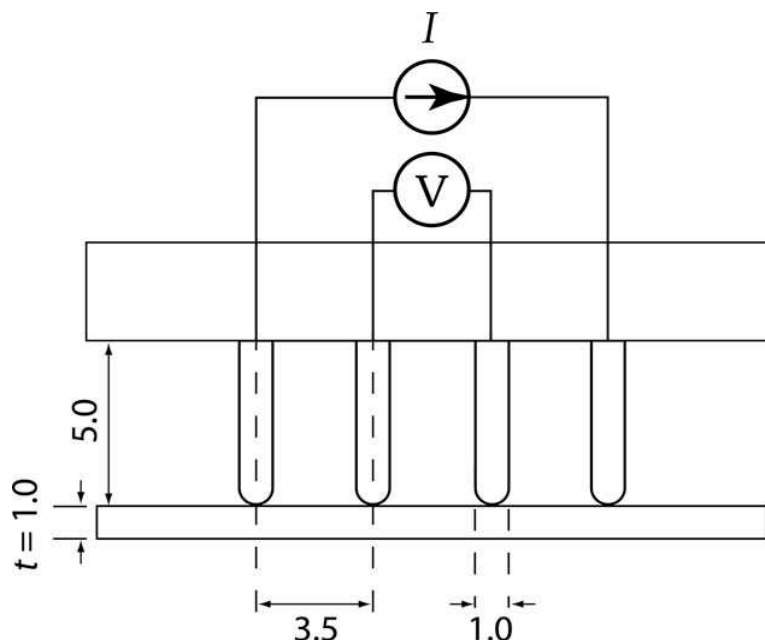


**Figure 3.8 Schematic representation of four-point collinear probe set-up (all dimensions in mm)**

The direct current (dc) conductivity for the PLA and nanocomposite samples was measured at room temperature (26 °C), using a four-point collinear probe method (Keithley 4200-SCS, USA). The data presented here are the average of five independent tests.

### 3.3.13 Transmission electron microscopy

TEM is an instrument that uses a high energy electron beam transmitted through a very thin sample to image and analyse the microstructure of materials with atomic scale resolution [28,29]. An image is formed from the interaction of the electrons transmitted through the specimen; the image is magnified and focused onto an imaging device, such as a fluorescent screen, a layer of photographic film, or is detected by a sensor such as a CCD camera (Figure 3.9). A TEM sample must be approximately 1000 Å or less in thickness in the area of interest. The entire specimen must fit into a 3 mm diameter cup and be less than about 100 microns in thickness.

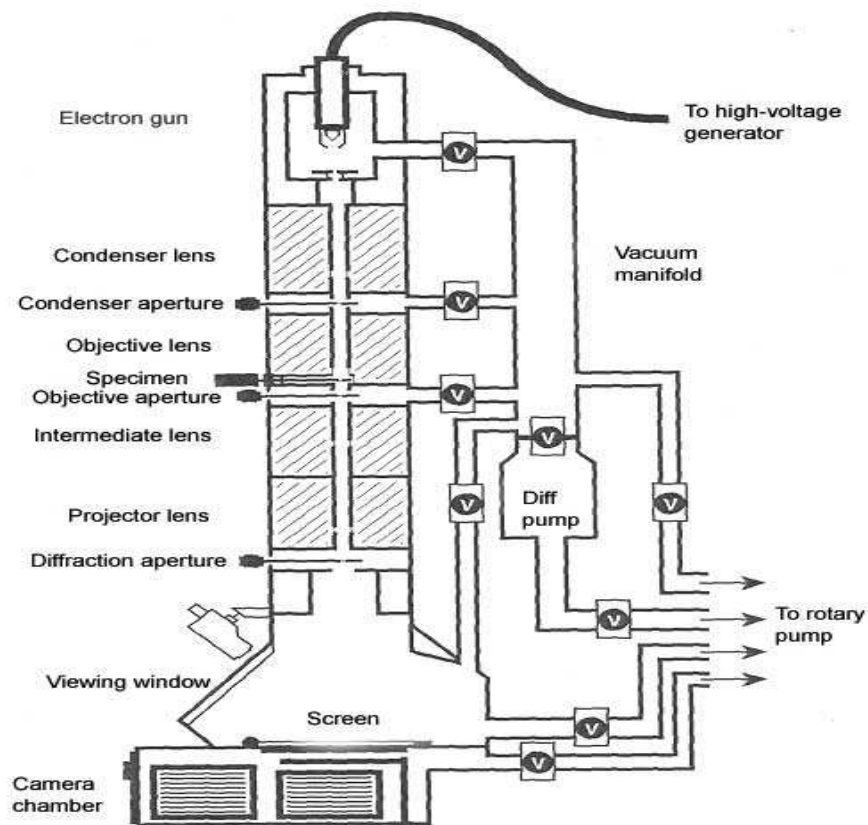


**Figure 3.9** Schematic representation of a transmission electron microscope [29].

The degree of dispersion of f-MWCNTs in the composite was investigated by means of transmission electron microscopy (JEOL JEM 2100) operated at an accelerating voltage of 100 kV. The composite sample was cut using a cryo-ultramicrotome (-70 °C), collected on a 300-mesh carbon coated copper grid, and observed without further treatment.

**3.3.14 Atomic force microscopy**

AFM is a technique that probe the sample and make measurements in three dimensions, x, y, and z (normal to the sample surface), thus allowing the presentation of three-dimensional images of a sample surface [30]. Clean samples with no excessively large surface features can have a resolution in the x-y plane ranging from 0.1 to 1.0 nm and in the z direction 0.01 nm (atomic resolution). AFM does not need a vacuum environment or any special sample preparation, and it can be used in either an ambient or liquid nitrogen environment. Because of its versatility, AFM can be used in different modes such contact (Figure 3.10), noncontact, or tapping modes.

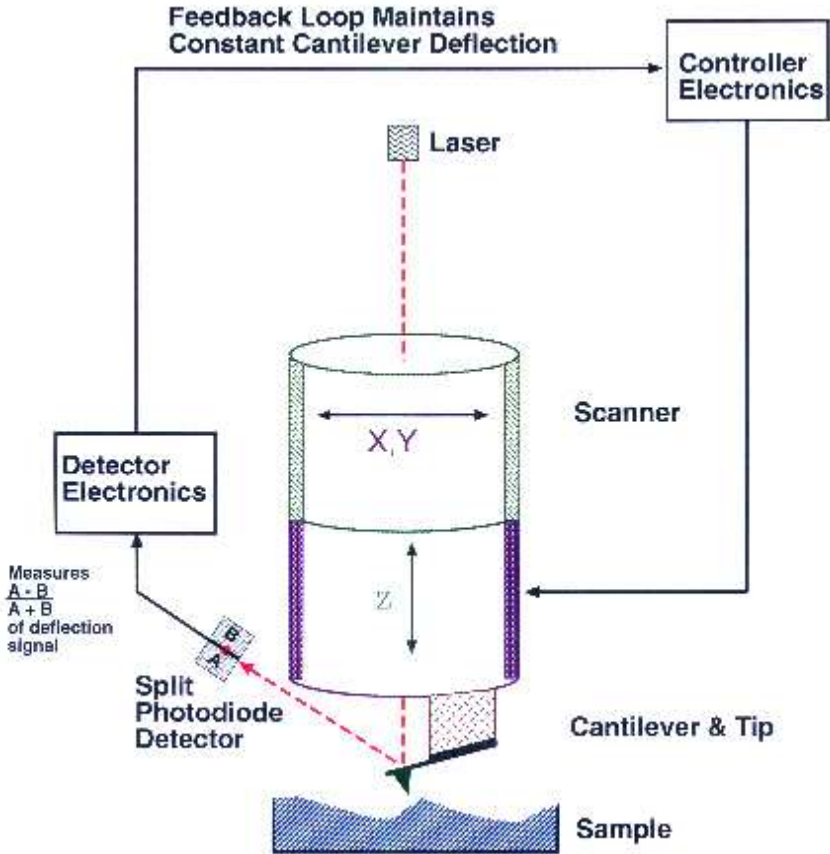


**Figure 3.10** Schematic diagram showing the operating principles of the AFM in the tapping mode [31].

The AFM topography examinations were carried out with a multimode AFM Nano Scope Version (R) IV using 0.5 – 2.0 Ω.cm phosphorous (n) doped tip with a radius of curvature of less than 10 nm. The tip mounted in a 125 μm long cantilever with the spring constant of 40

$\text{N m}^{-1}$  was employed for the tapping mode experiment. Samples were imaged using a scan rate of 0.5 Hz and tip frequencies ranging from 280 to 310 kHz.

Samples of PLA and its composite were separately dissolved in chloroform. Thin films were prepared on the glass substrates using a spin coater which was ramped at 500 rpm for 10 s and subsequently ramped at 1000 rpm for 20 s. The samples were annealed in a vacuum oven at 130 °C for 30 min and quenched with liquid nitrogen. The samples were then immediately taken for AFM experiments.

### 3.4 References

- [1] B.C. Smith. Fundamentals of Fourier Transform Infrared Spectroscopy, CRC Press, Boca Raton (1996).
- [2] FT-IR Spectroscopy – Attenuated Total Reflectance (ATR). Perkin Elmer Life and Analytical Sciences (2005).  
[http://las.perkinelmer.com/content/TechnicalInfo/TCH\\_FTIRATR.pdf](http://las.perkinelmer.com/content/TechnicalInfo/TCH_FTIRATR.pdf) (Retrieved 20 August 2010).
- [3] [http://www.nuance.northwestern.edu/KeckII/Instruments/FT-IR/keck-ii%20pages1.html#What is ATR?](http://www.nuance.northwestern.edu/KeckII/Instruments/FT-IR/keck-ii%20pages1.html#What%20is%20ATR?) (Retrieved 21 November 2010).
- [4] T.A. Carlson (Editor), X-ray Photoelectron Spectroscopy, Benchmark Papers in Physical Chemistry and Chemical Physics. Vol. 2, Dowden, Hutchinson and Ross (1978): p 352.
- [5] K.M Siegbahn. Electron Spectroscopy for Atoms, Molecules and Condensed Matter, Nobel Lecture, 8 December 1981.
- [6] [www.casaxps.com](http://www.casaxps.com) (Retrieved 22 August 2010).
- [7] M. El-Desawy. Characterization and Application of Aromatic Self-Assembled Monolayers. University of Bielefeld, PhD thesis (2007).
- [8] G.W. Faris, R.A. Copeland. Wavelength dependence of the Raman cross section for liquid water. Applied Optics 1997; 36:2686-2688.
- [9] A.J. Berger, Y. Wang, D.M. Sammeth, I. Itzkan, K. Kneipp, M.S. Feld. Aqueous dissolved gas measurements using near-infrared Raman spectroscopy. Applied Spectroscopy 1995; 49:1164-1169.

- [10] D.I. Ostrovskii, A.M. Brodin, L.M. Torell. Raman study of water in Nafion-117 membranes. *Solid State Ionics* 1996; 85:323-327.
- [11] L.A. Lyon, C.D. Keating, A.P. Fox, B.E. Baker, L. He, S.R. Nicewarner, S.P. Mulvaney, M.J. Natan. Raman spectroscopy. *Analytical Chemistry* 1998; 70:341-361.
- [12] P. Madl. Raman Spectroscopy. Comparison of Infrared Spectra with those gathered by Raman Spectroscopy of selected substances. Protocol. Salzburg, June 9th and 11th 1999. Also available on: <http://www.uni-salzburg.at/pls/portal/docs/1/359400.PDF>
- [13] G.R. Heal. Thermogravimetry & Derivative Thermogravimetry. In P.J. Haines (ed.). *Principles of Thermal Analysis & Calorimetry*. Royal Society of Chemistry, Cambridge (2002) p.10-54.
- [14] D.M. Price, D.J. Hourston, F. Dumont. Thermogravimetry of Polymers. *Encyclopedia of Analytical Chemistry*. R.A. Meyers (Ed.). John Wiley & Sons Ltd, Chichester (2000) p.8094-8105.
- [15] D. Braun, H. Cherdron, M. Rehahn, H. Ritter, B. Voit. *Polymer Synthesis: Theory and Practice* (4<sup>th</sup> Edition). Springer-Verlag: Heidelberg (2005) p.39-156.
- [16] W. Zhou, Z.L. Wang (Editors). *Scanning Microscopy for Nanotechnology: Techniques and Applications*. Springer Science + Business Media, LLC, New York (2006) p.1-40.
- [17] <http://www.britannica.com/EBchecked/topic-art/526571/110970/Scanning-electron-microscope>
- [18] <http://www.microscopyu.com/print/articles/polarized/polarizedintro-print.html>
- [19] D.M. Price. Thermomechanical, Dynamic Mechanical and Dielectric Methods. In: *Principles of Thermal Analysis and Calorimetry*. P.J. Haines (Ed.), Royal Society of Chemistry, Cambridge (2002): 94-128.
- [20] P. Thiyagarajan. Characterization of materials of industrial importance using small-angle scattering techniques. *Journal of Applied Crystallography* 2003; 36:373-380.
- [21] S. Chattopadhyay, D. Erdemir, J.M.B. Evans, J. Ilavsky, H. Amenitsch, C.U. Segre, A.S. Myerson. SAXS study of the nucleation of glycine crystals from a supersaturated solution. *Crystal Growth and Design* 2005; 5:523-527.
- [22] R. Mittelbach, O. Glatter. Direct structure analysis of small-angle scattering data from polydisperse colloidal particles. *Journal of Applied Crystallography* 1998; 31:600-608.
- [23] O. Glatter, O. Kratky. *Small Angle X-ray Scattering*. Academic Press Inc., London (1982).

- [24] H. Schnablegger, Y. Singh. A Practical Guide to SAXS: Getting Acquitted with the Principles. Anton Paar GmbH Publishers: Austria (2006).
- [25] <http://www.matweb.com/reference/tensilestrength.aspx>
- [26] M.P. Groover. Fundamentals of Modern Manufacturing: Materials, Processes, and Systems, 3rd Edition. John Wiley & Sons, Inc: USA (2006).
- [27] Four-Probe Resistivity and Hall Voltage Measurements with the Model 4200-SCS. [www.keithley.com/data?asset=15222](http://www.keithley.com/data?asset=15222)
- [28] [http://www.mauricewilkinscentre.org/bioviz/index.php?page\\_id=118](http://www.mauricewilkinscentre.org/bioviz/index.php?page_id=118) (Retrieved on 26 November 2010).
- [29] N. Tanaka. Present status and future prospects of spherical aberration corrected TEM/STEM for study of nanomaterials – A topical review. Science and Technology of Advanced Materials 2008; 9:014111-014122.
- [30] C.R. Blanchard. Atomic force microscopy. The Chemical Educator 1996; 1:1–8.
- [31] <http://www.nanoscience.com/education/afm.html> (Retrieved on 25 November 2010).

## Chapter 4

### High-performance carbon nanotube-reinforced bioplastic

#### 4.1 Introduction

Recently, a broad range of biodegradable aliphatic polyesters and their co-polymers have been commercialized by various companies [1]. One of the most well-studied and promising polymers in this area is polylactide (PLA), because it is made from renewable agricultural products and is readily biodegradable [2-4]. Another important property of PLA is its biocompatibility [5,6]. Commercially available PLA has a high modulus and strength comparable to those of most petroleum-based polymers. However, its low elongation at break and very slow crystallization rate present drawbacks for its biomedical applications such as implant materials, surgical sutures, and controlled drug delivery systems, as well as for the conventional applications where common thermoplastics are employed [4]. In this chapter, the different properties of PLA and its f-MWCNTs composites are discussed. The PLA composite contained 1.5 wt.% of f-MWCNTs. The f-MWCNTs used in this work contained ~10% (determined gravimetrically) of HDA.

The work on the PLA composite with non-functionalized MWCNTs is not presented here, because of variable results obtained due to poor dispersion of the MWCNTs.

#### 4.2 Results and discussion

##### 4.2.1 Fourier-transform infrared spectroscopy: Functionalization of MWCNTs

The functionalization of the outer surface of multi-walled carbon nanotubes (MWCNTs) and the presence of hexadecylamine (HDA) chains on the outer surface of the MWCNTs were examined by FTIR spectroscopy. The FTIR spectra of pure HDA, pure MWCNTs (p-MWCNTs), and functionalized MWCNTs (f-MWCNTs) are shown in Figure 4.1. The main

IR peaks of HDA, appearing at 1456, 1613, 2846, 2916, and 3336  $\text{cm}^{-1}$  are due to: C-H deformation, primary amine N-H deformation,  $\text{CH}_2$  rocking vibration due to tail-to-tail addition, -C-H- stretching, and N-H stretching, respectively [7]. The peaks at 1976 and 2160  $\text{cm}^{-1}$  on spectrum (a) correspond to pure MWCNTs, and can also be observed on the spectrum of f-MWCNTs (spectrum (b)). The HDA (spectrum (c)) peaks can also be observed on the spectrum of f-MWCNT. Thus, with a careful analysis of the FTIR spectra of pure HDA, p-MWCNTs, and f-MWCNTs, one can conclude that the MWCNTs outer surfaces are functionalized by HDA chains.

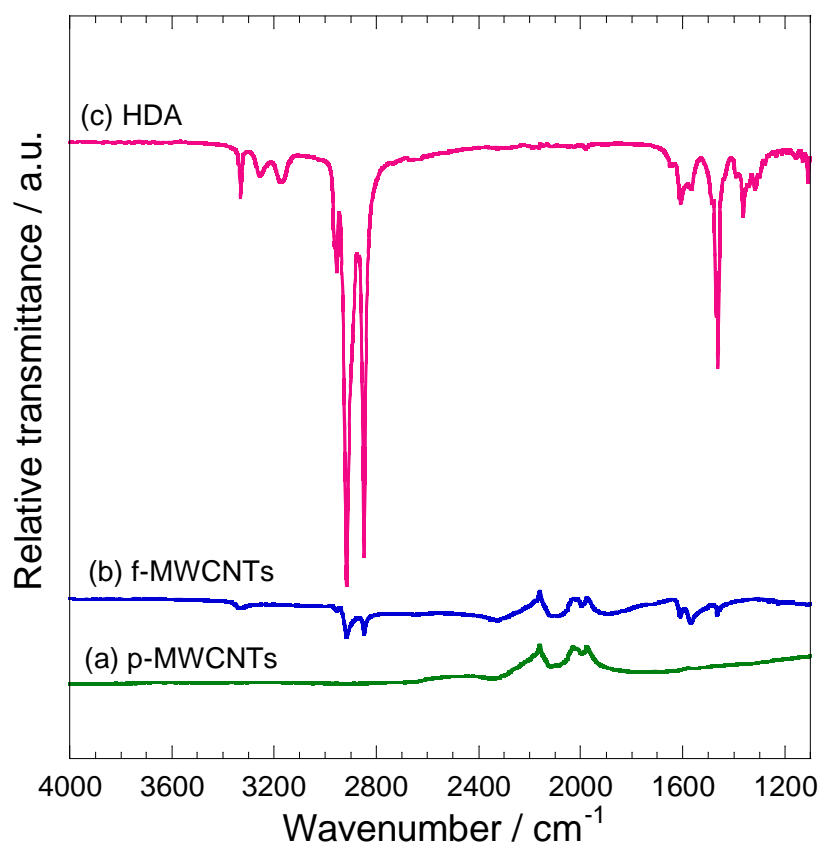


**Figure 4.1** Fourier-transform infrared spectra of (a) p-MWCNTs, (b) f-MWCNTs, and (c) pure HDA.

#### 4.2.2 X-ray photoelectron spectroscopy: Functionalization of MWCNTs

The presence of amine groups on the outer graphene layer of the MWCNTs can further be identified by comparing the XPS spectra of p-MWCNTs and f-MWCNTs. Figure 2 shows the

XPS spectra of p-MWCNTs and f-MWCNTs samples. Two distinct features can be identified from the XPS spectrum of the f-MWCNTs. First is the appearance of the ‘N 1S’ peak at 400 eV, suggesting the presence of amine groups on the MWCNTs’ outer surface. Secondly, the appearance of weak ‘O 1s’ and ‘O KLL’ peaks may be due to the presence of surface adsorbed oxygen in the sample. Another interesting observation is that the characteristic ‘C 1S’ peak of the f-MWCNTs remains at almost the same position as that of the p-MWCNTs, indicating that the MWCNTs’ surface carbon atoms were not damaged due to amine functionalization and there is also no indication of covalent bond formation.

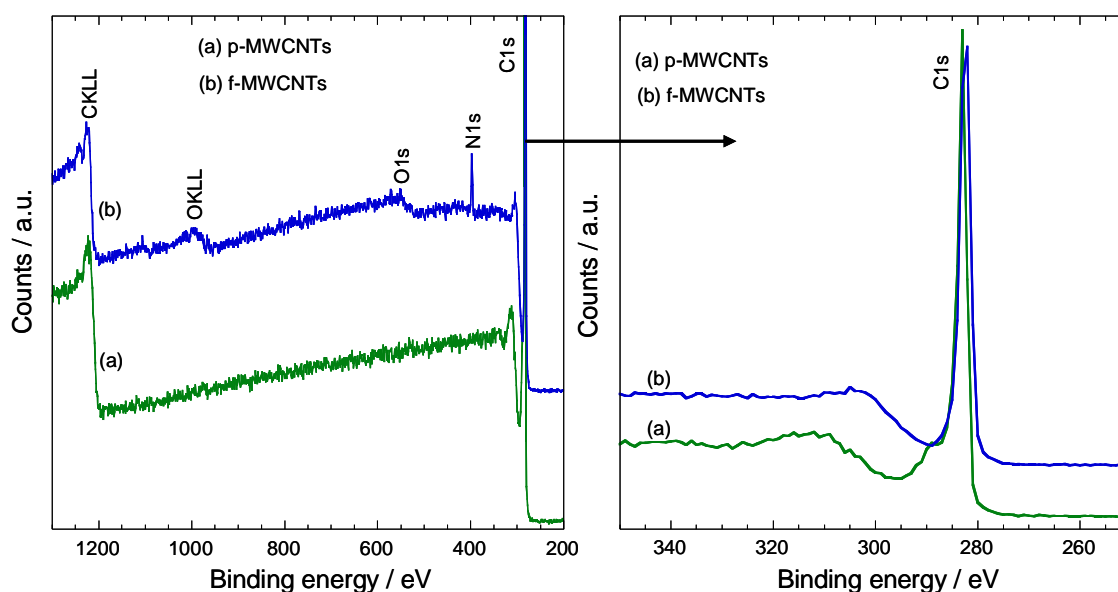


**Figure 4.2** XPS spectra of (a) p-MWCNTs and (b) f-MWCNTs. The right side is the enlarged peak position of ‘C 1S’.

### 4.2.3 Raman spectroscopy: Functionalization of MWCNTs

To investigate the nature of the bonding between the HDA chains with the outer graphene layer of the MWCNTs, Raman spectroscopy analyses were conducted on both p- and f-MWCNTs samples, and the results are presented in Figure 4.3. Both samples show the two characteristic peaks of the MWCNTs. The first peak appears at  $1350\text{ cm}^{-1}$ , which is due to the disordered C-atoms and is commonly known as the D-band. The second peak appears at  $1580\text{ cm}^{-1}$ , which is related to the  $sp^2$  hybridized C-atoms of the MWCNTs, and is known as the G-

band. It is interesting to note that there is no significant shift in the peak positions of both bands in the case of the f-MWCNTs. This observation indicates the non-covalent adsorption of the HDA chains on the MWCNTs outer surface. Another interesting observation is that in the case of f-MWCNTs, the intensity ratio of the *G*-band to the *D*-band remains almost the same as for the p-MWCNTs. This indicates the adsorption of HDA chains on the MWCNTs' outer surface without damaging the carbon atoms of the graphene layer.

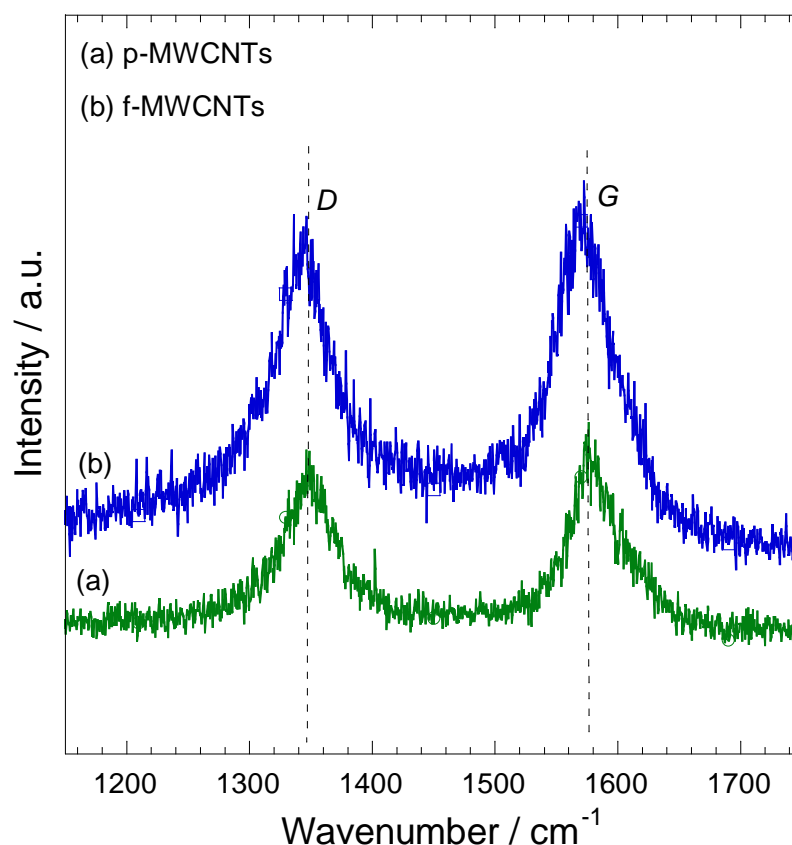


**Figure 4.3** Raman spectra of (a) p-MWCNTs and (b) f-MWCNTs. Excitation wavelength was 514.5 nm.

#### 4.2.4 Fourier-transform infrared spectroscopy: After composite formation

The question is how the HDA chains adsorb on the MWCNTs' outer surface without the formation of any covalent bonds with the MWCNT surfaces? It has already been established that CNTs are natural electron acceptors [8]. On the other hand, the amine group of the HDA chain is an electron donor. Thus, the free amine groups of the HDA chains interact with the MWCNTs' surfaces and get adsorbed through the formation of charge-transfer complexes [9].

Figure 4.4 shows the FTIR spectra of f-MWCNTs, pure PLA, and the PLA/f-MWCNT composite. The PLA spectrum shows the  $\text{-C=O}$ ,  $\text{-CH}_2$ ,  $\text{-C-O-C}$  ester group, and  $\text{-CH(CH}_3\text{)}$  stretching peaks at 1753, 3004 and 2942, 1184, and 1376  $\text{cm}^{-1}$ , respectively [10, 11]. The FTIR spectrum of the composite confirms the presence of the characteristic peaks of PLA, MWCNTs, and HDA. On the other hand, the characteristic N-H stretching peak of HDA in the IR spectrum of the composite (marked by an arrow in the figure) moved to a much higher wavenumber of 3503  $\text{cm}^{-1}$  compared to the 3336  $\text{cm}^{-1}$  of the f-MWCNTs (marked an by arrow in the figure). This indicates some degree of interactions between the amine groups of HDA chains and the polyester backbone of PLA.

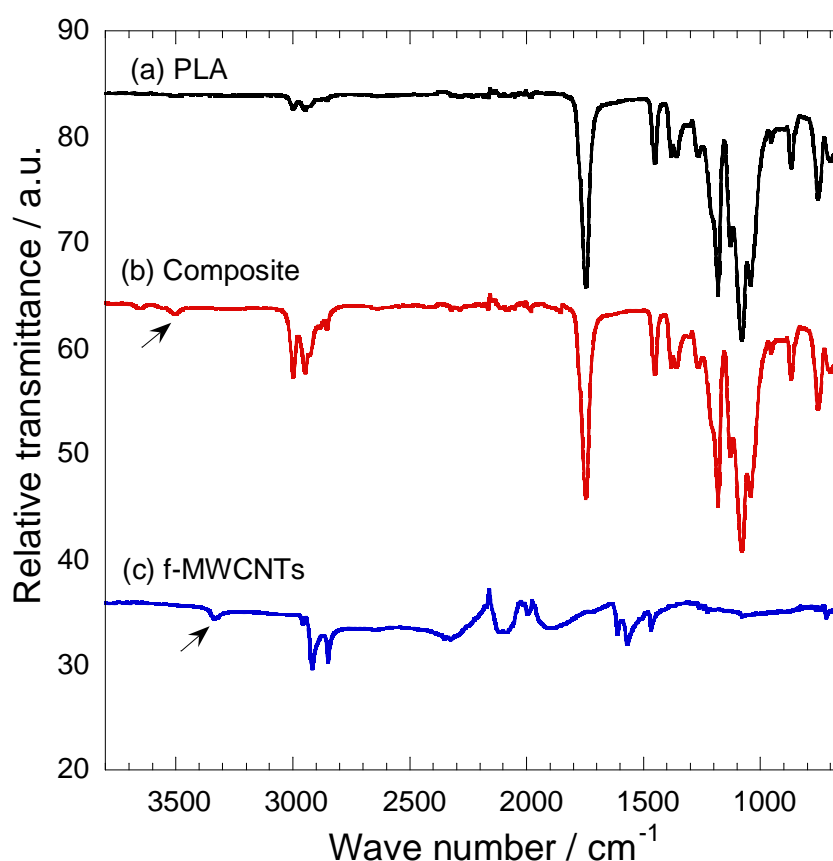


**Figure 4.4** FTIR of (a) pure PLA, (b) PLA/f-MWCNTs composite, and (c) f-MWCNTs.

#### 4.2.5 Raman spectroscopy: After composite formation

Further confirmation of the strong interactions between the f-MWCNTs' surface and the PLA chains is revealed by the Raman spectroscopic analysis. The Raman spectra of the f-MWCNTs and the corresponding composite with PLA are shown in Figure 4.5. The spectra show shifts of both the characteristic *D*- and *G*-bands of the MWCNTs in the composite to higher wavenumbers, which means that the system needs more energy to vibrate the individual tube or each tube becomes more bulky in the composite. The characteristic peak of the PLA matrix (see inset in Figure 4.5) is also at a higher wavenumber. These observations suggest the formation of strong bonds between the f-MWCNTs' surfaces and the PLA chains.

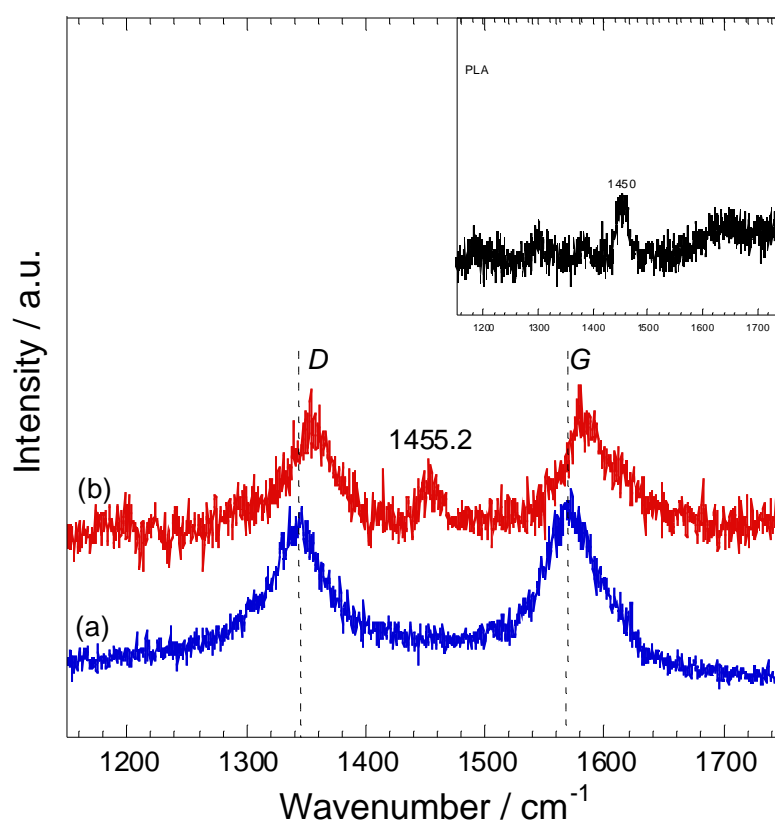


**Figure 4.5** Raman spectra of (a) f-MWCNTs and (b) the PLA/f-MWCNTs composite. The inset is the Raman spectrum of the pure PLA matrix. The excitation wavelength was 514.5 nm.

#### 4.2.6 Differential scanning calorimetry

To investigate the effect of the incorporation of f-MWCNTs on the thermal properties of the PLA matrix, DSC analyses were performed. Figure 4.6 shows the DSC curves for the annealed samples of neat PLA and its composite with f-MWCNTs. The  $T_g$  of the PLA increased from 63 °C for the neat PLA to 68 °C for the PLA in the nanocomposite with f-MWCNTs. Such an increase in the  $T_g$  suggests the presence of strong interactions between the f-MWCNTs surfaces and the PLA chains, which hinder the motion of the PLA chains. The slight increase in the melting temperature of the PLA from 167 °C for pure PLA to 168 °C for PLA in the composite suggests that the f-MWCNTs had some effect on the PLA matrix crystallinity. The melting enthalpy and degree of crystallinity ( $\chi_c$ ) of the PLA matrix increased from  $\Delta H = 39.9 \text{ J g}^{-1}$  and  $\chi_c = 42.9\%$  for the pure PLA to  $\Delta H = 47.9 \text{ J g}^{-1}$  and  $\chi_c = 51.5\%$  for the PLA in the composite, which is in line with the increase in the melting temperature.  $\chi_c$  was calculated according to the Equation 1.

$$\chi_c = \frac{\Delta H_{\text{sample}}}{\Delta H_{100\%}} 100 \quad (1)$$

where  $\Delta H_{\text{sample}}$  is the heat of fusion of the sample and  $\Delta H_{100\%}$  is the heat of fusion of 100% crystalline PLA ( $93 \text{ J g}^{-1}$ ) [12,13]. The increase in crystallinity indicates the active nucleating role of the dispersed MWCNTs on PLA matrix crystallization.

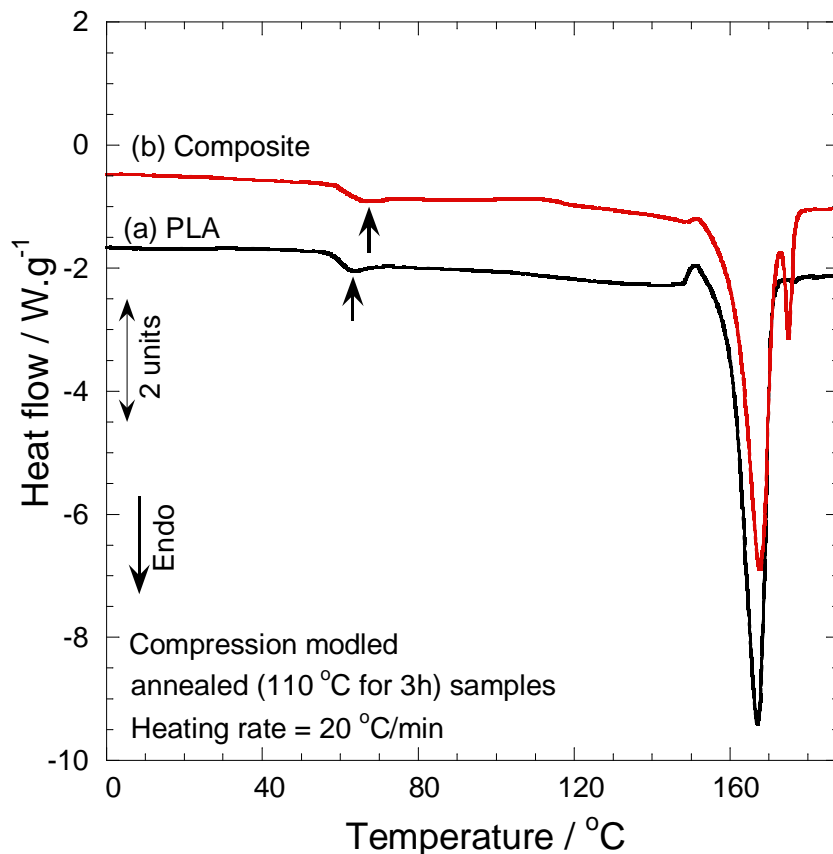


**Figure 4.6** DSC curves of (a) pure PLA and (b) the PLA/f-MWCNT composite. Both samples were annealed at 110 °C for 3h under vacuum prior to analysis.

#### 4.2.7 Polarized optical microscopy

To check the nucleating role of the MWCNTs, the spherulitic growth behaviour of the PLA from its melt at 130 °C was investigated by POM for both pure PLA and the nanocomposite. Figure 4.7 shows the POM images of pure PLA and the composite. The pure PLA matrix shows a well-defined large spherulitic morphology (Figure 4.7(a)). This shows that at a cooling rate of 10 °C.min<sup>-1</sup>, PLA crystals have enough time to grow undisturbed in the absence of f-MWCNTs. However, in the presence f-MWCNTs, at the same cooling rate, the sizes of the PLA spherulites are significantly reduced and highly disordered as shown in Figure 4.7(b). This observation indicates that the surface of the dispersed nanotubes act as strong nucleating agents for the PLA matrix crystallization. This is a very important

observation because the crystalline phase of the PLA can confer useful mechanical and other physical properties.

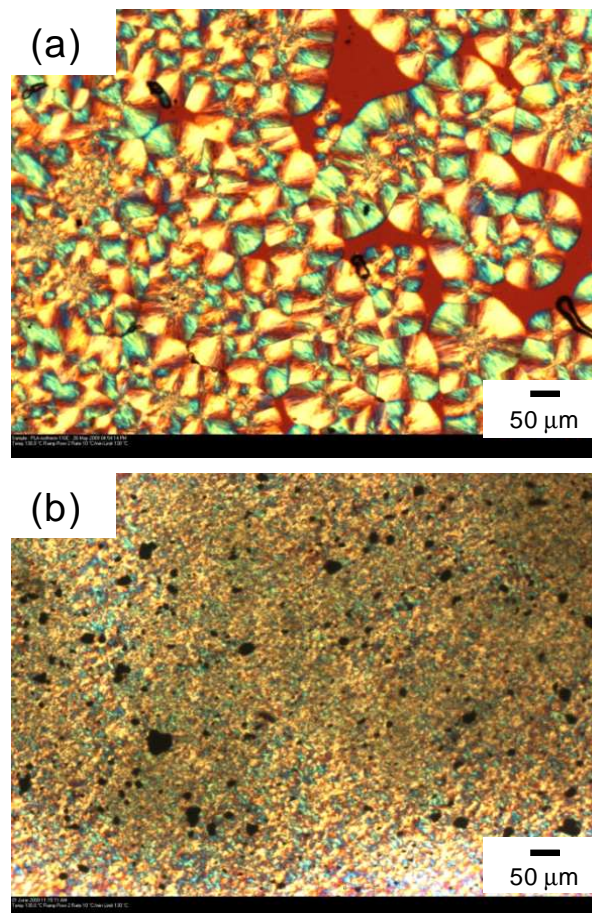


**Figure 4.7** Polarized optical micrographs of (a) pure PLA and (b) the PLA/f-MWCNT composite. Both samples were crystallized from their melts at 130 °C for 30 min.

The degree of dispersion-distribution of the nanotubes in the PLA matrix was analysed with POM in the transmission mode at 190 °C (Figure 4.8). Most of the tubes are homogeneously dispersed, but there is still some microscale dispersion of tube bundles in the PLA matrix.

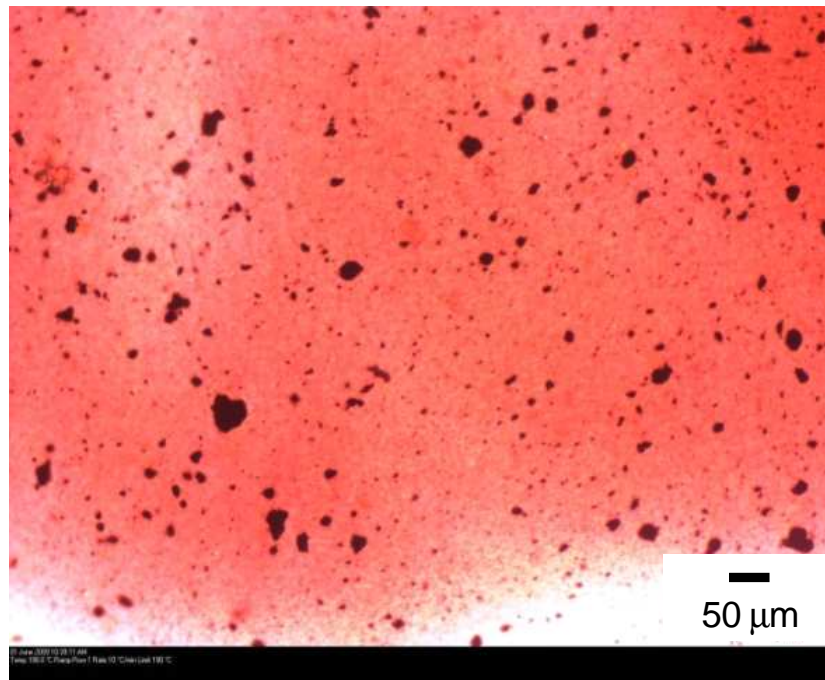


**Figure 4.8** POM image of the PLA/f-MWCNT composite taken at 190 °C in the transmittance mode. This is the most representative image after taking 5 pictures at different positions in the sample.

#### 4.2.8 Dynamic mechanical analysis

Upon the application of a harmonic strain, the dynamic mechanical response reveals the amount of energy stored as elastic energy and the amount of energy dissipated in the composite, which are strongly dependent on the level of dispersion-distribution of the nanotubes and their interaction with the PLA matrix. The temperature dependence of the storage modulus ( $G'$ ) and  $\tan \delta$  of the neat PLA and the composite is shown in Figure 4.8. The composite with 1.5 wt.% of f-MWCNTs shows an observable increase in the elastic modulus compared to that of the pure PLA, particularly in the glass transition and rubbery regions (Figure 4.9(a)).

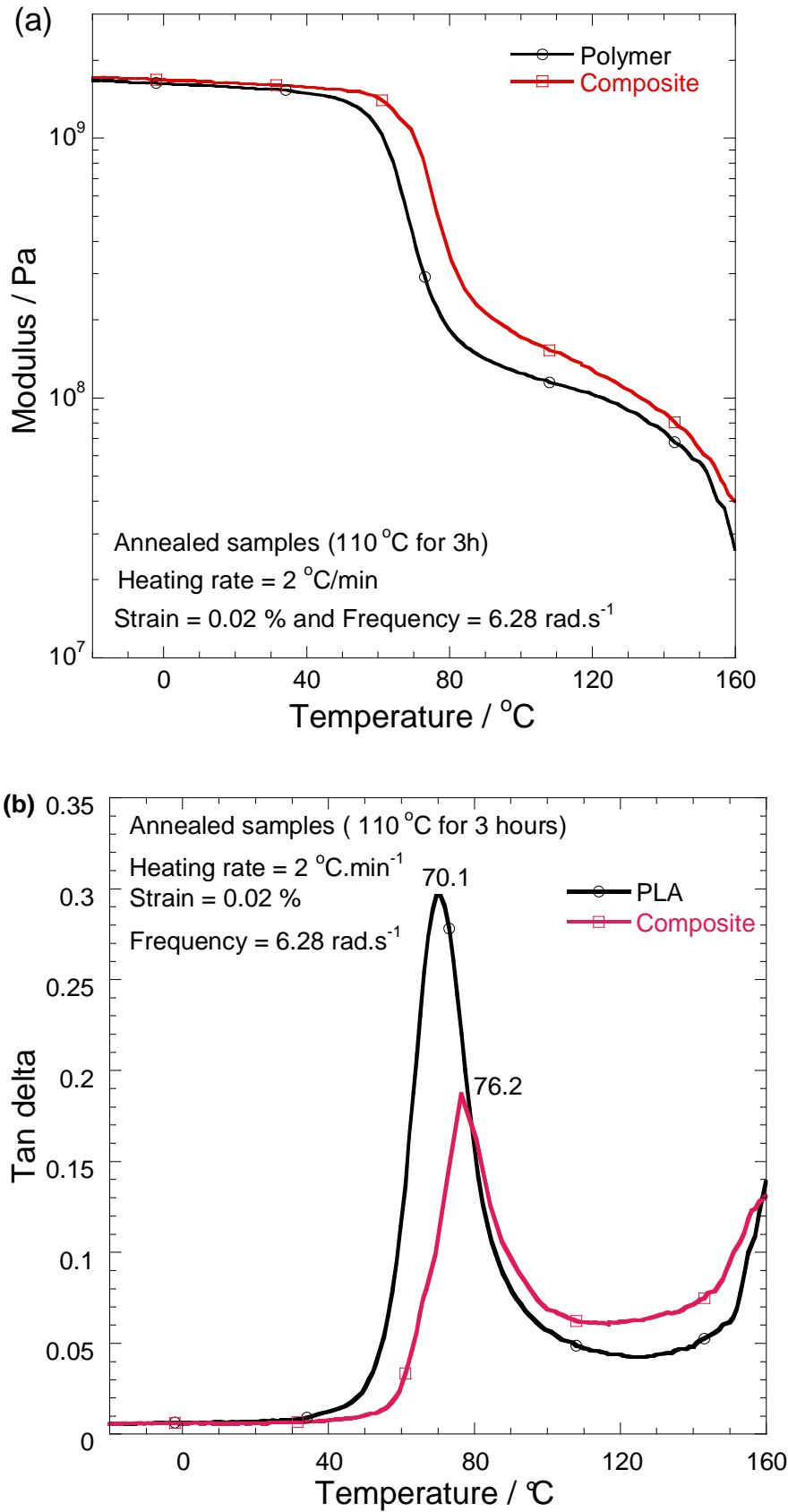


**Figure 4.9** Temperature dependence of the dynamic mechanical properties of pure PLA and the composite: (a) storage modulus and (b) tan  $\delta$ .

The increased modulus is accompanied by an increase in  $T_g$ , as is evidenced by the peak position in the  $\tan \delta$  curve that moves to a higher temperature for the composite (Figure 4.9(b)). The increase in modulus is related to the strong interaction between the f-MWCNTs' outer surface and the PLA matrix, which gives rise to the immobilization of the polymer chains. This immobilization becomes prominent in the glass transition region when the polymer chains start to relax.

#### 4.2.9 Tensile properties

The strong f-MWCNT–PLA interaction also leads to an improvement of elongation at break of the pure PLA matrix without significant loss of modulus. However, tensile strength at break does not change significantly. This is an important observation because even in the presence of CNTs, the original properties of PLA are not lost. The representative tensile curve is presented in Figure 4.10. The results are summarized in Table 4.1.

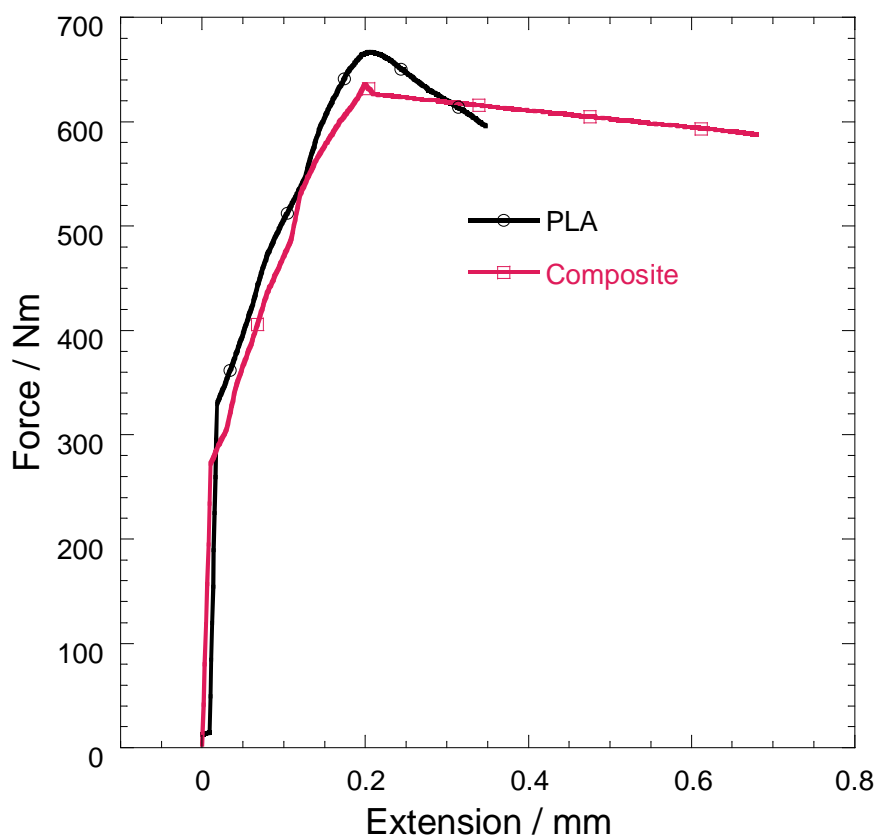


**Figure 4.10** Most representative (out of five tests for each sample) room temperature uniaxial tensile tests of neat PLA and composite samples at a constant cross head speed of 5 mm/min. Annealed (110 °C for 3h) injection moulded samples were used.

**Table 4.1** Various properties of neat PLA and its composite with f-MWCNTs

Samples	Tensile properties <sup>a</sup>		
	Modulus / GPa	Strength at break / MPa	Elongation at break / %
PLA	6.1 ± 0.4	61.0 ± 4.1	1.5 ± 0.4
Composite	4.7 ± 0.5	61.6 ± 4.6	2.7 ± 0.1

<sup>a</sup>Five measurements were carried out for each specimen and the results were averaged to obtain a mean value. Injection moulded samples (annealed at 110 °C for 3h under vacuum) were used for tensile property measurements. Compression moulded sheets (~0.6 mm, annealed at 110 °C for 3h under vacuum) were used for conductivity measurements.

#### 4.2.10 Direct current measurements

The incorporation of f-MWCNTs in PLA did not seem to have an influence on the dc electrical conductivity of the sample. The dc electrical conductivity measurements (average of 5 measurements) were recorded as  $(9.1 \pm 0.8) \times 10^{-4}$  for PLA, and  $(9.7 \pm 0.7) \times 10^{-4}$  S.cm<sup>-1</sup> for the composite. This suggests that the alkyl chains of HDA covered most of the nanotubes' outer surface and blocked the active flow of electrons between the matrix and filler. It can also be that the concentration of f-MWCNT was too low for the formation of percolation paths.

### 4.3 Conclusions

In summary, in this chapter we described a new and novel MWCNTs-reinforced approach for biodegradable/biocompatible PLA that results in a concurrent improvement in the inherent properties of PLA such as glass transition temperature, crystallization kinetics, dynamic mechanical properties, strength, and elongation at break. The results show that the concurrent improvement in PLA properties after composite formation with f-MWCNTs is due to the strong interfacial interaction between the nanotubes' outer surface and the PLA chains.

#### 4.4 References

- [1] S. Sinha Ray, M. Bousmina. Biodegradable polymers and their layered silicate nanocomposites in greening the 21st century materials world. *Progress in Materials Science* 2005; 50:962-1079.
- [2] R.E. Drumright, P.R. Gruber, D.E. Henton. Polylactic acid technology. *Advanced Materials* 2000; 12:1841-1846.
- [3] J. Lunt. Large scale production, properties and commercial applications of polylactic acid polymers. *Polymer Degradation and Stability* 1998; 59:145-152.
- [4] R. Auras, B. Harte, S. Selke. An overview of polylactides as packaging materials. *Macromolecular Bioscience* 2004; 4:835–864.
- [5] Y. Ikada, H. Tsuji. Biodegradable polyesters for medical and ecological applications. *Macromolecular Rapid Communications* 2000; 21:117-132.
- [6] N.C. Bleach, K.E. Tanner, M. Kellomaki, P. Tormala. Effect of filler type on the mechanical properties of self-reinforced polylactide-calcium phosphate composites. *Journal of Materials Science: Materials in Medicine* 2001; 12:911-915.
- [7] G. Socrates. *Infrared and Raman characteristic group frequencies*, 3<sup>rd</sup> edition, John Wiley and Sons, New York (2001).
- [8] M.G. Guldi, G.M.A. Rahman, F. Zerbetto, M. Prato. Carbon nanotubes in electron donor-acceptor nanocomposites. *Accounts of Chemical Research* 2005; 38:871-878.
- [9] R.J. Chen, Y. Zhang, D. Wang, H. Dai. Noncovalent sidewall functionalization of single-walled carbon nanotubes for protein immobilization. *Journal of the American Chemical Society* 2001; 123:3838-3839.
- [10] E. Meaurio, N. López-Rodríguez, J.R. Sarasua. Infrared spectrum of poly(L-lactide): application to crystallinity studies. *Macromolecules* 2006; 39:9291-9301.
- [11] L. Fang, R. Qi, L. Liu, G. Juan, S. Huang. Synthesis of poly(L-lactide) via solvothermal method. *International Journal of Polymer Science* 2009; 2009:1-7.
- [12] E.W. Fisher, H.J. Sterzel, G. Wegner. Investigation of the structure of solution grown crystals of lactide copolymers by means of chemical reactions. *Kolloid-Zeitschrift and Zeitschrift fur Polymere* 1973; 25:980-990.
- [13] S. Sinha Ray, K. Yamada, M. Okamoto, A. Ogami, K. Ueda. New polylactide/layered silicate nanocomposite: Nanoscale control over multiple properties. *Macromolecular Rapid Communications* 2002; 23:943-947.

## **Chapter 5**

### **The effect of surface functionalized carbon nanotubes on the morphology, as well as thermal, thermomechanical, and crystallization properties of polylactide**

#### **5.1 Introduction**

Over the last few years, a significant amount of work has been done on the preparation and characterization of polymer nanocomposites based on nanoclays such as montmorillinite, saponite, and synthetic mica [1-7]. These fillers moderately improved the mechanical and physical properties of the neat polymer matrices even though their amounts were small (~5 wt.%). The main reason for these improved properties in the case of the clay-containing polymer nanocomposites is the presence of interfacial interactions as opposed to the conventional composites.

Currently a number of researchers are focusing on the preparation and characterization of functionalized carbon nanotube containing polymer nanocomposites [8-20]. The main purpose is to prepare conducting composites with a balance of mechanical properties. This chapter summarizes various properties of a PLA composite containing 0.5 wt.% of functionalized multiwalled carbon nanotubes (f-MWCNTs). The f-MWCNTs used in this work contain  $\pm 20\%$  (determined gravimetrically) of hexadecylamine (HDA).

#### **5.2 Results and discussion**

##### **5.2.1 Attenuated total reflectance Fourier-transform infrared (ATR-FTIR) spectroscopy**

The functionalization of the MWCNTs outer surfaces' by HDA was studied by ATR-FTIR spectroscopy. Figure 5.1 shows the ATR-FTIR spectra of neat PLA, the f-MWCNTs and the

PLA/f-MWCNTs composite. The spectrum of the composite shows the characteristic peaks of PLA and the f-MWCNTs. The broad peak in the spectrum of the f-MWCNTs represents the N-H stretching of HDA. This broad peak also appears in the spectrum of the composite. The peak at  $1592\text{ cm}^{-1}$  (indicated by \*) in the spectrum of the f-MWCNTs represents the primary amine N-H deformation of HDA. This peak is also observed in the spectrum of the composite at  $1645\text{ cm}^{-1}$  (also indicated by \*). These results confirm the presence of f-MWCNTs in the composite. However, it is difficult to establish whether there is a possible interfacial interaction between the PLA and the HDA chains, because we could not get a clear peak of the N-H stretching in both the f-MWCNTs and the composite spectra.

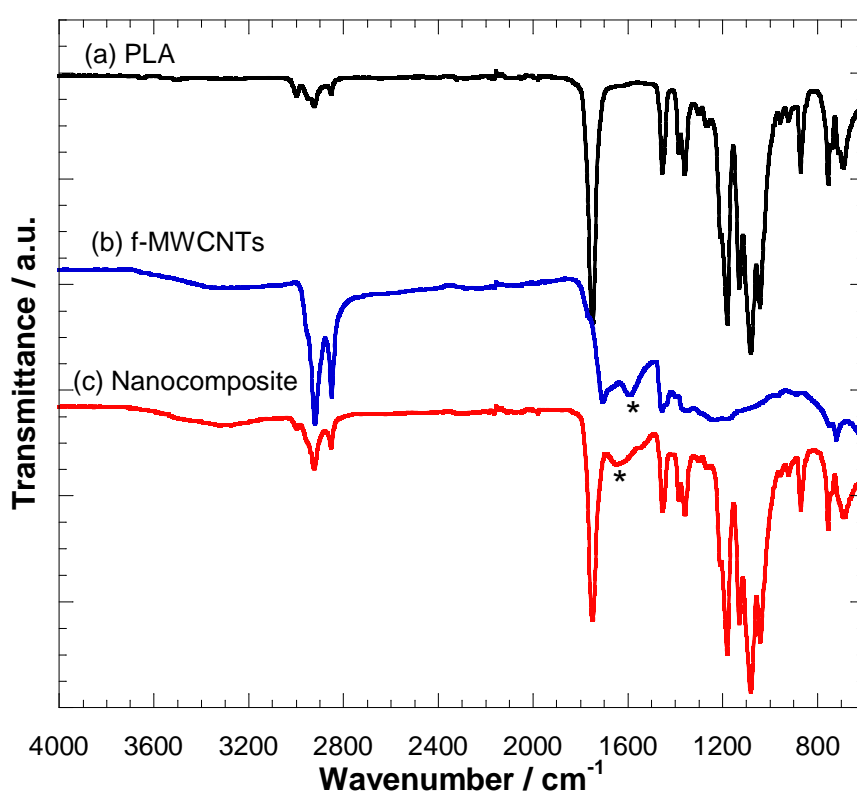


**Figure 5.1** FT-IR spectra of pure PLA, f-MWCNTs, and the nanocomposite.

### 5.2.2 Raman spectroscopy

Raman spectroscopy was used to verify the presence of possible interfacial interactions between f-MWCNTs and the matrix of PLA. Figure 5.2 shows the Raman spectra of the f-MWCNTs and the corresponding nanocomposite of PLA. It can be seen from the spectra that there is a small shift in the characteristic *D*-band and a quite significant shift in the *G*-band of

the f-MWCNTs to higher wavenumbers in the case of the nanocomposite. This indicates the presence of interfacial interactions between the PLA chains and the f-MWCNTs surfaces. It can also be seen that the characteristic peak of the PLA matrix (appearing at  $1450\text{ cm}^{-1}$  for neat PLA, refer to Chapter 4) moves toward higher a wavenumber of  $1453\text{ cm}^{-1}$ . This observation further confirms the presence of some interactions between the PLA matrix and the f-MWCNT surfaces.

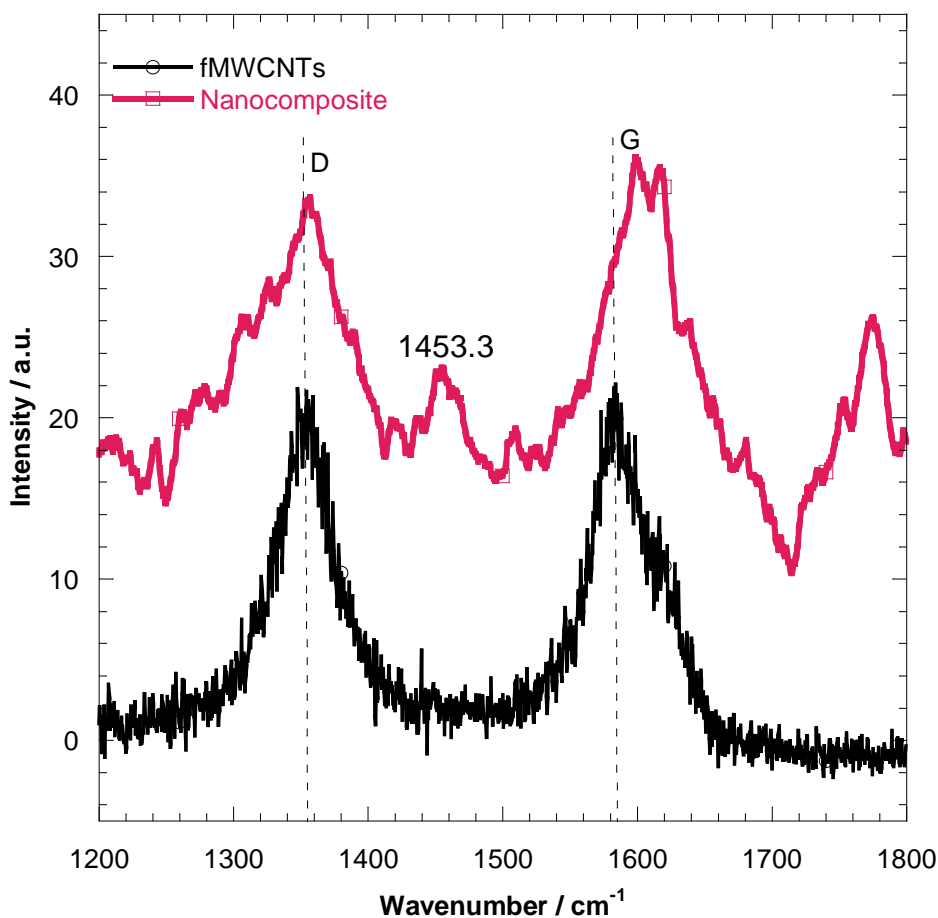


**Figure 5.2** Raman spectra of PLA and its nanocomposite.

### 5.2.3 Scanning electron microscopy

The dispersion of the f-MWCNTs in the PLA matrix was studied using a scanning electron microscope (SEM) operated at an accelerated voltage of 2 kV. Figure 5.3(a) represents the SEM image of the freeze fractured surface of the PLA/f-MWCNT nanocomposite. The polymer matrix surface with some white spots is clearly seen. Two areas, with and without

white spots, were selected and magnified. They are shown in Figure 5.3(b & c). In these pictures a fairly good dispersion of CNTs can be seen, but the white spots are clearly the result of agglomeration of f-MWCNTs in the PLA matrix at a micron scale level. Agglomeration of MWCNTs in the PLA matrix suggests that part of the surface area of CNTs could not be accessed during functionalization by HDA. This is due to the intrinsic van der Waals forces keeping the MWCNTs together as bundles. Based on these observations, it can be concluded that the homogenous dispersion of the f-MWCNTs is the result of improved interaction between the PLA matrix and the HDA chains on the surface of the MWCNTs, as established in Raman results.

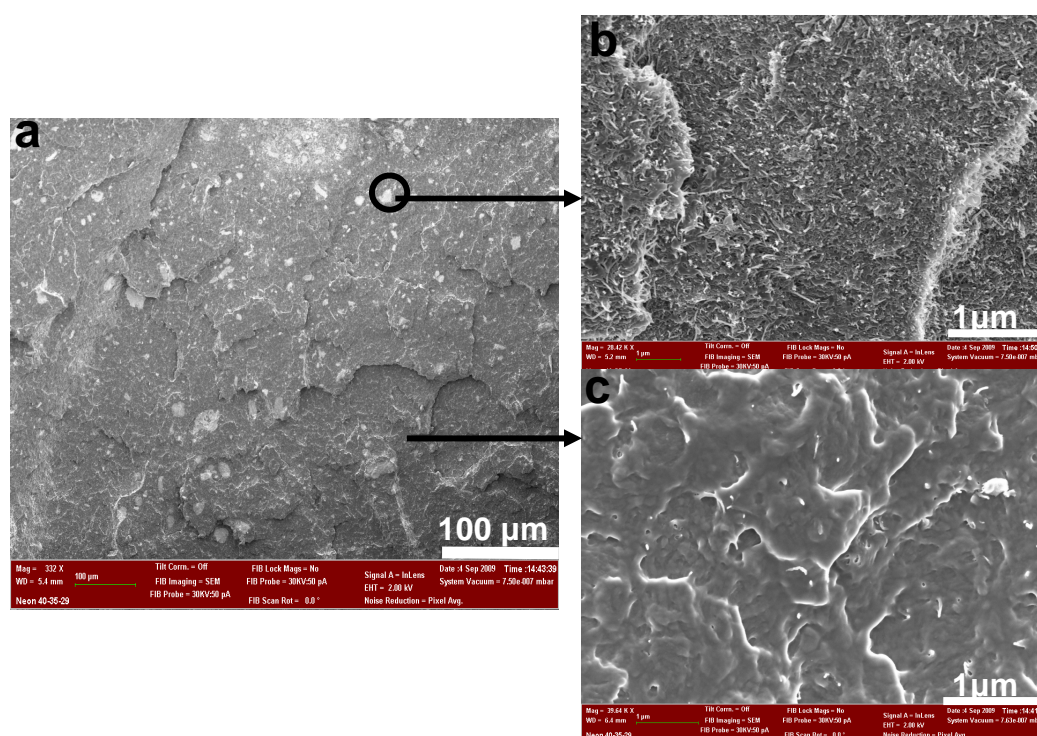


**Figure 5.3** Scanning electron microscopy images of a nanocomposite containing 0.5 wt.% f-MWCNTs with two selected spots at different magnifications.

### 5.2.4 Polarized optical microscopy

To further verify the good dispersion of the f-MWCNTs in the PLA matrix, the composite was investigated through an optical microscopy at 190 °C where PLA was in the molten state. These results are presented in Figure 5.4. The dark spots represent agglomerates of CNTs.

This image clearly shows that there is indeed homogenous dispersion of f-MWCNTs with few agglomerates at micron scale, as shown by the dark spots. Again, this results support the SEM results.

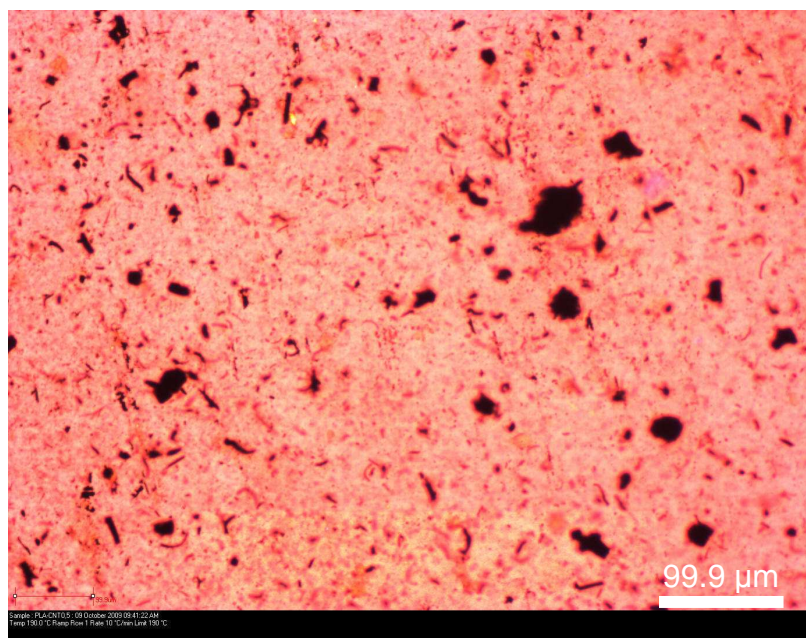


**Figure 5.4** Optical microscopic image of the PLA/f-MWCNTs nanocomposite taken at 190 °C in the transmittance mode. This is the representative image of images taken from five different positions.

### **5.2.5 The effect of cooling rate on the non-isothermal crystallization behaviour of PLA**

To study the influence of cooling rates on the non-isothermal crystallization behaviour of PLA, the samples were heated to 190 °C at a heating rate of 20 °C.min<sup>-1</sup>, kept at this temperature for 5 min, and then cooled down to -20 °C at different cooling rates. The cooling curves of pure PLA and its composite during non-isothermal crystallization from their melts at five different cooling rates are shown in Figure 5.5. In the case of neat PLA, a broad peak is observed when the sample was cooled from the melt at a rate of 0.5 °C.min<sup>-1</sup>. With an increase in cooling rate to 1 °C.min<sup>-1</sup>, a peak with a shoulder peak appears and shifts towards lower temperatures. The peak shoulders indicate a continuous change of enthalpy. It is clear

that at cooling rates higher than  $5\text{ }^{\circ}\text{C}\cdot\text{min}^{-1}$ , it is very difficult for the PLA matrix to fully crystallize and the polymer stays in a super-cooled state. The crystallization peak shifts to lower temperatures as the cooling rate is increased is a natural observation, because it is difficult for the polymer chains to crystallize at faster cooling rates. A small crystallization peak appears at  $126\text{ }^{\circ}\text{C}$  for the composite when the cooling rate from the melt is  $0.5\text{ }^{\circ}\text{C}\cdot\text{min}^{-1}$ . It is further observed that this peak does not clearly show the double thermal event that was observed in the case of the neat PLA. This peak also shifts to lower temperatures as the cooling rate increases to  $1\text{ }^{\circ}\text{C}\cdot\text{min}^{-1}$ . A further increase in the cooling rates to  $5\text{ }^{\circ}\text{C}\cdot\text{min}^{-1}$  also shows the presence of a double peak as in the case of PLA. The crystallization peaks for the nanocomposite, for all the investigated cooling rates, are more intense and better resolved than those for neat PLA. What is more interesting is that even at a faster cooling rate of  $10\text{ }^{\circ}\text{C}\cdot\text{min}^{-1}$ , the nanocomposite is still able to crystallize. Based on the observations above, it can be concluded that f-MWCNTs act as nucleating agents for the crystallization of the PLA matrix.

To confirm the nucleating effect of the f-MWCNTs during non-isothermal crystallization, the samples were investigated through POM. For the POM measurements, a cooling rate of  $10\text{ }^{\circ}\text{C}\cdot\text{min}^{-1}$  was selected because during injection moulding the cooling rates are usually very fast. The POM images of the PLA and its nanocomposite, taken at  $130\text{ }^{\circ}\text{C}$  during isothermal crystallization from their melt, are shown in Figure 5.6. The images show large spherulites for the neat PLA sample, but much smaller and more densely packed crystallites for the nanocomposite. This observation indicates that the f-MWCNT nanoparticles formed nucleating sites for the formation of small spherulites in the nanocomposite.

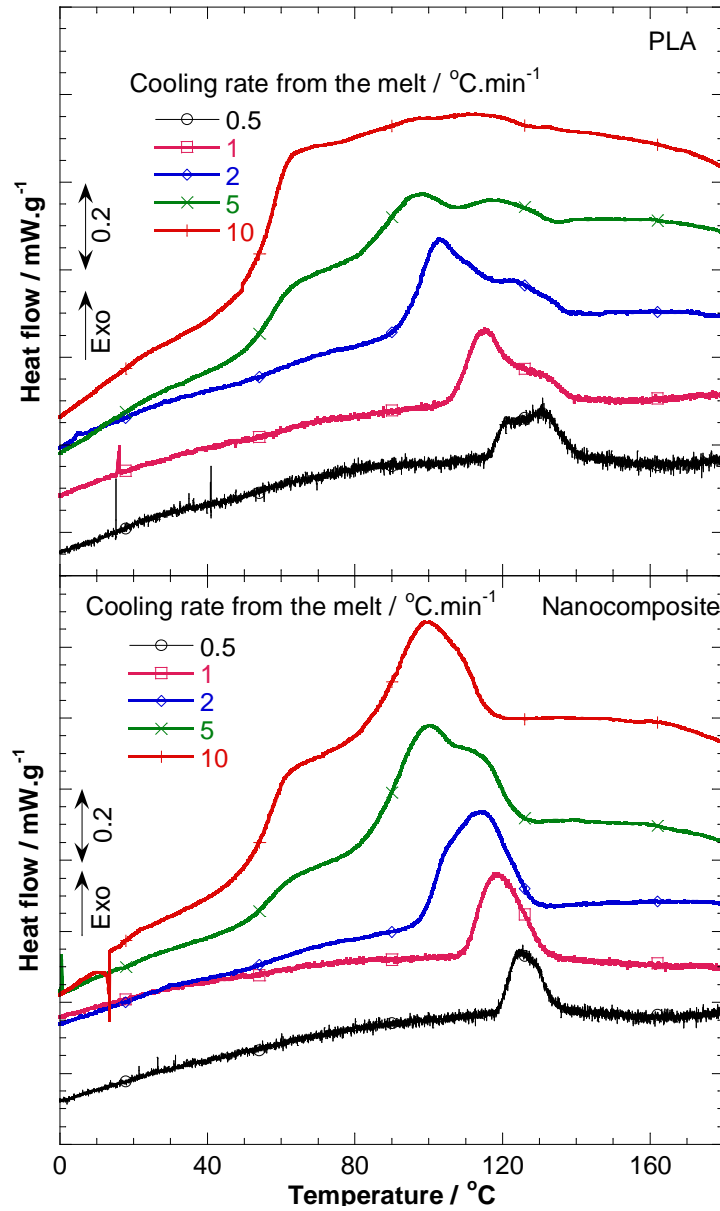


**Figure 5.5** DSC heating curve of PLA and its nanocomposite after non-isothermal crystallization at different cooling rates.

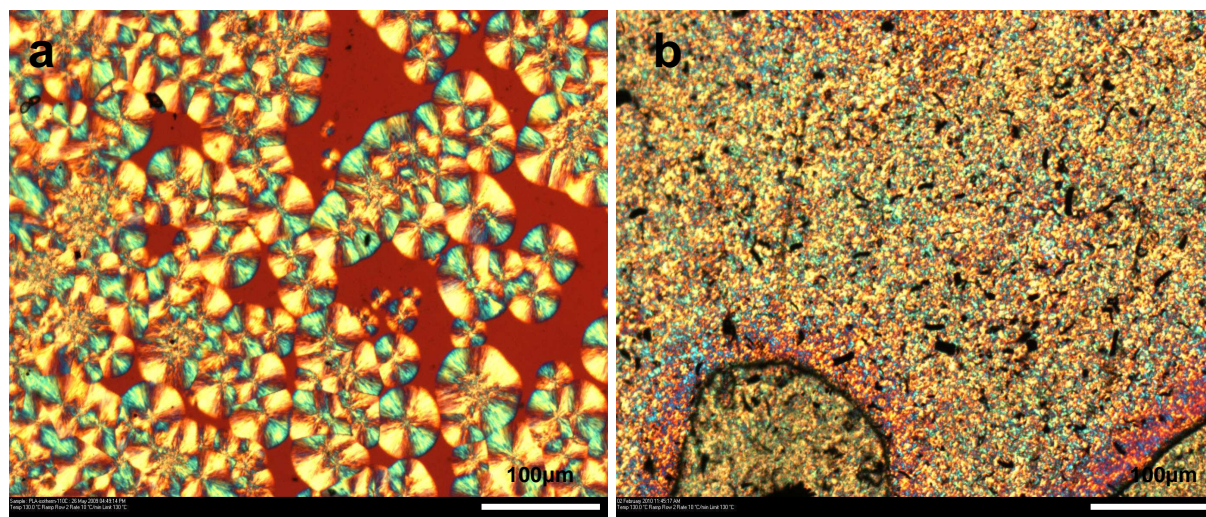


**Figure 5.6** Polarized optical micrographs of (a) neat PLA and (b) the PLA/f-MWCNT nanocomposite. Both samples were crystallized at 130 °C from their melts.

### 5.2.6 Effect of cooling rates on melting behaviour of PLA

In order to study the effect of cooling rates on the melting behaviour, PLA and its nanocomposite were heated from -20 to 190 °C at 20 °C.min<sup>-1</sup> as soon as the cooling was finished. These heating curves are presented in Figure 5.7, and the DSC data are summarized in Table 5.1. It can be seen that PLA only shows cold crystallization peaks and two melting peaks when the cooling rates were 5 and 10 °C min<sup>-1</sup>. The composite also shows cold crystallization peaks at the same cooling rates, but single melting peaks. This observation indicates that the crystallization of PLA chains was not completed during cooling at the faster cooling rates, and the crystallization process continued during heating. The double melting peaks indicate the presence of different types of crystals with different stabilities. Nam *et al.* [20] also suggested that the double melting peaks of PLA may be due to the presence of less perfect crystals having enough time to melt and rearrange into crystals with higher structural perfection, which re-melted at higher temperatures during heating in the DSC. However, when the cooling rates were 0.5, 1, and 2 °C.min<sup>-1</sup>, no cold crystallization peak was observed for both PLA and its nanocomposite. This indicates that the crystallization of PLA chains was completed at slower cooling rates during the non-isothermal cooling process. Single melting peaks were observed when the cooling rate was 0.5 °C.min<sup>-1</sup> for both samples. In brief, the

nanocomposite shows two distinct melting peaks when the cooling rate was 2 °C.min<sup>-1</sup> in comparison to the neat polymer. This is an indication that the nucleation effect of f-MWCNTs in the polymer matrix assisted in the formation of more perfect crystals.

By integrating the area under the endothermic region of the DSC curves, and by subtracting the extra heat absorbed by the crystallites formed during cold crystallization, the melting enthalpy ( $\Delta H_m$ ) of all the samples was calculated, and at the same time the degree of crystallinity ( $\chi_c$ ) was estimated by considering the melting enthalpy of 100% crystalline PLA as 93 J.g<sup>-1</sup> [21]. The  $\chi_c$  data in Table 5.1 show that the overall crystallinity of PLA was reduced when 0.5 wt.% f-MWCNTs was added. A decrease in overall crystallinity may be as a result of two factors: MWCNT agglomerates acting as active nucleation sites and at the same time, the non-agglomerated sites inhibiting mobility of the polymer chains. Because of the well-dispersed f-MWCNTs crystal growth was inhibited, thus leading to a decrease of crystallinity.

**Table 5.1 Cooling rate dependence of the melting enthalpy from two melting peaks of the PLA and the composite**

Sample	Cooling rate	Melting enthalpy / J g <sup>-1</sup> <sup>a</sup>	% crystallinity <sup>b</sup>
PLA	0.5	53.0	57.0
	1	44.4	47.8
	2	41.1	44.2
	5	37.6	40.4
	10	37.6	40.4
Nanocomposite	0.5	48.0	51.6
	1	40.1	43.1
	2	39.1	42.0
	5	38.8	41.7
	10	33.9	36.5

<sup>a</sup> The total melting enthalpy of PLA evaluated by integration of the area under the endothermic peaks from the heating scans after non-isothermal crystallization.

<sup>b</sup> Calculated using the melting enthalpy of 100% crystalline PLA, 93 J g<sup>-1</sup> [21].

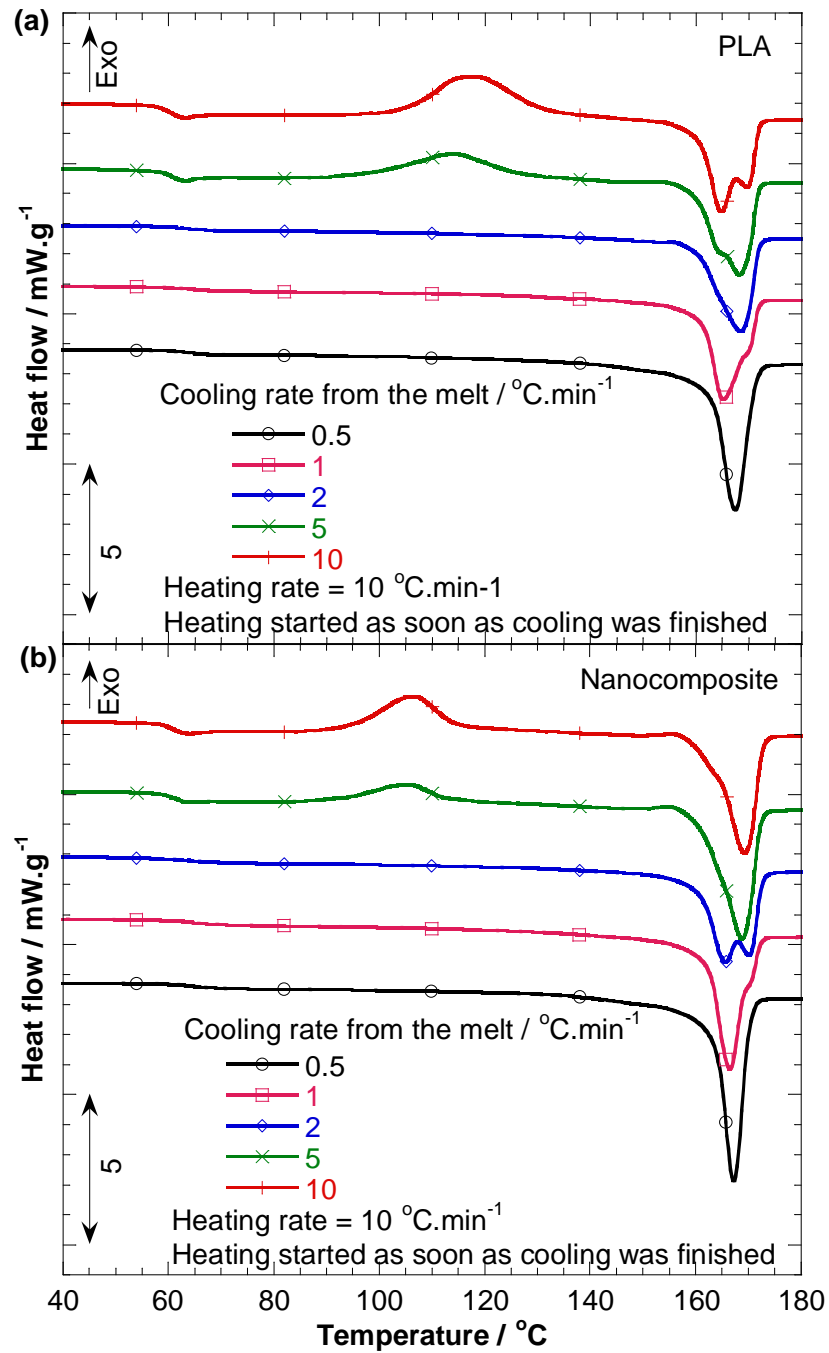


**Figure 5.7** DSC heating curves of PLA and the nanocomposite after non-isothermal crystallization at five different cooling rates.

### 5.2.7 Temperature modulated DSC

To separate the heat capacity and kinetically related components during cold crystallization and subsequent melting of neat PLA and its nanocomposite, TMDSC of melt quenched samples were done. TMDSC allows us to see whether any re-crystallization process occurs as soon as PLA begins to melt. This has been used to confirm the presence of melting, re-crystallization, and re-melting processes. Figure 5.8 illustrates the TMDSC curves of (a) neat PLA and (b) its nanocomposite during the second heating. The samples were first equilibrated at  $-20\text{ }^{\circ}\text{C}$  for 30 min., and then heated to  $190\text{ }^{\circ}\text{C}$  at a rate of  $2\text{ }^{\circ}\text{C}\cdot\text{min}^{-1}$ , kept at that temperature for 5 min. to destroy any previous thermal history, and cooled to  $-20\text{ }^{\circ}\text{C}$  at a rate of  $2\text{ }^{\circ}\text{C}\cdot\text{min}^{-1}$ . TMDSC was started as soon as the cooling was finished. For both samples the total heat flow (middle curve) is separated into well defined reversible heat flow (bottom curve) and non-reversible heat flow (top curve). For neat PLA, the following behaviour is observed: two melting signals on the reversible heat flow curve are accompanied by the subsequent re-crystallization on the non-reversible heat flow curve, with the total heat flow curve showing only the melting peaks. This observation may be due to the partial melting and perfection of different crystals at temperatures before their final melting. For the nanocomposite, two melting peaks are observed for all the heat flow curves with no apparent re-crystallization. What is more notable is that the two melting peaks of the nanocomposite on the reversible heat flow curve are now distinct in comparison with the peaks for the neat polymer. This indicates the presence of different forms of crystals with different thermal stabilities. Another interesting feature is that TMDSC enabled us to see partial re-crystallization occurring in the neat polymer, which is absent in the composite.

To estimate the percent crystallinity ( $\chi_c$ ) of the samples, we took the enthalpy of melting ( $\Delta H_f$ ) from the reversible heat flow curve, divided this value by the enthalpy of a 100% crystalline polymer ( $\Delta H_f$  for 100 % crystalline PLA is  $93\text{ J}\cdot\text{g}^{-1}$  [21]), and multiplied the answer by 100%. The data is reported in Table 5.2. These values indicate that the crystallinity of the PLA matrix decreased in the presence of the f-MWCNTs.

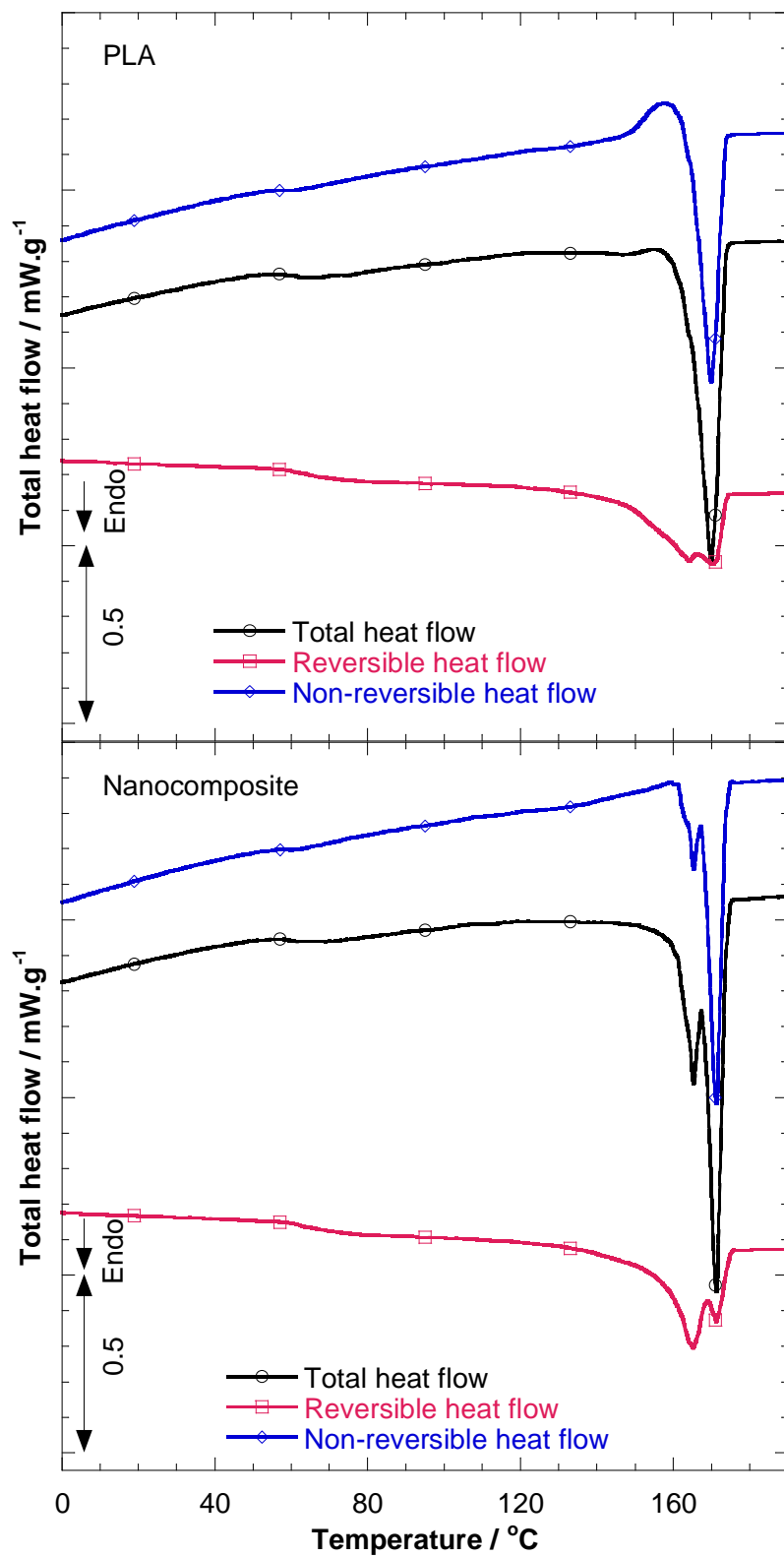


**Figure 5.8** TMDSC curves of (a) PLA and (b) the nanocomposite during second heating.

**Table 5.2 TMDSC data for PLA and its nanocomposite.**

Sample	Total			Reversible				Non-reversible			$\chi_c$ %
	$T_{m1}$ °C	$T_{m2}$ °C	$\Delta H_f$ J.g <sup>-1</sup>	$T_g$ °C	$T_{m1}$ °C	$T_{m2}$ °C	$\Delta H_f$ J.g <sup>-1</sup>	$\Delta H_c$ J.g <sup>-1</sup>	$\Delta H_f$ J.g <sup>-1</sup>	$T_m$ °C	
PLA	169.9	-	43.54	62.2	164.2	169.8	30.1	8.9	26.7	169.9	19.1
Composite	165.3	171.2	44.94	62.0	165.3	171.2	26.9	1.7	24.3	171.0	24.3

### 5.2.8 Wide angle X-ray scattering

To study the presence of different PLA crystals and their modification, WAXS of the neat PLA and nanocomposite samples were performed. The measurements were taken from room temperature to the melting temperature, and then back to room temperature. The samples were kept at each temperature for 5 minutes, including 1 minute exposure to the X-rays. Figure 5.9 shows the one-dimensional WAXS patterns of PLA and the nanocomposite obtained under these conditions. Overall, there is no sign of the modification of existing crystals or the formation of new crystals. The notable observation is when both samples were cooled from their melts. It is clear that it is very difficult for PLA to crystallize during cooling. However, crystals are formed in the presence of f-MWCNTs as shown by the fully resolved peaks in the spectra of the nanocomposite. Again, this supports the nucleation effect of f-MWCNTs in the polymer matrix. However, a very small peak is observed on the spectra of both samples at around  $2\theta = 22.5^\circ$ . This observation suggests the growth of another type of crystal.

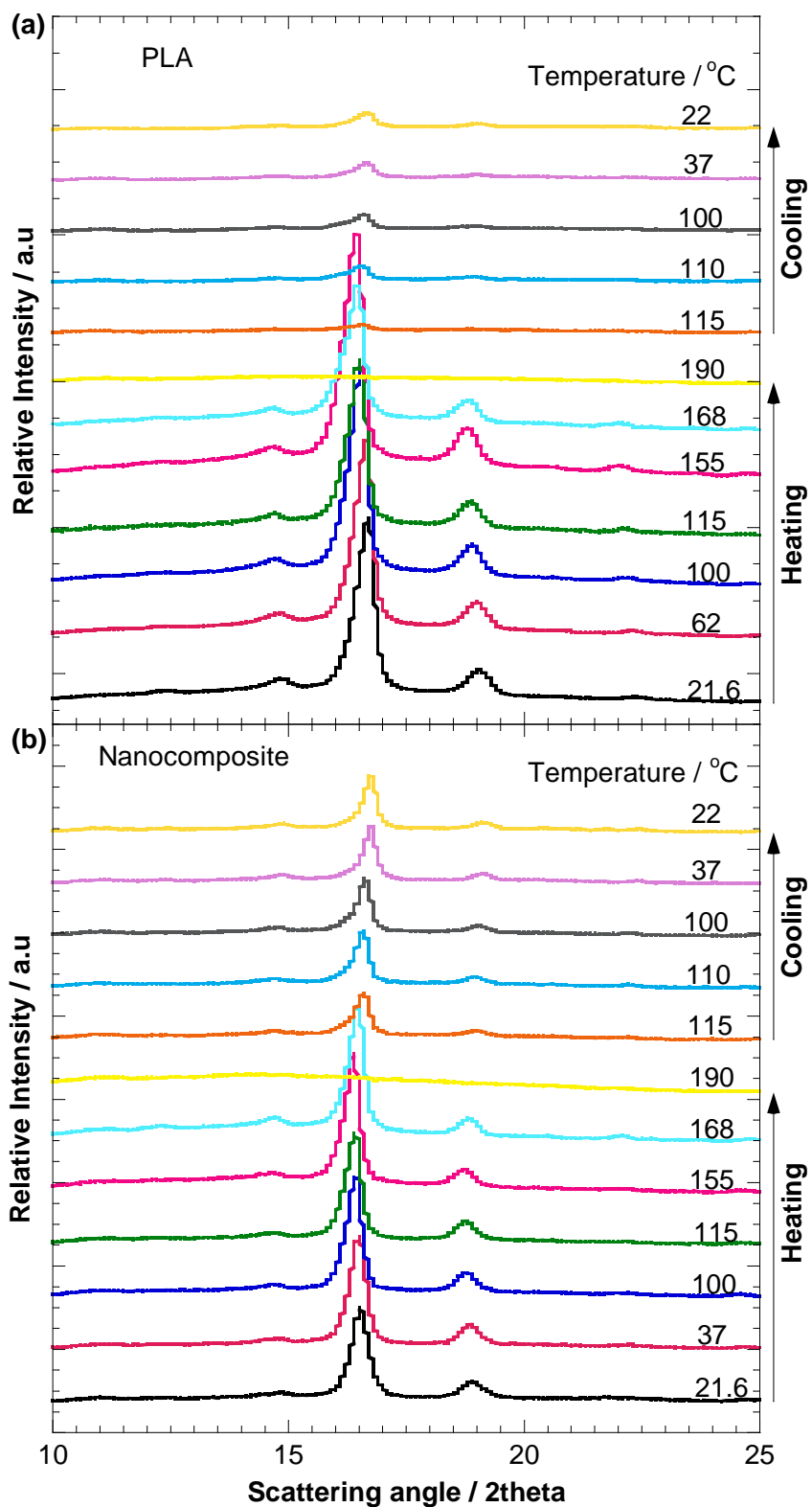


**Figure 5.9** Temperature dependence wide-angle X-ray scattering patterns of (a) neat PLA and (b) the nanocomposite samples during both heating and cooling cycles.

### 5.2.9 Thermogravimetric analysis

This section discusses the thermal stabilities of neat PLA and the nanocomposite in a thermo-oxidative environment. The TGA and the first dTGA curves of neat PLA and the nanocomposite obtained under oxygen flow are presented in Figure 5.10. The dTGA are presented because they more clearly show the difference in thermal stabilities between the samples. Both samples show a one-step decomposition. The thermal stability of the nanocomposite is higher than that of the neat PLA. This improvement can be attributed to the fairly homogenous dispersion of the f-MWCNTs. The thermal stability of the nanocomposite may also be due to the higher thermal stability of the CNTs in comparison to that of PLA. The dTGA peak of the nanocomposite shifts to a higher temperature compared to that of the neat PLA sample. This is also an indication of the improvement in thermal stability of PLA in the presence of the f-MWCNTs.

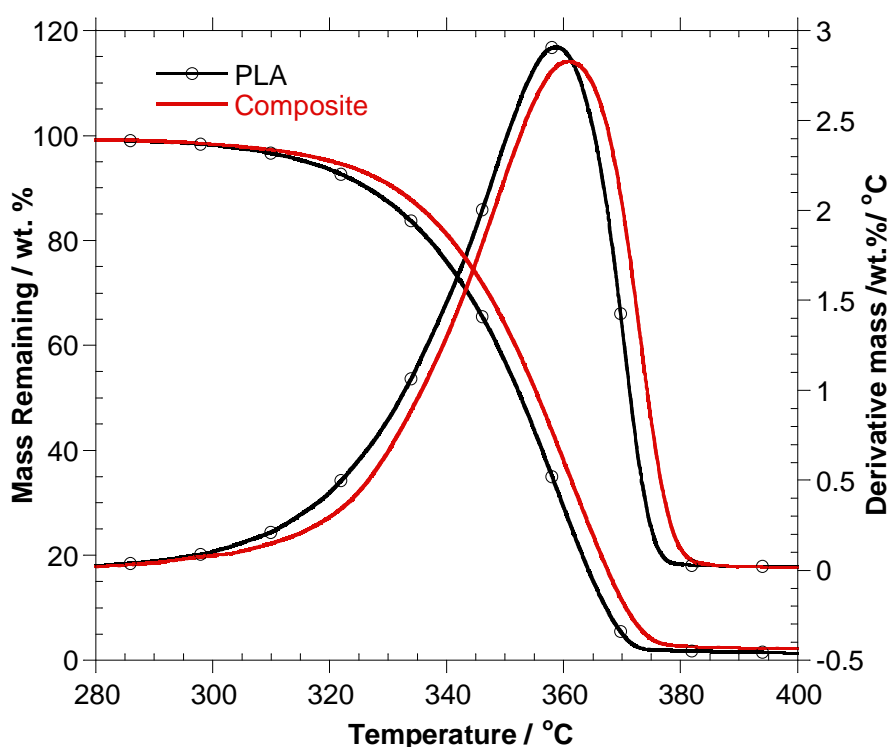


**Figure 5.10** TGA and derivative TGA curves of PLA and the nanocomposite under oxygen flow at a heating rate of  $10\text{ }^{\circ}\text{C min}^{-1}$ .

### 5.2.10 Dynamic mechanical analysis

DMA generally reveals the amount of energy stored in the nanocomposite as elastic energy, and the amount of energy dissipated during mechanical strain, which strongly depends on the geometrical characteristics and the level of dispersion of the filler in the matrix. It also depends on the degree of interaction between the matrix and the filler [22]. Figure 5.11 (a and b) represents the storage modulus ( $G'$ ) and the damping factor ( $\tan \delta$ ) curves for PLA and the nanocomposite, respectively. The damping factor provides information on the relative contributions of the viscous and elastic components of the viscoelastic material. Figure 5.11a shows three phenomena: (1) from 0-50 °C, there is an increase in modulus. This is because both samples are stiff because there is not yet chain mobility, but the nanocomposite is stiffer due to the presence stiff f-MWCNTs; (2) from 50-80 °C, there is a sudden drop of modulus because the chains of the surfactant (HDA) exhibits a plasticizing effect on the polymer matrix just below and above the glass transition temperature; (3) from 80-160 °C, there is a slight improvement of modulus because the presence of fairly homogeneously dispersed f-MWCNTs inhibits the PLA chain mobility. Figure 5.11b clearly indicates that there is a decrease in the glass transition temperature from 74 to 71 °C. This supports the observation of a plasticizing effect of the HDA chains in the PLA matrix. From these observations it may be concluded that the fairly homogeneously dispersed f-MWCNTs in the PLA matrix improved the storage modulus below and above the glass transition temperature. Also, the f-MWCNTs acted as a plasticizer of the PLA matrix at around the glass transition temperature.

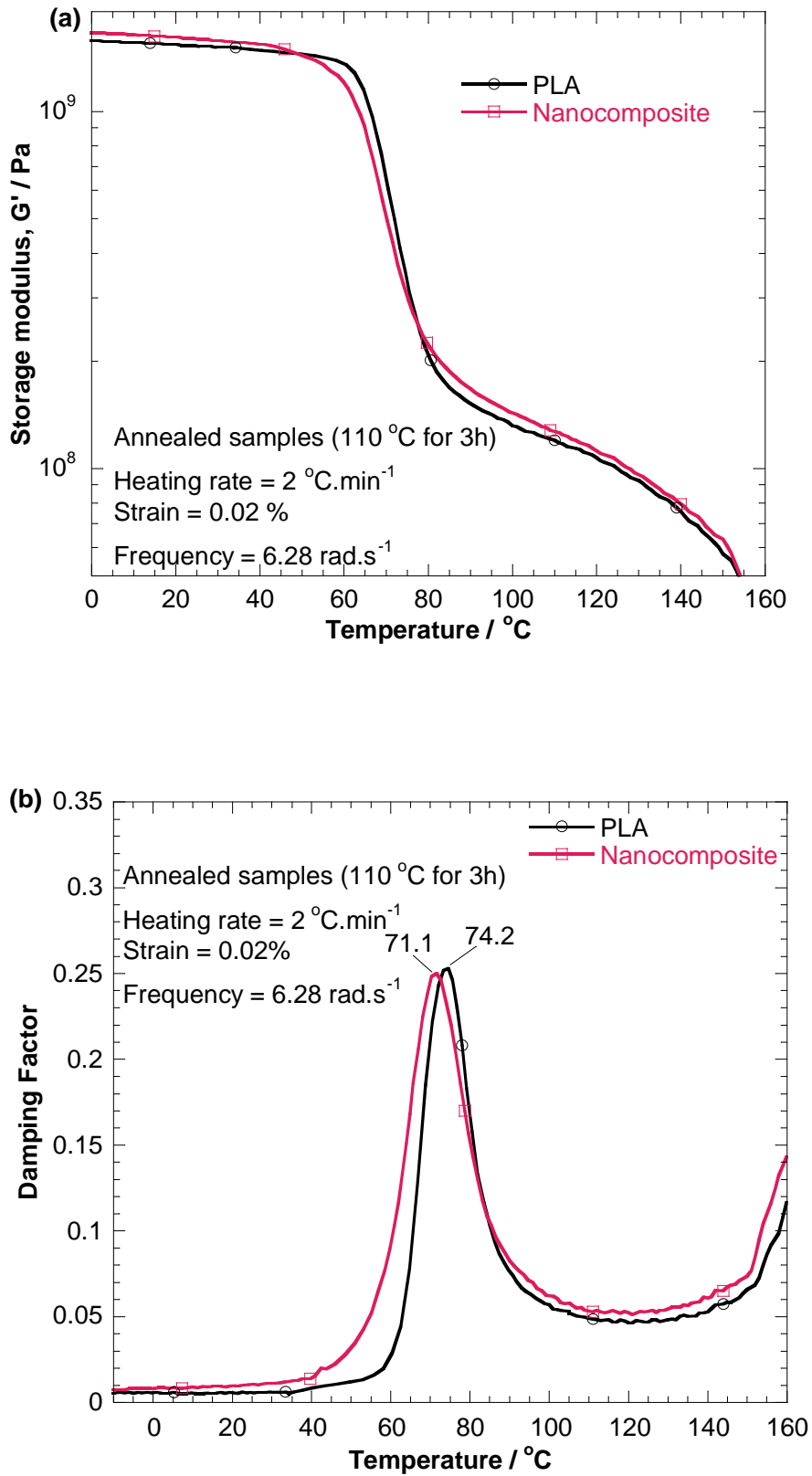


**Figure 5.11** Temperature dependence of dynamic mechanical properties of neat PLA and its nanocomposite: (a) storage modulus and (b) damping factor.

### 5.3 Conclusions

This chapter discussed the morphology, thermal, and thermomechanical properties of a PLA nanocomposite containing 0.5 wt.% of f-MWCNTs (with an amine content of 20 %). The SEM and POM (of the samples in the molten state) results confirm the homogenous dispersion of f-MWCNTs in the PLA matrix, with some micro-agglomeration. The POM results also show the formation of much smaller PLA crystallites in the presence of f-MWCNTs. The f-MWCNTs were found to play a nucleation role in the crystallization of PLA, as observed from the DSC, SEM, and WAXS results. The DMA and TGA results show that the presence of f-MWCNTs had only a slight influence on the thermomechanical properties and thermal stability of the PLA. FTIR and Raman spectroscopy confirmed the functionalization of the MWCNTs, and the presence of facial interaction between f-MWCNTs and the PLA matrix.

### 5.4 References

- [1] S. Sinha Ray, P. Maiti, M. Okamoto, K. Yamada, K. Ueda. New polylactide/layered silicate nanocomposites. I. Preparation, characterization and properties. *Macromolecules* 2002; 35:3104–3110.
- [2] S. Sinha Ray, K. Yamada, M. Okamoto, A. Ogami, K. Ueda. New polylactide/layered silicate nanocomposites. 3. High performance biodegradable materials. *Chemistry of Materials* 2003; 15:1456–1465.
- [3] S. Sinha Ray, K. Yamada, M. Okamoto, K. Ueda. Biodegradable polylactide/montmorillonite nanocomposites. *Journal of Nanoscience and Nanotechnology* 2003; 3:503-510.
- [4] C.R. Tseng, J.Y. Wu, Y.H. Lee, F.C. Chang. Preparation and crystallization behaviour of syndiotactic polystyrene-clay nanocomposites. *Polymer* 2001; 42:10063-10070.
- [5] R.A. Vaia, H. Ishii, E.P. Giannelis. Synthesis and properties of two-dimensional nanostructures by direct intercalation of polymer melts in layered silicates. *Chemistry of Materials* 1993; 5:1694-1696.
- [6] M. Okamoto, S. Morita, T. Kotaka. Dispersed structure and ionic conductivity of smectic clay/polymer nanocomposites. *Polymer* 2001; 42:2685-2688.

- [7] B. Lepoitevin, N. Pantoustier, M. Alexandre, C. Calberg, R. Jerome, P. Dubois. Polyester layered silicate nanohybrids by controlled grafting polymerization. *Journal of Materials Chemistry* 2002; 12:3528-3532.
- [8] F.T. Fisher, R.D. Bradshaw, L.C. Brinson. Effects of nanotube waviness on the modulus of nanotube-reinforced polymers. *Applied Physics Letters* 2002; 80:4647-4649.
- [9] Z. Yao, N. Braidy, G.A. Botton, A. Adronov. Polymerization from the surface of single-walled carbon nanotubes – Preparation and characterization of nanocomposites. *Journal of the American Chemical Society* 2003; 125:16015–16024.
- [10] S. Qin, D. Qin, W.T. Ford, D.E. Resasco, J.E Herrera. Functionalization of single-walled carbon nanotubes with polystyrene via grafting to and grafting from methods. *Macromolecules* 2004; 37:752–757.
- [11] J. Chen, R. Ramasubramaniam, C. Xue, H. Liu. A versatile molecular engineering approach to simultaneously enhanced, multifunctional carbon-nanotube–polymer composites. *Advanced Functional Materials* 2006; 16:114-119.
- [12] P. Calvert. Nanotube composites: A recipe for strength. *Nature* 1999; 399:210-211.
- [13] H.S. Kim, B.H. Park, J.S. Yoon, H.J. Jin. Thermal and electrical properties of poly(L-lactide)-graft-multiwalled carbon nanotube composites. *European Polymer Journal* 2007; 43:1729–1735.
- [14] Y.T. Shieh, G.L. Liu. Effects of carbon nanotubes on crystallization and melting behaviour of poly(L-lactide) via DSC and TMDSC studies. *Journal of Polymer Science Part B Polymer Physics* 2007; 45:1870–1881.
- [15] G.X. Chen, H.S. Kim, B.H. Park, J.S. Yoon. Synthesis of poly(L-lactide)-functionalized multiwalled carbon nanotubes by ring-opening polymerization. *Macromolecular Chemistry and Physics* 2007; 208:389–398.
- [16] H. Tsuji, Y. Kawashima, H. Takikawa, S. Tanaka. Poly(L-lactide)/nano-structured carbon composites: Conductivity, thermal properties, crystallization, and biodegradation. *Polymer* 2007; 48:4213–4225.
- [17] G.X. Chen, H. Shimizu. Multiwalled carbon nanotubes grafted with polyhedral oligomeric silsesquioxane and its dispersion in poly(L-lactide) matrix. *Polymer* 2008; 49:943–991.
- [18] D. Wu, L. Wu, M. Zhang, Y. Zhao. Viscoelasticity and thermal stability of polylactide composites with various functionalized carbon nanotubes. *Polymer Degradation and Stability* 2008; 93:1577–1584.

- [19] J. Ramontja, S. Sinha Ray, S.K. Pillai, A.S. Luyt. High-performance carbon nanotube-reinforced bioplastic. *Macromolecular Materials and Engineering* 2009; 294:839-846.
- [20] J.Y. Nam, S.S. Ray, M. Okamoto. Crystallization behaviour and morphology of biodegradable polylactide/layered silicate nanocomposite. *Macromolecules* 2003; 36:7126–7131.
- [21] E.W. Fisher, H.J. Sterzel, G. Wegner. Investigation of the structure of solution grown crystals of lactide copolymers by means of chemical reactions. *Kolloid-Zeitschrift and Zeitschrift fur Polymere* 1973; 25:980-990.
- [22] E.T. Michelson, C.B. Hoffman, A.G. Finzler, R.E. Smalley, R.H. Hauge, J.L. Margrave. Fluorination of single-wall carbon nanotubes. *Chemical Physics Letters* 1998; 296:188-194.

## **Chapter 6**

### **Unusual crystallization behaviour of carbon nanotubes-containing biodegradable polylactide composite**

#### **6.1 Introduction**

In recent years, various types of nano-fillers have been used as reinforcement materials for polymer matrices [1-12]. Among these nano-fillers, carbon nanotubes (CNTs) have been receiving special attention because of their extraordinary high modulus and strength, their excellent electrical conductivity along with their important thermal conductivity and stability and finally, their very low density [13-15]. The homogeneous dispersion of CNTs in a polymer matrix can lead to a moderate improvement in the electrical properties with a balance of mechanical properties.

The incorporation of CNTs can also affect the crystallization kinetics, spherulite growth and morphology, and the degree of crystallinity of a semicrystalline polymer matrix [16–20]. In general, it has been found that the incorporation of CNTs, which act as nucleation sites, tends to increase the rate of crystallization of the matrix [21]. In most reported studies it was found that the dispersed CNTs are strongly agglomerated and hence crystallization of the polymer chains occurs in a bulk and not in confined spaces. In this chapter, we found that the crystallization behaviour of a semicrystalline polymer such as PLA is completely changed when CNTs are homogeneously dispersed in the matrix. This chapter summarizes various properties of a PLA composite containing 1.5 wt.% of f-MWCNTs prepared through a solution casting method. The f-MWCNTs used in this work contain  $\pm 10\%$  (determined gravimetrically) of HDA.

#### **6.2 Results and discussion**

POM was used to check the spherulitic growth behaviour of the PLA matrix before and after composite formation. Figure 6.1 shows the crystal growth behaviour of neat PLA and the

composite at 130 °C from their melts. It can be seen from the POM images that it is very difficult for PLA crystals to grow fast in the presence of f-CNTs. This result implies that the nucleating role of f-CNTs in the crystallization of the PLA matrix is almost non-existent. Such an observation is completely contrary to what was observed when the PLA/f-CNT composite was prepared by a melt-mixing technique (Chapter 4), and also quite uncommon to the general understanding of the role of CNTs towards semicrystalline polymer crystallization [21]. We believe this observation is the result of a superstructure templating effect associated with the non-agglomerated (nano-level) dispersion of the CNTs in the PLA matrix that, in turn, retards the PLA crystals to grow fast.

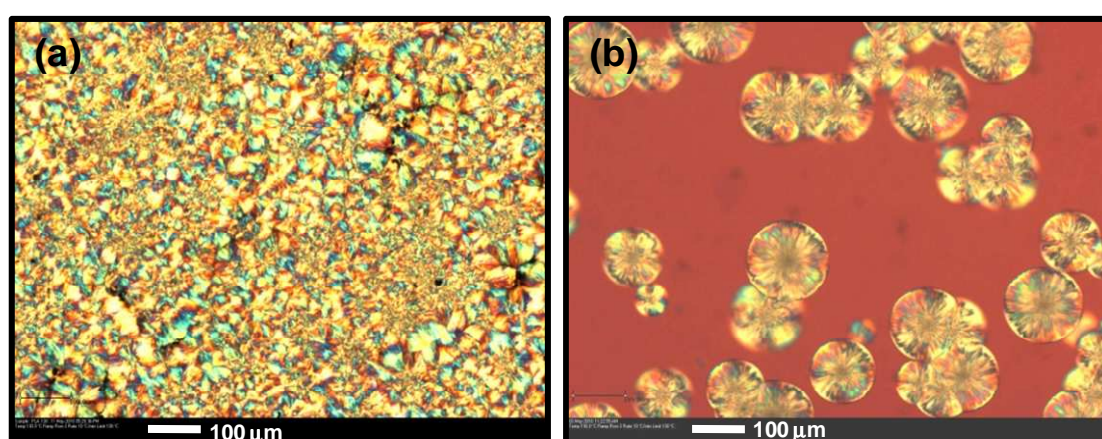


**Figure 6.1** Polarized optical micrographs of (a) neat PLA and (b) the PLA/f-MWCNT composite. Both samples were crystallized at 130 °C from their melts.

To understand the effect of f-MWCNTs incorporation on the crystallization behaviour of the PLA matrix, DSC experiments of neat PLA and the PLA/f-CNTs composite samples were carried out. The crystallization exotherms of neat PLA and its f-CNTs-containing composite during non-isothermal crystallization from their melts at a cooling rate of 10 °C.min<sup>-1</sup> are shown in Figure 6.2(a). Both samples show two exotherms – the first one is prominent (from the low temperature side) and the other one is very small. This indicates the growth of two different crystal fractions during cooling. On the other hand, in the case of the composite, both exotherms appear at much lower temperatures than those of neat PLA. This result again supports the inactive nucleation role of f-CNTs for PLA crystallization.

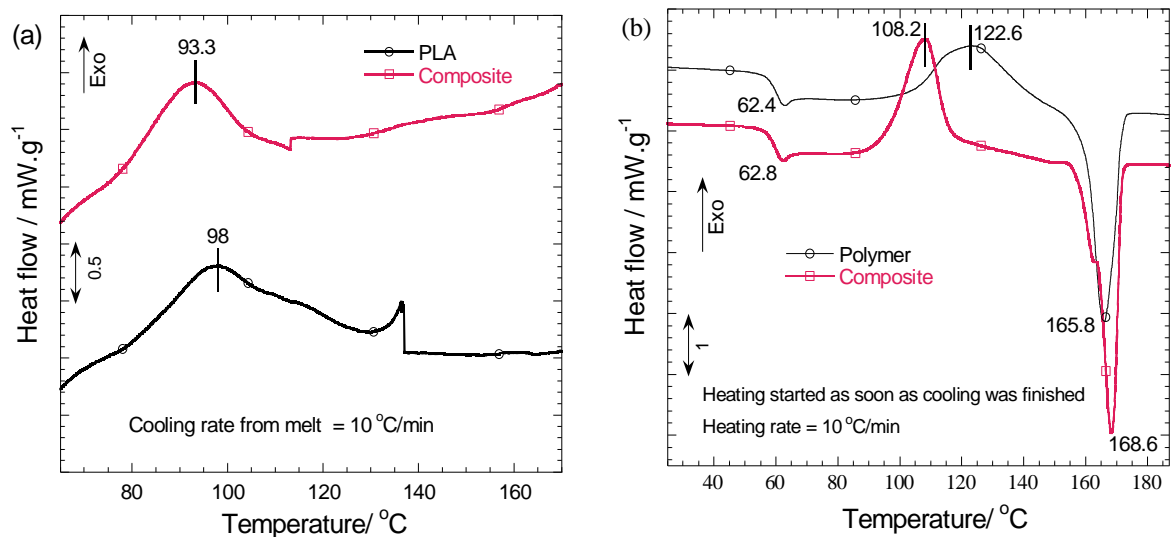


**Figure 6.2 DSC curves of neat PLA and the PLA/f-CNT composite: (a) during cooling from the melt and (b) during heating as soon as the cooling was finished.**

To study the influence of nonisothermal crystallization on the melting behaviour of the matrix, both neat PLA and the composite samples were heated at a rate of 10 °C.min<sup>-1</sup> directly from -20 °C as soon as the cooling was finished. Figure 6.2(b) shows the DSC curves of neat PLA and the composite during heating after non-isothermal crystallization, and the following main features are observed from these curves:

(i) For both samples, a sharp crystallization exotherm appears. Only one prominent exotherm indicates that for both samples the cold crystallization process takes place from a single homogeneous phase. However, the cold crystallization peak of neat PLA (122.6 °C) appears at a much higher temperature than that of the PLA/f-CNTs composite (108.2 °C). This indicates that the crystallization process is much more complete in the case of neat PLA than for the composite, or we can say that the neat PLA is in a much more stable state than the composite. Therefore, it is expected that the composite will go through the relaxation and crystal growth process much faster than the neat PLA, since each system tries to attain a thermodynamically stable state. For this reason, the composite shows a cold crystallization peak at a much lower temperature than the neat PLA matrix. It can also be seen from the DSC curves that the cold crystallization peak is more well-defined in the case of the composite than in the case of neat PLA. This suggests the formation of more perfect crystals in the case of the composite during heating.

(ii) The melting peak of the composite (168.6 °C) is at a slightly higher temperature than that of neat PLA (165.8 °C). This may be the result of the formation of much more stable and perfect PLA crystals in the case of the composite.

Dynamic mechanical analysis in the tension-torsion mode has been used to examine the temperature dependence of the  $E'$  of PLA upon composite formation with f-CNTs, which are strongly dependent on the level of dispersion-distribution of the nanotubes and their interaction with the PLA matrix. The temperature dependence of  $E'$  and  $\tan \delta$  of the neat PLA and the composite is presented in Figure 6.3. For both samples, in the  $\tan \delta$  curves, a prominent relaxation appears at around 28.4°C (as marked by the dotted line). However, the degree of relaxation is much higher in the case of the composite than in the case of the neat PLA. Such an observation indicates that the initial relaxation of the polymer chains is much faster in the composite than in neat PLA, although both samples were annealed under the same conditions. This relaxation probably facilitates faster crystal growth in the case of the composite during the second heating cycle (refer to Figure 6.2(b)).

On the other hand, the composite shows a substantial increase in the  $E'$  compared to that of the neat PLA, particularly above room temperature. Such an increase in  $E'$  occurs with the modification of the  $T_g$  of the neat PLA, as is evidenced by the peak position in the  $\tan \delta$  curve that moves quite significantly to higher temperatures upon f-CNTs addition. We believe that such a relative enhancement in the modulus is related to the presence of the f-CNT network structure, which eventually retards the mobilization of the PLA chains. The immobilization of the PLA chains becomes prominent above room temperature when the macromolecule chains start to relax. For this reason, the composite shows significant improvement in modulus close to or above the  $T_g$  of the matrix.

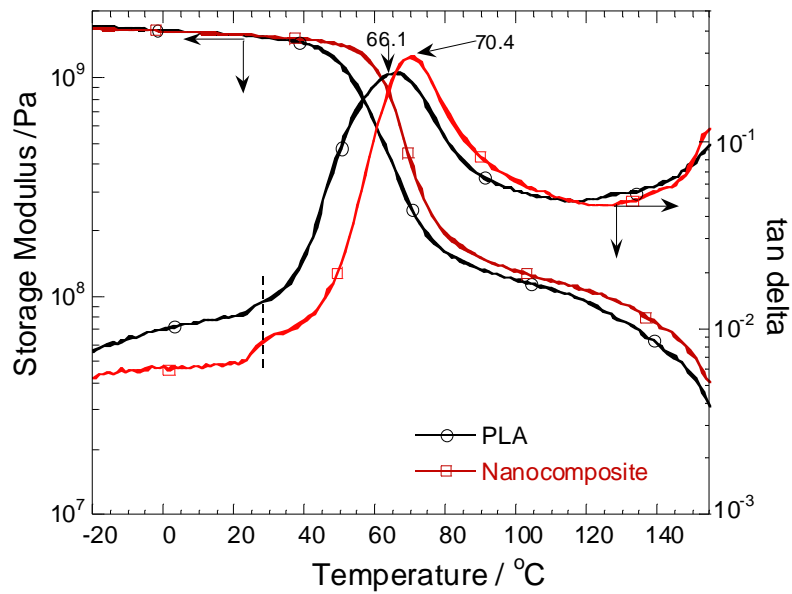


**Figure 6.3** The temperature dependence of elastic storage modulus and  $\tan \delta$  curves of neat PLA and the PLA/f-CNTs composite. Compression moulded, annealed (at  $110^{\circ}\text{C}$  for 3h under vacuum) samples were used.

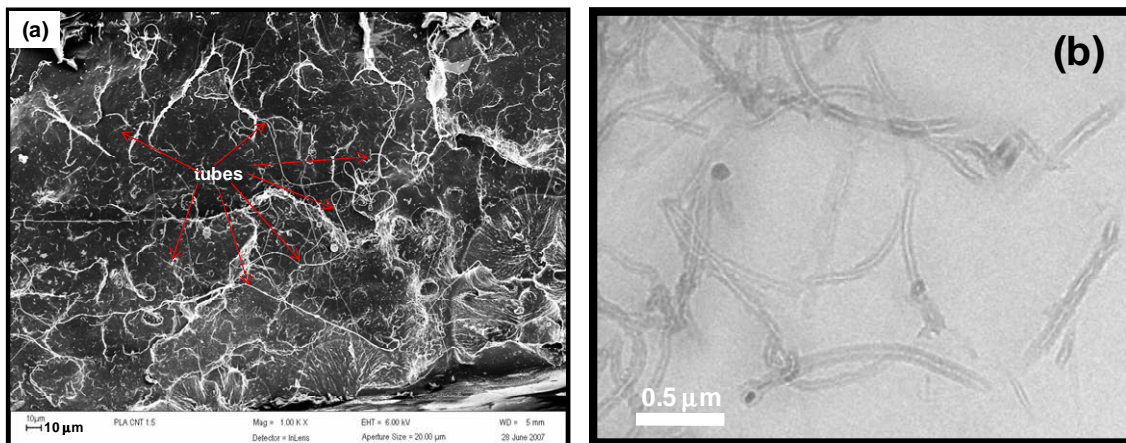


**Figure 6.4** (a) Field-emission scanning electron microscopic image of the freeze-fractured surface of the composite and (b) bright-field transmission electron microscopic image of the composite.

The degree of dispersion-distribution of f-CNTs in the PLA matrix was studied by FE-SEM and TEM. Figure 6.4(a) shows the freeze-fractured surface image of the composite. It can be seen from the FE-SEM image that most of the tubes separated and nicely dispersed in the PLA matrix, and formed a network-like structure. The bright-field TEM image of the composite further supports the conclusion made on the basis of the SEM image. Such a network-like structure is responsible for the unusual crystal growth behaviour and increase in mechanical properties of the composite.

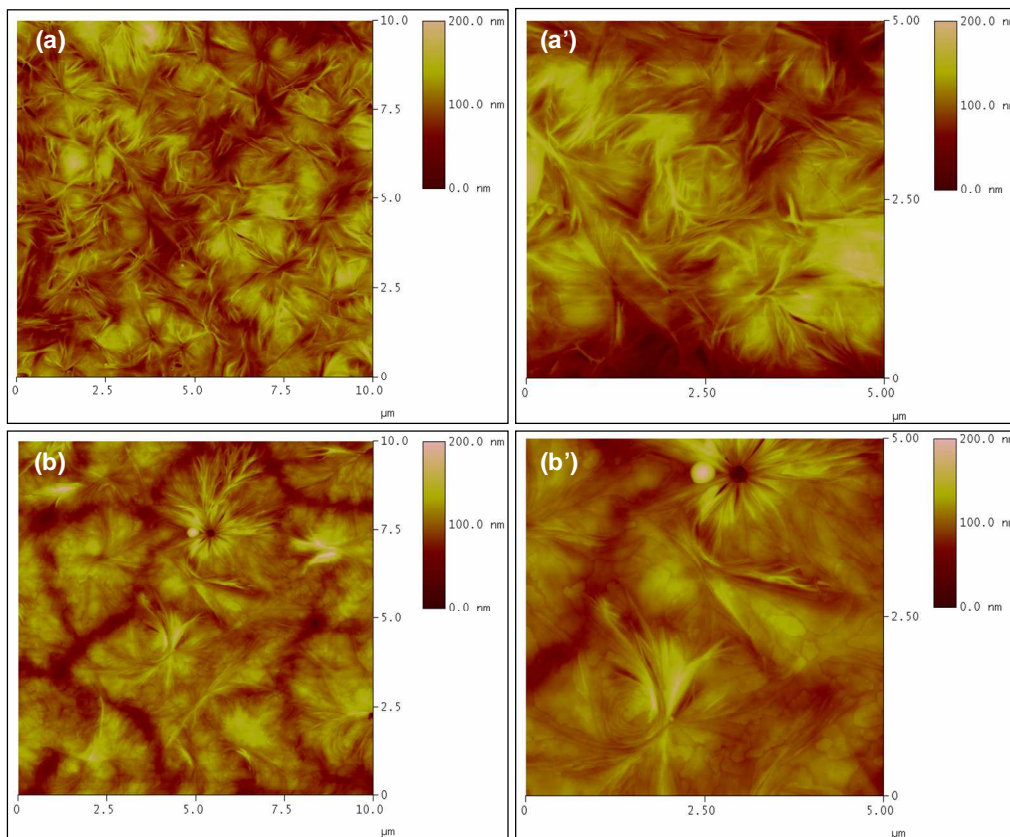


**Figure 6.5** Tapping mode atomic force microscopy height images of (a, a') neat PLA and (b, b') PLA/f-CNTs composite thin films at two different magnifications.

Finally, to see the effect of the incorporation of f-CNTs on the crystallization behaviour of the PLA matrix in a confined space, the crystal growth behaviour of the neat PLA and the PLA/f-CNTs composite thin films was studied by AFM. Figure 6.5 shows the tapping mode AFM height images (at two different magnifications) of neat PLA and its composite thin-film samples after being annealed at 130 °C for 30 min. It is clear from the height images (a, a') that the crystals were not perfectly grown in the case of neat PLA. This may be due to the

presence of a secondary crystallization or impingement effect. On the other hand, the crystals were more perfectly grown in the case of the PLA/f-CNTs composite (Figure 6.5(b, b')). Such an observation is the result of the presence of homogeneously dispersed f-CNTs in the PLA matrix. Because of the homogeneous dispersion of the tubes, the crystals are tightly bound and there is no chance of further impingement among themselves, which means that the crystals grow slowly and more perfectly. This result supports the conclusions made on the basis of the POM and DSC results.

### **6.3 Conclusions**

In this chapter we have discussed the effect of f-CNTs incorporation on the crystallization behaviour of PLA in both bulk and confined spaces. POM observations, AFM images and DSC curves show that the incorporation of f-CNTs changed the crystallization behaviour of PLA in a way that is quite uncommon from the general understanding of CNTs filled semicrystalline polymer systems. This is attributed to the non-agglomerated dispersion of the CNTs in the PLA matrix, which eventually formed a network-like structure as evidenced by SEM and TEM. This network-like structure acts as an obstacle for the mobility and flexibility of the PLA chains to fold and join the crystallization growth front. However, the network-like structure increases the elastic storage modulus of the composite.

### **6.4 References**

- [1] S. Sinha Ray, M. Bousmina. Polymers and their layered silicate nanocomposites. *Progress in Materials Science* 2005; 50:962-1079.
- [2] S. Sinha Ray, M. Okamoto. Polymer/layered silicate nanocomposites: A review from preparation to processing. *Progress in Polymer Science* 2003; 28:1539-1641.
- [3] F.F. Fang, H.J. Choi, J. Joo. Conducting polymer/clay nanocomposites and their applications. *Journal of Nanoscience and Nanotechnology* 2008; 8:1559-1581.
- [4] S. Pavlidou, C.D. Papaspyrides. A review on polymer-layered silicate nanocomposites. *Progress in Polymer Science* 2008; 33:1119-1198.

- [5] M. Alexandre, P. Dubois. Polymer-layered silicate nanocomposites: Preparation, properties and uses of a new class of materials. *Materials Science and Engineering* 2000; A28:1-63.
- [6] J.H. Park, H.M. Lee, I.J. Chin, H.J. Choi, H.K. Kim, W.G. Kang. Intercalated polypropylene/clay nanocomposite and its physical characteristics. *Journal of Physics and Chemistry of Solids* 2008; 69:1375-1382.
- [7] F.F. Fang, H.J. Choi, W.S. Ahn. Electroactive response of mesoporous silica and its nanocomposites with conducting polymers. *Composites Science and Technology* 2009; 69:2088-2092.
- [8] R. Hiroi, S. Sinha Ray, M. Okamoto, T. Shiroi. Organically modified layered titanate: A new nanofiller to improve the performance of biodegradable polylactide. *Macromolecular Rapid Communications* 2004; 25:1359-1364.
- [9] S.T. Kim, J.Y. Lim, B.J. Park, H.J. Choi. Dispersion-polymerized carbon nanotube/poly(methyl methacrylate) composite particles and their electrorheological characteristics. *Macromolecular Chemistry and Physics* 2007; 208:514-519.
- [10] S. Singh, S. Sinha Ray. Polylactide based nanostructured biomaterials and their applications. *Journal of Nanoscience and Nanotechnology* 2007; 7:2596-2615.
- [11] M. Moniruzzaman, K.I. Winey. Polymer nanocomposites containing carbon nanotubes. *Macromolecules* 2006; 39:5194-5205.
- [12] M.J. Percy, J.I. Amalvy, D.P. Randall, S.P. Armes, S.J. Greaves, J.F. Watts. Synthesis of vinyl polymer-silica colloidal nanocomposites prepared using commercial alcoholic silica sols. *Langmuir* 2004; 20:2184-2180.
- [13] E.T. Thostenson, Z.F. Ren, T.W. Chou. Advances in the science and technology of carbon nanotubes and their composites: A review. *Composites Science and Technology* 2001; 61:1899-1912.
- [14] X. Cui, M.H. Engelhard, Y. Lin. Preparation, characterization and anion exchange properties of polypyrrole/carbon nanotube nanocomposites. *Journal of Nanoscience and Nanotechnology* 2006; 5:547-553.
- [15] K. Kim, S.J. Cho, S.T. Kim, I.J. Chin, H.J. Choi. Formation of two-dimensional array of multiwalled carbon nanotubes in polystyrene/poly(methyl methacrylate) thin film. *Macromolecules* 2005; 38:10623-10626.
- [16] Y.T. Shieh, Y.K. Twu, C.C. Su, R.H. Lin, G.L. Liu. Crystallization kinetics study of poly(L-lactic acid)/carbon nanotubes nanocomposites. *Journal of Polymer Science Part B: Polymer Physics* 2010; 48:983-989.

- [17] L. Li, B. Li, M.A. Hodd, C. Li. Carbon nanotube-induced polymer crystallization. *Polymer* 2009; 50:953-965.
- [18] M.R. Nouri, M.G. Ahangari, A. Fereidoon, M. Jahanshahi. Kinetics and morphology of polypropylene. *Polymer Testing* 2009; 28:46-52.
- [19] K.A. Anand, U.S. Agarwal, R. Joseph. Carbon nanotubes induced crystallization of poly(ethylene terephthalate). *Polymer* 2006; 47:3976-3980.
- [20] G. Hu, X. Feng, S. Zhang, M. Yang. Crystallization behaviour of poly(ethylene terephthalate)/multiwalled carbon nanotubes composites. *Journal of Applied Polymer Science* 2008; 108:4080-4089.
- [21] A.P. Bhattacharyya, T.V. Sreekumar, T. Liu, S. Kumar, L.M. Ericson, R.H. Hauge, R.E. Smalley. Crystallization and orientation studies in polypropylene/single wall carbon nanotube composite. *Polymer* 2003; 44:2373-2377.

## Chapter 7

### Conclusions, publications and conference presentations

#### 7.1 Conclusions

The purpose of the study was to prepare polymer nanocomposites based on biodegradable poly(L-lactide) (PLA) with f-MWCNTs. The polymer nanocomposites were prepared by melt extrusion and solvent casting methods. A new and novel MWCNTs-reinforced approach for biodegradable/biocompatible PLA was presented.

In the case of poly(lactide) nanocomposite containing 1.5 wt.% of f-MWCNTs (with an amine content of ~10 % content) prepared by a melt extrusion method, an improvement in the inherent properties of the PLA such as the glass transition temperature, crystallization kinetics, dynamic mechanical properties, strength, and elongation at break were reported. The results showed that these property improvements were due to the strong interfacial interaction between the nanotubes's outer surface and the PLA chains.

In the case of the PLA nanocomposite containing 0.5 wt.% of f-MWCNTs (with an amine content of ~20%) prepared by melt extrusion, the morphology, thermal, and thermomechanical properties of the PLA and its nanocomposite were discussed. The SEM and POM (of the samples in the molten state) results confirmed the good dispersion of the f-MWCNTs in the PLA matrix, with some micro-agglomeration. The POM results also show the formation of much smaller PLA crystallites in the presence of f-MWCNTs. The f-MWCNTs were found to play a nucleation role in the crystallization of PLA, as observed from the DSC, SEM, and WAXS results. However, the overall crystallinity of the PLA was reduced when 0.5 wt.% f-MWCNTs was added. A decrease in the overall crystallinity was found to be the result of two factors: f-MWCNT agglomerates acting as active nucleation sites and at the same time, the non-agglomerated sites inhibiting mobility of the polymer chains. The DMA and TGA results showed that the presence of f-MWCNTs had only a slight influence on the thermomechanical properties and thermal stability of the PLA. FTIR and

Raman spectroscopy confirmed the functionalization of the MWCNTs, and the presence of interfacial interaction between the f-MWCNTs and the PLA matrix.

In the case of the PLA nanocomposite containing 1.5 wt.% f-MWCNTs (with an amine content of ~10%) prepared through solution casting method, the effect of the f-MWCNTs incorporation on the crystallization behaviour of PLA in both the bulk and confined spaces was investigated. POM observations, AFM images and DSC curves showed that the incorporation of f-MWCNTs changed the crystallization behaviour of the PLA in a way that is quite uncommon from the general understanding of CNTs filled semicrystalline polymer systems. This was attributed to the non-agglomerated dispersion of the CNTs in the PLA matrix, which eventually formed a network-like structure as evidenced by SEM and TEM. This network-like structure acted as an obstacle for the mobility and flexibility of the PLA chains to fold and join the crystallization growth front. However, the network-like structure was found to increase the elastic storage modulus of the composite.

## **7.2 Publications from the project**

1. S. Sinha Ray, J. Ramontja. "Biodegradable Polymer Blends and Composites from Renewable Resources", John Wiley & Sons, ISBN-13: 9780470146835, 2008, 389-409.
2. J. Ramontja, S. Sinha Ray, S.K. Pillai, A.S. Luyt. High-performance carbon nanotube-reinforced bioplastic. *Macromolecular Materials and Engineering* 2009; 294:839-846.
3. J. Ramontja, S. Sinha Ray, S.K. Pillai, A.S. Luyt. Uncommon crystallization behaviour of biodegradable polylactide in presence of functionalized carbon nanotubes. *Macromolecular Materials and Engineering* (provisionally accepted).
4. J. Ramontja, S. Sinha Ray, A.S. Luyt. The effect of surface functionalized carbon nanotubes on the morphology, as well as thermal, thermomechanical, and crystallization properties of polylactide (submitted to the *Journal of American Ceramic Society*).

### **7.3 Future work**

We intent to study crystallization kinetics and rheological properties of the samples we prepared. Furthermore, different functional groups will be attached to the surface of CNTs, composites will be prepared by melt extrusion and solution casting techniques. These will be characterized and studied in details for orthopaedic applications.

### **7.4 Conference presentations**

1. High-performance carbon nanotube-reinforced bioplastic. 11<sup>th</sup> Pacific Polymer Conference, Cairns, Australia, 06-10 December 2009.
2. High-performance carbon nanotube-reinforced bioplastic. Nanoscience Young Researchers Symposium, CSIR, Pretoria, South Africa, 18 September 2009. (winner of the 2<sup>nd</sup> best oral presentation on the PhD category).
3. Properties of polylactide nanocomposite based on functionalized carbon nanotubes. NanoAfrica 2009, CSIR, Pretoria, South Africa, 1-4 February 2009.
4. Uncommon crystallization behaviour of biodegradable polylactide in presence of functionalized carbon nanotubes. 35<sup>th</sup> International Conference & Exposition on Advanced Ceramics and Composites, Daytona Beach, Florida, USA, 23-28 January 2011.